Preparation of $K_{1-x}Na_xNbO_3$ Ferroelectrics Composite for Solar Energy Harvesting Application

A Thesis

Submitted to the College of Science, Al-Nahrain University in Partial Fulfillment of the Requirements for Degree of Master of Science in Physics.

By

Amer Abdullah Salman

B.Sc., Al-Nahrain University (2010)

Supervised by
Prof. Dr. Emad K. Al-Shakarchi

2016 A.D   *1437A.H*

Acknowledgement

*Praise is to **Allah** and peace and blessings on the Prophet **Mohammed** great of senders.*

*I would like to express its sincere thanks and gratitude to my supervisor, Prof. Dr. **Emad K. Al-Shakarchi** for proposed this project, advice, encouragement, valuable guidance in my research and insightful comments during the writing process.*

And I wish to express my sincere thanks to the head of the physics department and dean of College of Sciences for their support to post graduate student.

The nicest words of thanks express to my father, my mother, my brothers. Thanks to them for the incredible amount of patience that they have given me, especially throughout my thesis-writing period. I am deeply grateful to them.

Amer

I

Abstract

In this study, $K_{1-x}Na_xNbO_3$ were prepared with different substitutions (x), where x = (0, 0.5 and, 1) by conventional solid state reaction (SSR). The sample with (x=0) was prepared for different value of sintering temperature (900, 950, 1000 and 1050 °C). while the samples with (x=0.5 and 1) with sintering temperature (1000°C). The resulted powders have polycrystalline structure with a starting to produce a single crystal for the sample with (x=0) above sintering temperature (1000 °C). Also this appeared for (x=0.5 and 1). Crystal structure, space group, crystallite size, and grain size were determined from structural analysis (XRD and, SEM). Using special software for specifications and estimations the XRD, which help in calculations and to make a comparison with some international databases like ICDD, PDF2 database and, COD database.

Physical properties represented by density, dielectric measurements, optical energy gap and the refractive index for $K_{1-x}Na_xNbO_3$ system. The dielectric measurements were studied under two conditions, the first was by changing frequency at room temperature, the second was by changing temperature at fix frequency in role to measure the dielectric constant (ε_r) and loss tangent (D). Curie temperature (Tc) and dielectric constant were determined from dielectric measurements.

From dielectric measurements for $KNbO_3$, the maximum dielectric constant was appeared at the sample with sintering temperature (1000°C). While for all sample sintered at (1000 °C) the maximum dielectric constant was for (x=0.5). The Curie temperature was shifted to a lower temperature as the Na ratio increase in the system.

The optical energy gap was calculated for the system and its value was in the range (4.23-4.27 eV). The refractive index also calculated from the reflectance spectrum and from the LCR- measurement. The maximum value of the refractive index from the reflectance pattern was in the range

(1.2, 1.8 and 1.24) for x = 0, 0.5 and 1 respectively. The refractive index also concluded form the LCR-measurement for the same frequency of its the maximum value the reflectance pattern calculation. It was (0.72, 0.96 and 0.67) for x = 0, 0.5 and 1 respectively.

The total results showed that the ability of using this composition ($K_{1-x}Na_xNbO_3$) in the field of solar energy harvesting

Table of Contents

List of Figures

List of Tables

Chapter One

Introduction and Literature

Review

1.1 Introduction

The ferroelectric is a material that exhibited the spontaneous polarization in the absence of applied electric field over a wide temperature range. This polarization can be reversed by an applied field in opposite direction. The most commonly used of ferroelectrics having the Perovskite structure. The ideal simple of perovskite unite cell, represented by ABX_3 where A and B are cations with different sizes, and X is an anion that bonded to both[1].

Ferroelectric materials have many applications like capacitors, memory devices, transducers, photonic devices, communications, thermal photography (IR photography), and ferroelectric-photovoltaic (FE-PV) device [1, 2].

Ferroelectric materials have recently more active as a candidate class of materials for using in photovoltaic devices. These materials have a strong inversion symmetry that was due to the spontaneous electric polarization promotes the desirable separation of photo-excited carriers and allows voltages higher than the band gap. This might be enable in the efficiency beyond the maximum possible in a conventional p–n junction solar cell. The ferroelectric oxide is a stable in a wide range of mechanical, chemical and thermal conditions. They were being fabricated by using low-cost methods. The decreasing in the ferroelectric layer thickness and ferroelectric–electrode interfaces are greatly increase the current harvesting from ferroelectric absorber materials. This is causing increasing in the power conversion efficiency about 10^{-4} to about 0.5 per cent. Further improvements in photovoltaic efficiency have been inhibited by the wide band gap in the range (2.7–4eV) of ferroelectric oxides, which allow the use of only 8–20 per cent of the solar spectrum[3].

2

1.2   General aspect

Polarizability is a consequence of the fact that the molecules, which are the building blocks of all substances, are composed of both positive charges (nuclei) and negative charges (electrons). When a field acts on a molecule, the positive charges are displaced along the field, while the negative charges are displaced in a direction opposite to that of the field. The effect is therefore to pull the opposite charges apart, i.e., to polarize the molecule[4, 5]. There are different types of polarization processes, depending on the structure of the molecules which constitute the solid[1, 4]. If the molecule has a permanent moment, i.e., a moment even in the absence of an electric field, means a dipolar molecule. When a field is applied to the substance, however, the molecular dipoles tend to align with the field, and this results in a net non-vanishing polarization. This leads to the so-called dipolar polarizability [4, 5]. If the molecule contains ionic bonds, then the field tends to stretch the lengths of these bonds. This result from the field tends to displace the positive ion to the right, and the negative ion to the left, resulting in a stretching in the length of the bond. The effect of this change in length is to produce a net dipole moment in the unit cell where previously there was none. Since the polarization here is due to the relative displacements of oppositely charged ions, we speak of ionic polarizability [4]. The third type of polarizability arises by the individual ions or atoms in a molecule are themselves polarized by the field. This type is called electronic polarizability [4, 5].
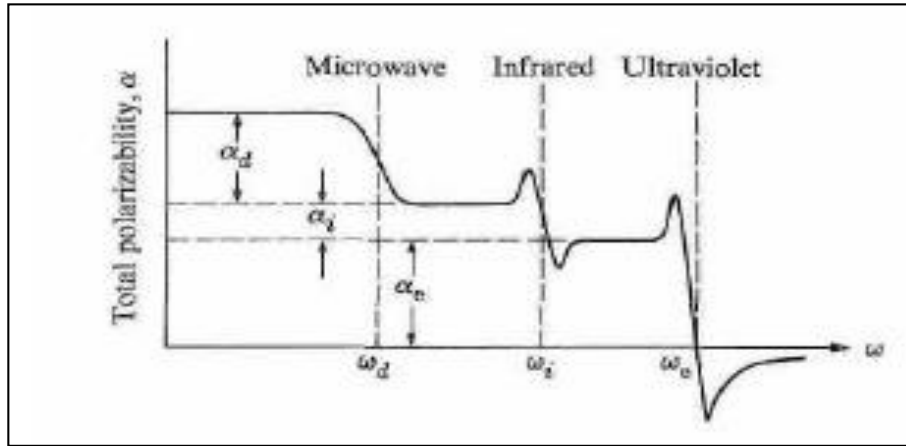
Fig. 1.1: Frequency dependence of the several contributions to the polarizability[4].

Another important distinction between the various polarizabilities emerges when one examines the behavior of the polarizability that is induced by an alternating field. Fig. 1.1 shows a typical dependence of this polarizability on frequency over a wide range, extending from the static all the way up to the ultraviolet region. It can be seen that in the range from $\omega = 0$ to $\omega = \omega d$, where ω_d (d for dipolar) is some frequency usually in the microwave region, the polarizability is essentially constant. In the neighborhood of ω_d, however, the polarizability decreases by a substantial amount. This amount corresponds precisely, in fact, to the dipolar contribution $\boldsymbol{\alpha}_d$. The reason for the disappearance of $\boldsymbol{\alpha_d}$ in the frequency range $\omega > \omega_d$ is that the field now oscillates too rapidly for the dipole to follow, and so the dipoles remain essentially stationary. The polarizability remains similarly unchanged in the frequency range from ω_d to ω_i and then drops down at the higher frequency. The frequency ω_i lies in the infrared region, and corresponds to the frequency of the transverse optical phonon in the crystal. For the frequency range $\omega > \omega_i$ the ions with their heavy masses are no longer able to follow the very rapidly oscillating field, and consequently the ionic polarizibility αi, vanishes[4, 5].

4

The term ferroelectrics is similar to analogy of ferromagnetic, because they have the same characteristics under electric field for dielectric materials. The prefix ferro- derived from ferum, which means the in Iron by Latin form. The feature of Iron is showed the presence the ordering of magnetic dipole moment. This is the element of ferromagnetic materials. The elements of ferroelectric materials are the presence of electric dipole moments. The ordering of this dipoles are the reason to produce ferroelectric behavior in those dielectric materials and there after the presence of hysteresis loop. It implies the similarity in characteristics to ferromagnetic but the difference in the ordering elements. The ferroelectric is exhibiting a spontaneous electric polarization below the Curie temperature (T_C) producing a hysteresis loop under mechanical strain as shown in (Fig.1.2). However, the ferroelectrics is differ from ferromagnetic in their fundamental mechanisms and also in some of their applications[1].

In ferroelectric materials the ionic susceptibility is sensitive to variations in temperature. In these substances, the static dielectric constant changes with temperature according to the Curie–Weiss relation[1].

$$\varepsilon = \frac{C}{T - T_c} \qquad\qquad (1.1)$$

where C is known as the Curie constant, and T_C is the Curie temperature. At temperatures above T_C, the crystal is no longer ferroelectric and transfer to paraelectric exhibiting normal dielectric behavior.
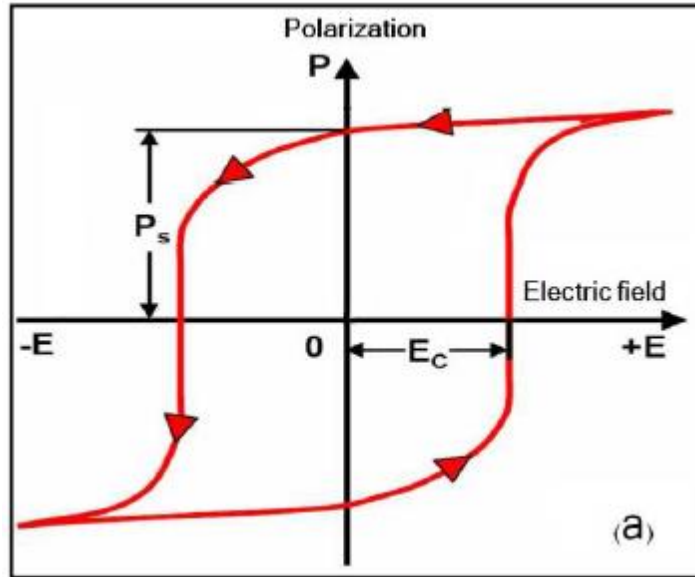
Fig. 1.2 : A typical ferroelectric hysteresis loop[1]

Piezoelectricity is referring to the fact that, when a crystal is strained, there is electric field produced within the substance. The potential difference is developed across the sample, the last has direct effect in measuring the electric field. The inverse effect - that an applied field produces by strain has also been observed, such that in quartz [3].

The pyroelectric material is a crystalline substance and capable of generating an electric charge in response to heat flow. The pyroelectric effect is very closely related to the piezoelectric effect [6].

All these types of materials (Piezoelectric, Ferroelectric, and Pyroelectric) are belonged to dielectric materials. The ferroelectric materials are special type of pyroelectric materials, and the pyroelectric materials are special type of piezoelectric materials, all these types are belonged to dielectric materials as shown in Fig.1.3 [7].
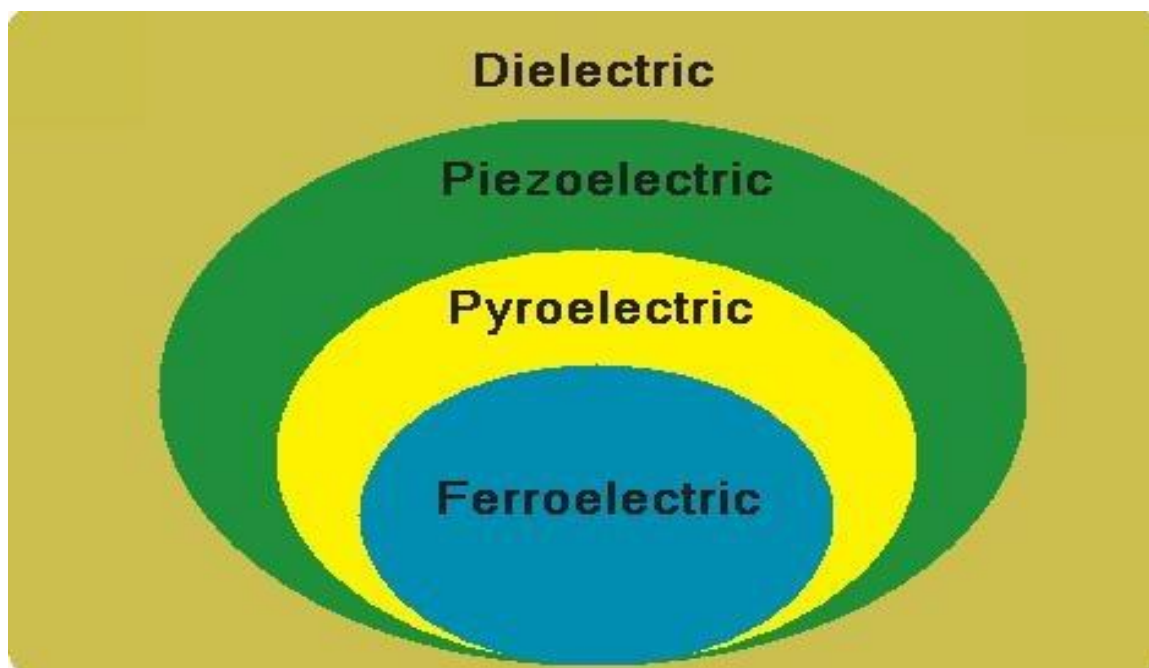
Fig. 1.3 :The relation between ferroelectric, pyroelectric,piezoelectric and dielectric materials[7].

The crystal can be classified into (32) classes according to their symmetry operation with respect to point groups. Among the (32) point classes, there are (11) of them possess to a center of symmetry, and the remaining (21) classes are non-centrosymmetric. One of the (21) classes is possess other combined symmetry elements, thus rendering no piezoelectricity. The remaining (20) classes of non-centrosymmetric crystals would exhibited piezoelectric effects. Only the (10) of the (20) classes, have induced polarization by a mechanical stress (piezoelectric effect). While the other (10) classes have possess a spontaneous polarization. The last(10) classes have exhibiting all three effects ferroelectric, piezoelectric, and pyroelectric[1].So it is obvious that only ferroelectric crystals are piezoelectrics, but the reverse is not true[1, 7].
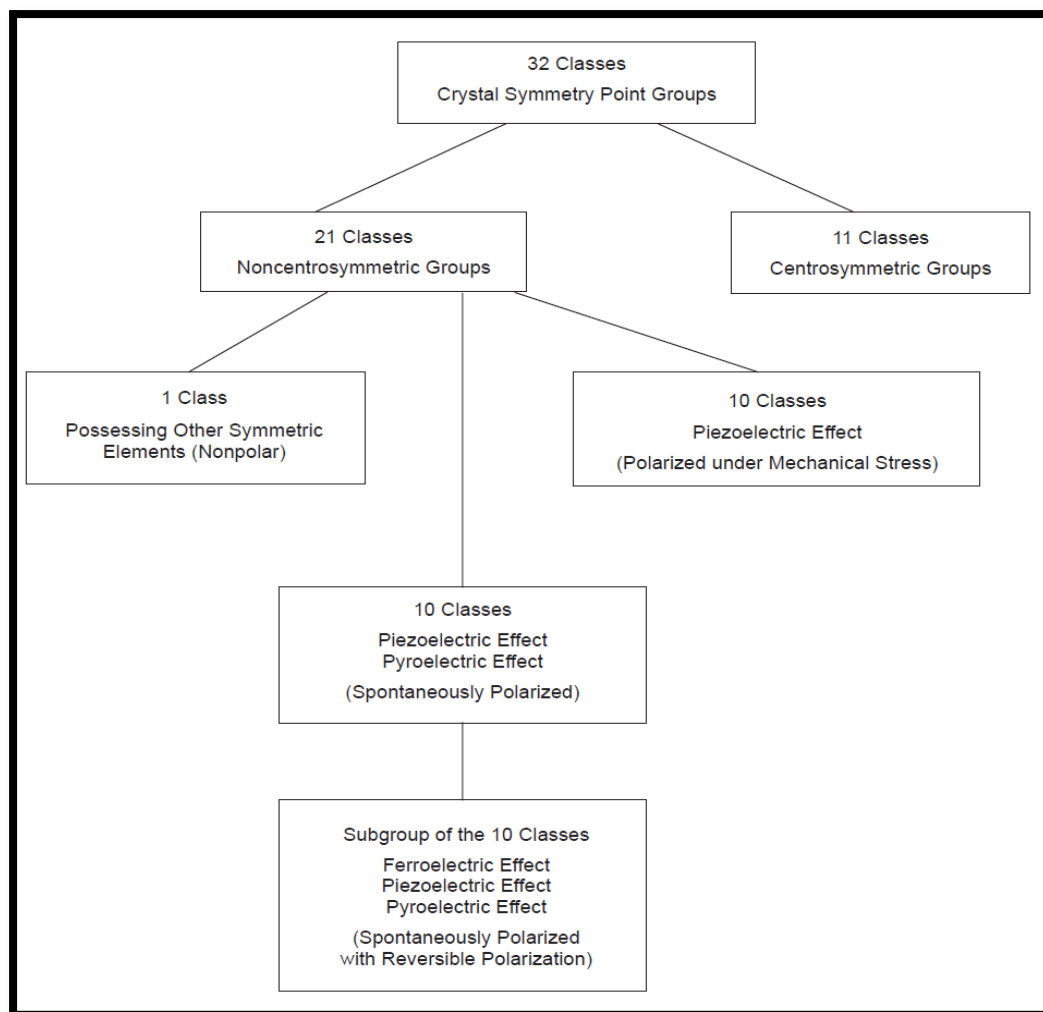
Fig. 1.4:Classification of crystals showing the classes with piezoelectric, pyroelectric, and ferroelectric phenomenon [1]

1.3 Relaxor Ferroelectrics

The relaxor ferroelectricity (RF) is closely related to conventional ferroelectricity (FE). The relaxor ferroelectrics are dielectrics, often crystallizing in an ABO_3 perovskite structure. It is capable in exhibiting strong piezoelectric coupling and large field-induced strains while their microstructure features polar regions, which are decisive for the functional properties. Despite these similarities, both groups of materials are inherently different in several aspects, as summarized by in Fig.1.5.
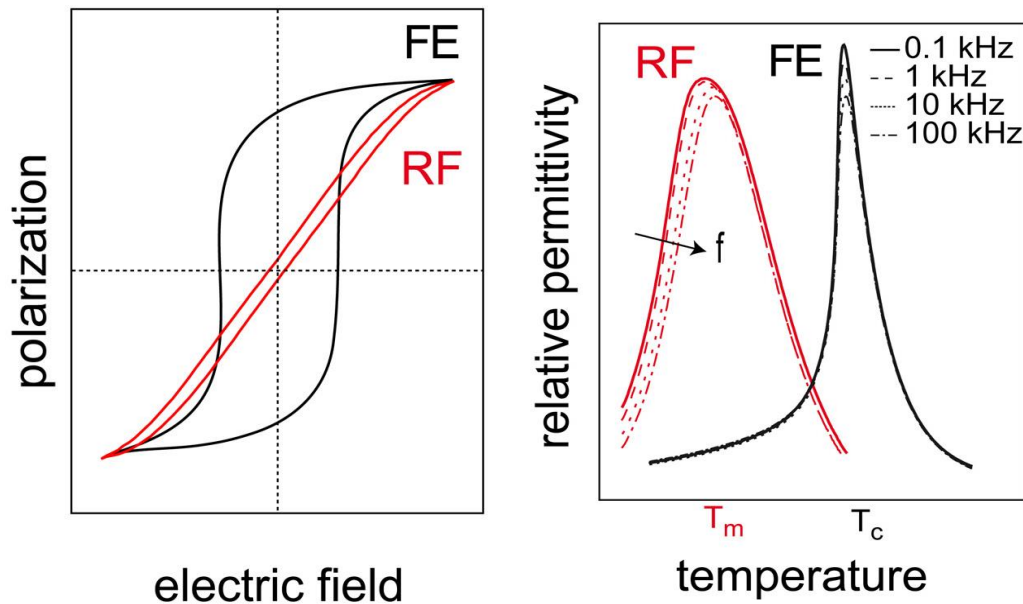
Fig. 1.5: Comparison of ferroelectrics and relaxor ferroelectrics in terms of field-induced polarization (left), and relative permittivity (right) [8]

In contrast to the rectangular polarization hysteresis observed for conventional FE, the P(E)loops of RF might be remain slim with little remanence and minute 'coercive field'. Moreover, the temperature-driven FE-PE phase transition of ferroelectrics is associated with symmetry breaking and a peak in permittivity at T_C, above which the Curie-Weiss law applies. While the $\varepsilon_r(T)$ curve of RFs also exhibits a maximum at temperature T_m, the values of both T_m and $\varepsilon_r(T=T_m)$ depend on the measurement frequency. This effect, referred to the frequency dispersion, is one of the most characteristic features of RFs. In contrast to FE, this peak in permittivity is not associated with a structural phase transition and the permittivity does not obey the Curie-Weiss law for all $T>T_m$. Also, the remnant polarization may assume finite nonzero values in excess of T_m. Relaxor ferroelectrics, however, do not only stand out because of these properties but also due to their high applicability. Large dielectric constants are beneficial in capacitors, high electrostrictive coefficients are exploited

in actuators, and the electro-optical characteristics are employed in devices such as shutters or optical modulators [8].

1.4 Perovskite structure

The perovskite structure is one of the most extensively studied structures in solid state physics, chemistry, materials science, and geology. It is one of the most popular structures that showed the ferroelectric behavior [9].

The ideal form the crystal structure is a perovskie cubic structure with a chemical formula ABX_3.It can be described by two types of cation A and B. The B-cation has 6-foldcoordination surrounded by an octahedron of anions, and the A-cation has12-fold cuboctahedral coordination. The X is often oxygen but also other large ions such as F^- and Cl^- are possible[10].
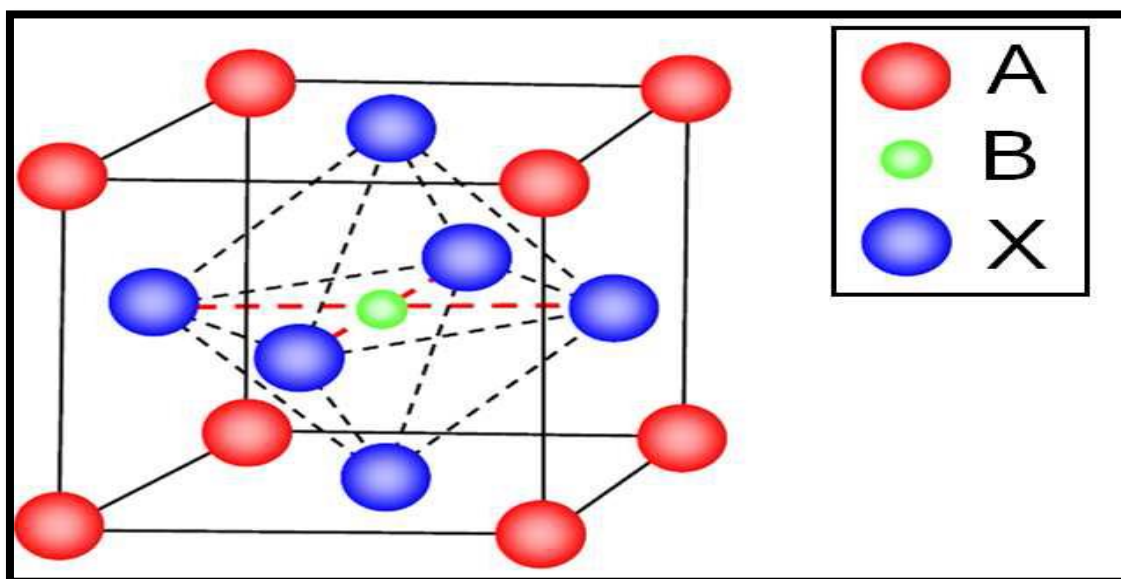
Fig. 1.6: Perovskite structure[10]

The relative ion size is quite stringent for the stability of cubic structure. The slight distortion can produce several lower-symmetry distorted versions. The coordination numbers of A, B cations are both reduced. The

tolerance factor (t) of perovskite structure can be estimated by the following equation[1, 7]

$$t = \frac{r_A + r_0}{\sqrt{2}(r_B + r_0)}$$ 1-2

Where (r) is the ionic radius.

1.5 Solid State Reaction (SSR).

It is a conventional method which means a chemical reaction between solids. Solid state reaction routes from oxides and carbonates have been extensively used to synthesize ferroelectric powders with good control of particle morphology [11] .

The mixture of oxides and carbonates were grounded with suitable solvent, like ethanol. The calcinations many time process is a suitable to produce the sample under study until getting the net powder[12].

Moreover, the solid state reaction synthesis is a low cost technique and requires only simple processing. Thus, this technique would be highly desirable for technological applications [11].

1.6 Properties of the system $K_{1-x}Na_xNbO_3$

Potassium Niobate $KNbO_3$ is a ferroelectric material possessing high electro-optic and nonlinear optical coefficients. It is exhibited a large bandgap, and its optical properties can be sensitively altered by the application of electric field. The $KNbO_3$ has been applied in optical waveguides and holographic storage systems because of its specific electro-optic properties [13].
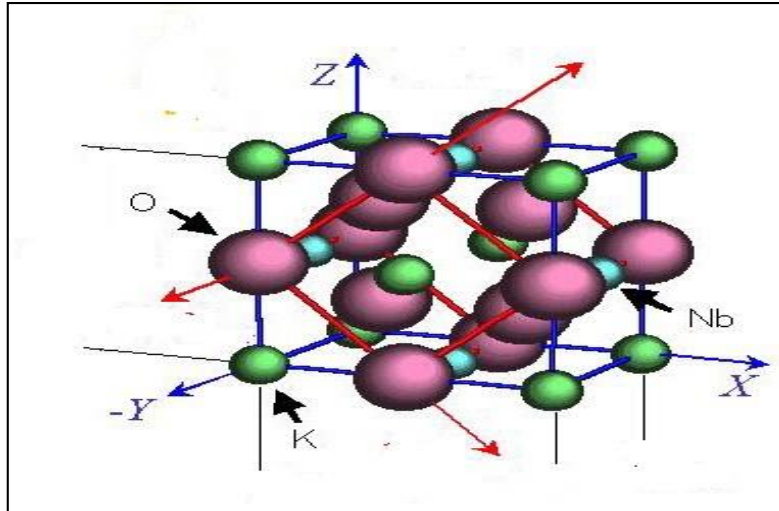
Fig. 1.7 : Crystal structure of Orthorhombic $KNbO_3$[14]

The composition $KNbO_3$ with an orthorhombic structure at room temperature, which has promising applications in electromechanical, nonlinear optical and other technological fields[15]. At high temperature (T > 435 ℃), the $KNbO_3$ is paraelectric with a cubic structure. When the temperature decrease, the $KNbO_3$ crystal undergoes a series of ferroelectric phase transitions. On the other words, there is a multiphase transformation from cubic to tetragonal phases at temperature (435°C) and to orthorhombic at temperature(225°C), and orthorhombic to rhombohedral at temperature (−50°C). All of these ferroelectric phases are first-order and involve thermal hysteresis as a result of the lattice deformation. The reason for this multiphase transformation return to the shift of Nb ion involved in the transitions[16].
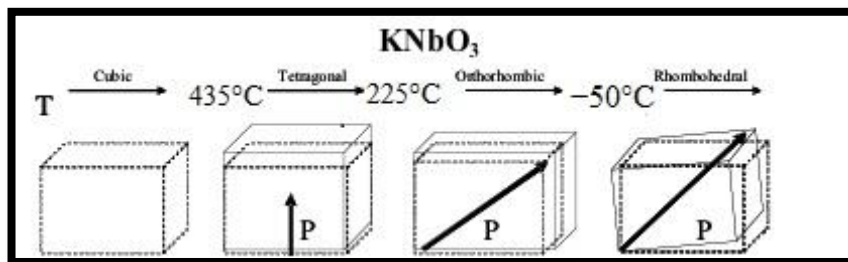
Fig. 1.8: Phase transition of $KNbO_3$

Potassium Sodium Niobate (KNN) is a ferroelectric system with a complex perovskite structure. The word complex is referred to the fact that the A-site is shared by more than one type of ion. The KNN is a mixed system of orthorhombic ferroelectric Potassium Niobate (KN) displaying similar phase transitions to barium titanate but at higher temperatures[16]. Potassium Sodium Niobate (KNN) is one of the most commonly investigated lead-free ferroelectric systems today. The others are being Bismuth Sodium Titanate-Barium Titanate (BNT-BT). The KNN is well known as lead-free system with a perovskite structure, which has a higher Curie temperature than the commonly used lead zircona tetitanate (PZT) and piezoelectric properties are in the same order of magnitude[12].

The drawbacks are still prevent wide scale industrial used today. The KNN is made from volatile alkali metal compounds, that require carefully controlled manufacturing conditions and low reaction temperatures. Furthermore, the KNN was exhibited a poor densification behavior in pressure-less sintering conditions. There is also a phase transition between two ferroelectric phases above room temperature. The heating above this transition temperature is causing accelerated aging. The best piezoelectric properties were achieved at morphotropic phase boundary (MPB) 50/50 Potassium Sodium Niobate composition [12].

The mixture of $NaNbO_3$ (NN) is probably the most complex perovskite structure as shown in Fig. 1.9. It is lead-free piezoelectric ceramics. It has a variety of structures and exhibited unusual complex sequence of temperature driven structural phase transitions which are not clearly understood [17].
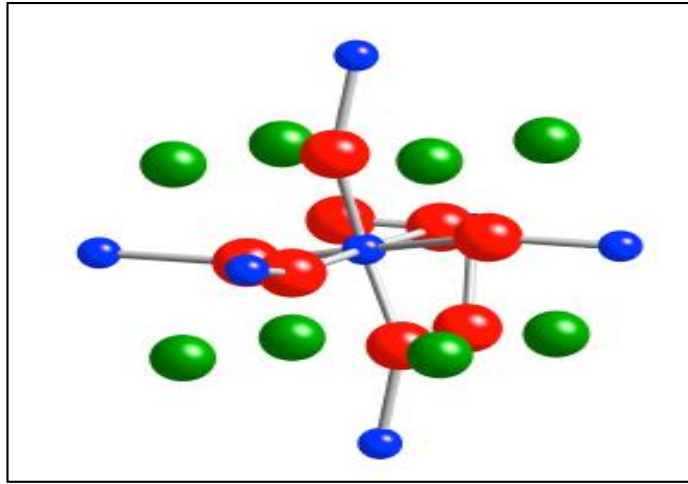
Fig. 1.9: NaNbO$_3$ structure with an Orthorhombic structure,Blue, red

and green spheres represent niobium, oxygen and sodium atoms, respectively [18].

The high-temperature phase is the cubic perovskites structure in the form ABO$_3$. The whole series of structural phase below 640°C had been found at least six phases were identified. The successive phases, which are labeled by T2 , T1 , S, R ,Q and P, are of orthorhombic symmetry except T2 that has tetragonal phase [19]. The NaNbO$_3$has great potential applications in electromechanical and also used in enhancing nonlinear optical properties and finds applications in Hologram recording materials [20].
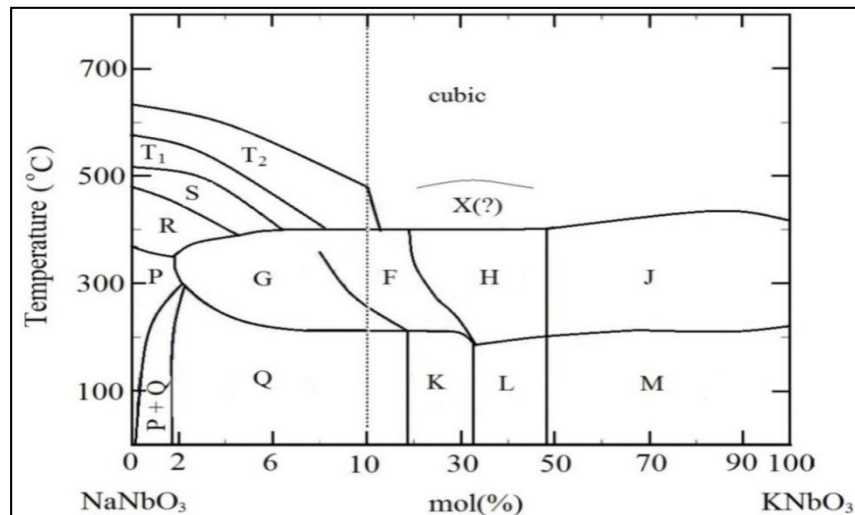
Fig. 1.10: Phase diagram of K$_{X-1}$Na$_X$NbO3. Regions labelled with Q, K, and L are monoclinic (or orthorhombic in most literature) ferroelectric, M, G is orthorhombic ferroelectric; F, H and J are tetragonal ferroelectric. Region P is orthorhombic[12]

14

1.7   Solar energy harvesting

The energy-harvesting and conversion devices using nano technology have been interesting recently, because they have potential applications in self-powered nano devices and nano systems. The piezoelectric nanowires have been extensively investigated for nano-generators (NGs). The nanowire-based solar cells can only work under light-illumination conditions. It had been reported that the size-driven enhancement of the pyroelectric coupling lead to a giant pyroelectric current and voltage generation by the polarized ferroelectric nanomaterials as a function of temperature fluctuations[20].

The solar energy is the most promising source in renewable energy to replace the traditional energy reliance on fossil fuels. Unfortunately, the solar cell power conversion efficiency (PCE) is limited in conventional solar cells, in which the excited carriers are separated by the internal electric field at p-n junction or other material interface. The ferroelectric possess an intrinsic spontaneous polarization. This is the reason to provide an alternative way to separate charge by the bulk material. This is called the bulk photovoltaic effect, since charge carriers are separated by a single phase material[21].

The wide bandgap of typical ferroelectric perovskite structure ABO_3 is due to the fundamental characteristics of the metal‑oxygen bonds(A–O) and (B‑O). The excitation across the bandgap is essentially a charge transfer from the oxygen O_{2p} state at the maximum valence band for the transition-metal d-states at the minimum conduction band. In transition-metal the B-cations enable in the perovskite oxide to exhibit ferroelectricity. Owing to a large difference in electronegativity between the oxygen and transition-metal atoms. The theoretical bandgap is quite

large within the range (3‑5 eV)[3].Ferroelectric oxides are also stable in a wide range of mechanical, chemical and thermal conditions[3].

There are many studies have been shown how the decreasing in ferroelectric layer thickness and judicious engineering of domain structures and ferroelectric–electrode interfaces can greatly increase the current harvested from ferroelectric absorber materials, which tend to increase the efficiency of power conversion. The unique characteristic of ferroelectric-photovoltaic (FE-PV) devices is the photocurrent direction can be switched by changing the spontaneous polarization direction of a ferroelectric material FE with the applied of electric field[3].

The ferroelectric photovoltaic effect is completely different from the traditional p–n junction photovoltaic effect as shown in (Fig.1.11aand b). In traditional p–n junction solar cells (Fig.1-11 a), for such semiconductor materials, the absorbed photons can jump the electrons from the top of valence band to the bottom of conduction band, the holes are left behind in the valence band. The electron-hole pairs generated are quickly separated by the built-in electric field inside the p–n junction and collected by the respective electrodes. Theoretically, the magnitude of V_{oc} in p–n junction solar cells is determined by the quasi-Fermi energy difference of photo-generated electrons and holes which is limited by the bandgap of the light absorbing semiconductors[2]. Nevertheless, the FE-PV devices as shown in Fig.1-6b, it was observed that the output photo voltage is proportional to the magnitude of electric polarization and electrode spacing. The unique and important characteristic of the FE-PV devices is the anomalous photovoltaic (APV) effect, i.e. the output V_{oc} can be a few orders of magnitude larger than the bandgap of the FE materials[2].
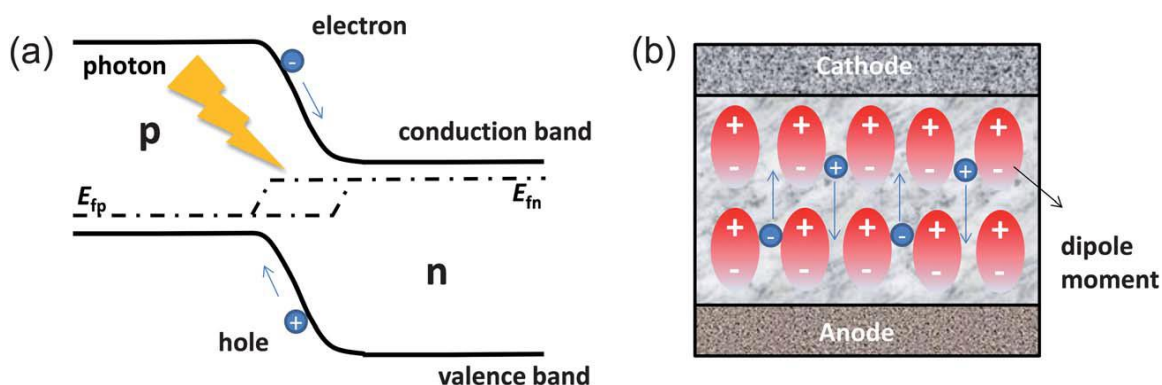
Fig. 1.11 : The working principle of (a) p–n junction solar cells and (b) FE-PV devices.[2]

1.8 Literature Review

Zhuang *et al*,[22] prepared a single phase and well crystallized of the compound $K_{0.5}Na_{0.5}NbO_3$ (KNN) as nano powder using a sol–gel method with a calcinations temperature of (750 ^oC). The average grain size of KNN powder was determined of about (450 nm). A flexible and implantable energy harvesting device fabricated using the KNN nano powder exhibited an output power was about (0.13 μW) with a load resistance of about (100 MΩ). The Young modulus of the device was determined to be (10.4 GPa) by atomic force microscopy (AFM).

Macutkevic *et al*,[23] obtained $NaNbO_3$ ceramics by solid state reaction. The calcination was at temperature (947 ^oC) for (3 hr). The second calcinations were at temperature (897 ^oC) for (2 hr). The sintering was at temperature (1147 ^oC) for (2 hr). They observed that the phase transitions of $NaNbO_3$ceramicby cooling during the broadband of frequency (20 Hz-1 GHz) in the temperature range (-248 ^oC-727 ^oC). There are multi points of phase transition at temperature (567 ,430 ,330 ,133 and -131 ^oC).

Vendrell *et al*,[24] prepared ZrO_2 and TiO_2 modified lead-free $(K_{0.5}Na_{0.5})NbO_3$ (KNN) piezoelectric ceramic. The addition of TiO_2or$ZrO_2$was tend to shift the phase transition toward lower temperature as confirmed by different techniques. This effect being higher than the samples doped with TiO_2. The addition of low amount of doping was acted

17

as an acceptor. It was promoted the densification, improving functional properties of KNN ceramic. The piezoelectric properties of the ceramic is greatly enhanced when doping with small concentrations of TiO_2 or ZrO_2.

Gaur *et al*,[25] synthesized $(K_{0.5}Na_{0.5})_{1-x}Li_x(Nb_{0.96}Sb_{0.04})O_3$ (x=0, 0.02,0.03,0.04,0.05,0.06) by conventional solid state reaction. The calcinations was at temperature (900ºC) for (3hr). The powder was sintered for (2–3 hr) within the temperature range (1050–1090 ºC). The resultant ceramic possesses orthorhombic symmetrical perovskite structure. The effect of (Li) substitution was discussed during the shifting in Curie temperature (T_C) and orthorhombic-tetragonal phase transition temperature. It was slightly to higher and lower temperatures respectively. The addition of (Li)was leading to high grain size and poorer density.

Kim *et al*,[26] prepared KN ceramic using conventional solid-state method. The powder was calcined at temperature (600ºC) for (4 hr) then reheated at temperature (1000ºC) for (4 hr) and sintered at temperatures (1020 and 1040◦C) for (0.5 ,1 ,2 and 6 hr). A porous microstructure was consisting a small grains in the formation of the KN ceramic that was sintered at (1020ºC) for (2 hr) or at temperature (1040ºC) for (0.5 hr). Specimens that was sintered at (1020◦C) for (6 hr) or at temperature (1040ºC) for (1.0 hr) exhibited a dense micro structure with a large relative density that was equivalent to 95% of the theoretical density. The KN ceramic was sintered at (1020ºC) for (6 hr) exhibited good dielectric and piezoelectric properties. There were a similar results obtained for the specimen sintered at (1040ºC) for (1hr).

Cheng *et al*, [27] fabricated $(0.99-x)K_{0.48}Na_{0.52}NbO_3-0.01B_{0.5}Na_{0.5}$ $TiO_{3\_x}Bi_{0.5}(Na_{0.7}K_{0.2}Li_{0.1})_{0.5}ZrO_3$ through typical solid state method. The strong dielectric, piezoelectric, and ferroelectric properties had been obtained in the ceramic with Rhombohedral–tetragonal (R–T) phase

transition. Then the ceramic possesses optimum electrical properties at (x=0.035) has an optimum electrical behavior (d_{33} = 310pC/N, P_r=23.4 $\mu C/cm^2$, E_C= 17.4 kV/cm, ε_r= 1249, tanδ= 0.025, and T_C=338 ^{o}C).

Li *et al*,[28], they prepared the KNN–BNZ–xZnO system (x=0, 0.01,0.02,0.03,0.04,and0.05) lead-free piezo-ceramics by the conventional solid-state method. The powder was calcinated at temperature (850^oC) for (6 hr). It was sintered at temperature (1090^oC) for (3hr). The obtainable phase structure was identified by both XRD patterns and ε_r–T curves. The ceramic with (x=0.01) was possessed a mixture of Rhombohedral–Orthorhombic and Orthorhombic–Tetragonal phase boundaries. The ceramic with (x=0.01) showed optimal electrical properties with a high (T_C) of about (320^oC). The ceramic with (0.01) of (ZnO) has possesses a higher (T_C) as compared with a pure one.

Acker *et al*,[29] they investigated the influence of high alkaline vapor pressure in the sintering atmosphere on the microstructure of sodium potassium niobate ceramic with alkaline/niobium ratios ranging (1.02 - 0.98).The densities were decreased for KNN with alkaline excess and stoichiometric KNN, whereas they were tend to increase for niobium excess material.

Wang *et al*, [21] they demonstrated a new band engineering strategy is necessary of the design of semiconductor perovskite ferroelectrics for photovoltaic and other applications from first principles. They studied a six ferroelectric solid solutions created by partially substituting Zn^{2+} for Nb^{5+} into the parent $KNbO_3$. The results showed there was a low band gap of about 2.11 eV for KN-SLZN (75% $KNbO_3$ - 25% $(Sr_{0.5}La_{0.5})$ $(Zn_{0.5}Nb_{0.5})$ O_3. There was also a decreasing in the energy gap value by (0.54–0.72 eV) due to strain effect, it was about (1% and 2%). This feature has a benefit in the developing a bulk photovoltaic energy conversion.

Rezaie *et al*,[30] used the streaming process for Electrode-less Electrochemical Deposition (SPEED) method to create complex thin-film structures like $[KNbO_3]_{1-x}[BaNi_{1/2}Nb_{1/2}O_{3-\delta}]_x$ mentioned by "KBNNO". The KBNNO has a relatively large polarization and could possibly produce high open-circuit voltages exceeding its bandgap. The KBNNO films have shown high absorption in the visible range with a good match of the solar spectrum. The fabricated KBNNO films also possess an excellent adhesion to the substrate surface. They were stable under a wide range of chemical, mechanical and thermal conditions, which makes them desirables in solar cell applications.

Mahesh *et al*,[31] synthesized $(K_{0.5}Na_{0.5})NbO_3$ (KNN) ceramics by solid state reaction method. The effect of calcination temperature on structural, microstructure and dielectric properties was investigated. The powder was calcined at different temperatures (600, 700, 800 and 900°C) for (5 hr). They were sintered at temperature (950 °C) for (5 hr). The phase transitions from orthorhombic to tetragonal was happened at temperature (165°C). The ferroelectric tetragonal to paraelectric cubic phase transition was happened at temperature (335°C). The prepared ceramic was exhibited a fine ferroelectric properties of remnant polarization and coercive field. They were (8.8°C/cm^2) and (11.01kV/cm) respectively.

Michael *et al*,[32] were fabricated and studied the characterization of lithium-doped KNN ceramic. It had been reported that the excellent piezoelectric properties for sample under study. The samples containing (0-9 mol%) Li were synthesized by a conventional mixed oxide method. The addition of lithium was found to promote the grain growth within the microstructure, causing a denser ceramic. A phase transformation from the orthorhombic to tetragonal crystal structure was also identified at temperature (200°C).

Chen *et al*,[33] were prepared lead-free piezoelectric ceramics (KNL-NTS, KN) by solid state reaction. The effect of sintering temperature on the structure, density and electrical properties of ceramics were investigated. The phase structure for both (KNL-NTS) and (KN) was Orthorhombic. The KNL-NTS ceramic was sintered at (1160 °C), it showed the maximum piezoelectric coefficient of about ($199pC \cdot N^{-1}$) and the maximum remnant polarization of (18.75 $\mu C \cdot cm^{-2}$), and the corresponding coercive field was about (10.95 $kV \cdot cm^{-1}$) and the density (4.74 g/cm^3).

Yang *et al*, [20] were fabricated a composite of the $KNbO_3$ nanowire and PDMS polymer in a volume ratio of (3:7).The $KNbO_3$ nano wire was synthesized by the hydrothermal method. The molecular ratio was about (0.63 mol) of KOH (35.3 g) that was dissolved in the (50 mL) of distilled water and then (1.24 mmol) of Nb_2O_5 (0.33 g) was added into the KOH solution. Thoroughly, the stirred solution was transferred to a stainless-steel autoclave with a (100 mL) Teflon was undergo a hydrothermal reaction at (150 °C) for (124 hr). The obtainable of white powder was further annealed at temperature (400°C) for (12 hr). The pyroelectric coefficient of the fabricated composite structure (the $KNbO_3$ nanowires and PDMS polymer in a volume ratio of 3:7) is about 0.8 nC/cm^2 K, which is smaller than the bulk of $KNbO_3$those were (5 nC/cm^2 K at 300 K).

Jinachai *et al*,[34]were synthesized (KN) powder under solvothermal conditions, with the use of mixed water-ethyl alcohol as the reacted medium. The influence of ethyl alcohol on particle shape and size, and the sintering condition of the synthesized powder was investigated. The density of KN ceramic was 95% from the theoretical value.

Song *et al*,[35] were prepared nano-crystal of ferroelectric $NaNbO_3$ by hydrothermal method. The compound of Nb_2O_5 was well dispersed in aqueous sodium hydroxide solution (25 mL) with magnetic stirring for (40

min). The mixture was then transferred to a Teflon-lined autoclave (50 mL). After several hours of reaction at selected temperatures, the resultant product was separated and washed neutrally by de-ionized water. Then it was dried at temperature (60^oC) for (24 hr). The NaOH and Nb_2O_5 concentrations have a remarkable influence on the sample morphology. The lower concentration of Nb_2O_5 is propitious to form $NaNbO_3$nanorods and nano-plates, while the lower concentration of NaOH facilitates is the formation of $NaNbO_3$ cubes. Both have a little effect on the crystalline structure of $NaNbO_3$. The Orthorhombic phase $NaNbO_3$ is more likely formed with lower ratio of $NaOH/Nb_2O_5$.

Kanie *et al*,[36] obtained the mixture of Potassium and Sodium Niobates fine particles with Orthorhombic crystal structures by hydrothermal reaction at (100^oC) for (24 hr) and ($150–250^oC$) for (3 hr)by using highly concentrated KOH or NaOH aqueous solution and a Niobium pent chloride aqueous solution. The preheating of the precursor solution at temperature (100^oC) for (24 hr) was played an important role to obtain the desired alkali metal niobate fine particles with flat and smooth surfaces. The present of potassium niobate fine particle was exhibited a good sintering property keeping with the original particle. The densities of the KN and KNN ceramics were reached to (4.07and 4.05 g/cm^3), at 1040^oC respectively.

Rubio-Marcos *et al*,[11]were studied the effect of stoichiometry and milling processes in the synthesis the pizo ceramic, the piezoelectric properties of KNN-modified nano-particles by solid state reaction. The system of (K, Na, Li) (Nb, Ta, Sb)O_3, KNN-modified, were synthesized by solid state reaction procedure. The mixtures of the components were calcineted at temperature (700^oC) for (2 hr). The sintering was carried out at temperature (1125 ^oC) for time duration (1 - 16 hr). The obtainable particles with particle size was ranging (50- 200 nm) as a function of the stoichiometry. The result of XRD was showed a tetragonal and

orthorhombic phases. The sintered samples were showed an improvement on the inhibition of abnormal grains growth and stabilization of the tetragonal symmetry.

Bruncková *et al*,[37]were prepared lead-free ferroelectric 2-layered $KNbO_3$ (KN) and $NaNbO_3$ (NN) thin films using modified sol-gel method. The prepared samples were deposited by spin-coating method on Pt/Al_2O_3 and $Pt/SiO_2/Si$ substrates, then sintered at (650°C). The produced particles of KN and NN thin films were observed and also the cross-section thickness of two layers was about (100 nm).

Wang *et al*,[38] were prepared $KNbO_3$ nano rods by hydrothermal synthesis at (180ºC) in a KOH solution using sodium dodecyl sulfate surfactant for (24 hr).The nanorods were (100–300nm) in diameter, up to (5 mm)in length. The phase transition temperatures from the orthorhombic to tetragonal and tetragonal to cubic transition of the nanorod were about (190, 400 º C) respectively. It had lower than that of the bulk $KNbO_3$ materials due to finite size effect or disorder.

Paula *et al*,[39] were synthesized $KNbO_3$ nanostructures through the reaction between Nb_2O_5 and KOH under microwave-assisted hydrothermal synthesis. The obtainable result was showed that it was a very fast synthesis in producing of single phase powders. The reaction between KOH and $Nb_2O_5$was carried out in a Teflon vessel model in a microwave system operating at frequency (2.45 GHz) with an output power of (300 W). The synthesis was carried out at temperature (200 °C) for different periods and the pressure inside the vessel increased to (150 PSI) for different periods (1, 2, 4, 8 and 12 hr). The $KNbO_3$ nanofinger were about (200 nm) in diameter was obtained after (1, 2 and 4 hr) of reaction.

Li *et al*,[15] were synthesized the Potassium niobate ($KNbO_3$) powders by hydrothermal method in supercritical water. The potassium hydroxide(KOH) concentration was employed in the synthesis reaction can

be greatly reduced (0.1-0.5M). It was far less than the very high concentration prerequisite to the hydrothermal synthesis of $KNbO_3$ powders in subcritical water. The $KNbO_3$ powders prepared in supercritical water have Rhombohedral and orthorhombic structures depending on the alkaline concentration.

Bomlai *et al*,[40]were prepared a Sodium potassium niobate (($Na_{1-x}K_x$)NbO_3) powder with (x = 0.2, 0.4, 0.6 and 0.8)by a solid state reaction. It was found that the high calcination temperature and long dwell time clearly favored particle growth and the formation of large and hard agglomerates. The results were showed that the presence of Orthorhombic phase structure. The result shows that large particle size, cubic shape and a low calcination condition were observed in ($Na_{1-x}K_x$) NbO_3 powder with low K_2CO_3 content (x = 0.2).

Hsiao *et al*,[41] were synthesized a bulk ceramic of composition $NaNbO_3$.The mixture of raw materials were pressed and sintered into ceramic pellet without the calcination stage involved. The $NaNbO_3$ phase was obtained at sintering temperatures of (1100–1200◦C). The maximum linear shrinkage and minimum porosity percentage of the $NaNbO_3$ was (22.9 and 1.6%) at temperature (1200 ◦C). Some rhomb-shaped grains in pellets did not occur until it got higher atomic mobility sintered at temperature of (1200 ◦C) for (3 hr). The growth mechanism of rhomb-shaped grains might be had a potential application in crystal growth and other crystallography.

Pribošič *et al*, [42]were prepared the composition of $KNbO_3$ (KN) and $KNbO_3$-$BaTiO_3$ (KN-BT) as a solid solution by the Polymerised Complex Method (PC method).The calcination was at temperature from (460 to 900°C). The SEM-images of the KN powder calcined at (900ºC) was showed a strongly agglomerated .Those were composed of smaller nano-sized particles.

Rojac *et al*, [43]were synthesized NaNbO$_3$, KNbO$_3$ and K$_{0.5}$Na$_{0.5}$NbO$_3$. The starting materials were mechanochemically treated for (10, 20 and 40 hr). They had been shown that NaNbO$_3$ can be prepared by a single-step mechanochemical synthesis after (20 hr) of high-energy milling. The mechanochemical reaction between (K$_2$CO$_3$ and Nb$_2$O$_5$) does not occur even after (40 hr) of milling. Similar observations were noticed for the (Na$_2$CO$_3$, K$_2$CO$_3$and Nb$_2$O$_5$) mixture.

Goh *et al*,[44]were synthesized (KN and KNN) powders by using hydrothermal method using KOH and NaOH solutions (6.7–15 M) at temperature (150 and 200 °C).The Orthorhombic phase structure of NaNbO$_3$ powder was hydrothermally synthesized at temperature(200°C) by (8.4 M) of NaOH solutions and (0.25 M) Nb$_2$O$_5$ powder. The Orthorhombic phase structure of KNbO$_3$powder obtained by the reaction between Nb$_2$O$_5$ (0.0015–0.38 M) and KOH solutions with different concentrations in the range (6.7–15 M) at temperature (150 and 200°C).

Sundarakannan *et al*,[45] were prepared Potassium niobate ceramics by the conventional solid state reaction. The dielectric and conductivity measurements were carried out on the potassium niobate ceramics bot has a function of temperature range (50 - 550 °C) and frequency range (10^2-10^{6}Hz).A low-frequency dielectric relaxation in the temperature range of (100 to 200 °C)was observed and analyzed with the Cole–Cole function. The activation energy of dielectric relaxation was estimated to be (0.84 eV).

Yun *et al*,[46] were synthesized Sodium niobate (NaNbO$_3$) powder high-energy milling of commercially available Na$_2$CO$_3$ and Nb$_2$O$_5$ powders. The starting powders were loaded in a high-energy shaker mill with a cylindrical ZrO$_2$ vial of (52 mm) length and (38 mm) inner diameter and ZrO$_2$ of (10 mm) diameter or WC milling balls of (11 mm) diameter. A high-energy milling apparatus used higher collision energy compared to

a planetary mill or an attrition mill. For the milling, the ball-to-powder ratio (BPR) was (30: 1) and the milling time from (10 to 300 min). Also ($NaNbO_3$) was prepared by solid state reaction for comparison. The powder was calcinaed at temperature (850 ^{o}C) for (5 hr). SEM images showed that the size of particles for the prepared powder is (100 to 600 nm), while the mechano chemically synthesized powder consists of agglomerates of small crystallites of (10–20 nm) size. The results showed that the time required for powder synthesis decreased as the density of balls increased.

1.9   The aims of this work

The literature review that was made on the $K_{1-x}Na_xNbO_3$ system led to have a huge knowledge before the starting of project. The main purpose of this research is to find the ability of the system mention above to applied as a solar energy harvester. The present work is summarized in the following points:

1- Preparation of Potassium Sodium Niobate ($K_{1-x}Na_xNbO_3$) for (x=0, 0.5 and, 1) by using the method of Solid State Reaction (SSR), in order to study the effect of (x) on the physical meaning between the compounded.

2- Studying the structural properties of the resultant Potassium Sodium Niobate (crystal structure, particle size) and using special software and databases.

3- Studying the effect of substitutions factor (x) on some physical properties of KNN system such as Curie temperature, dielectric constant, density, crystal structure, lattice parameters, energy gap and refractive index.

4- Studying the effect of sintering temperature of the system for (x=0) on some physical properties such as Curie temperature, dielectric constant and the density.
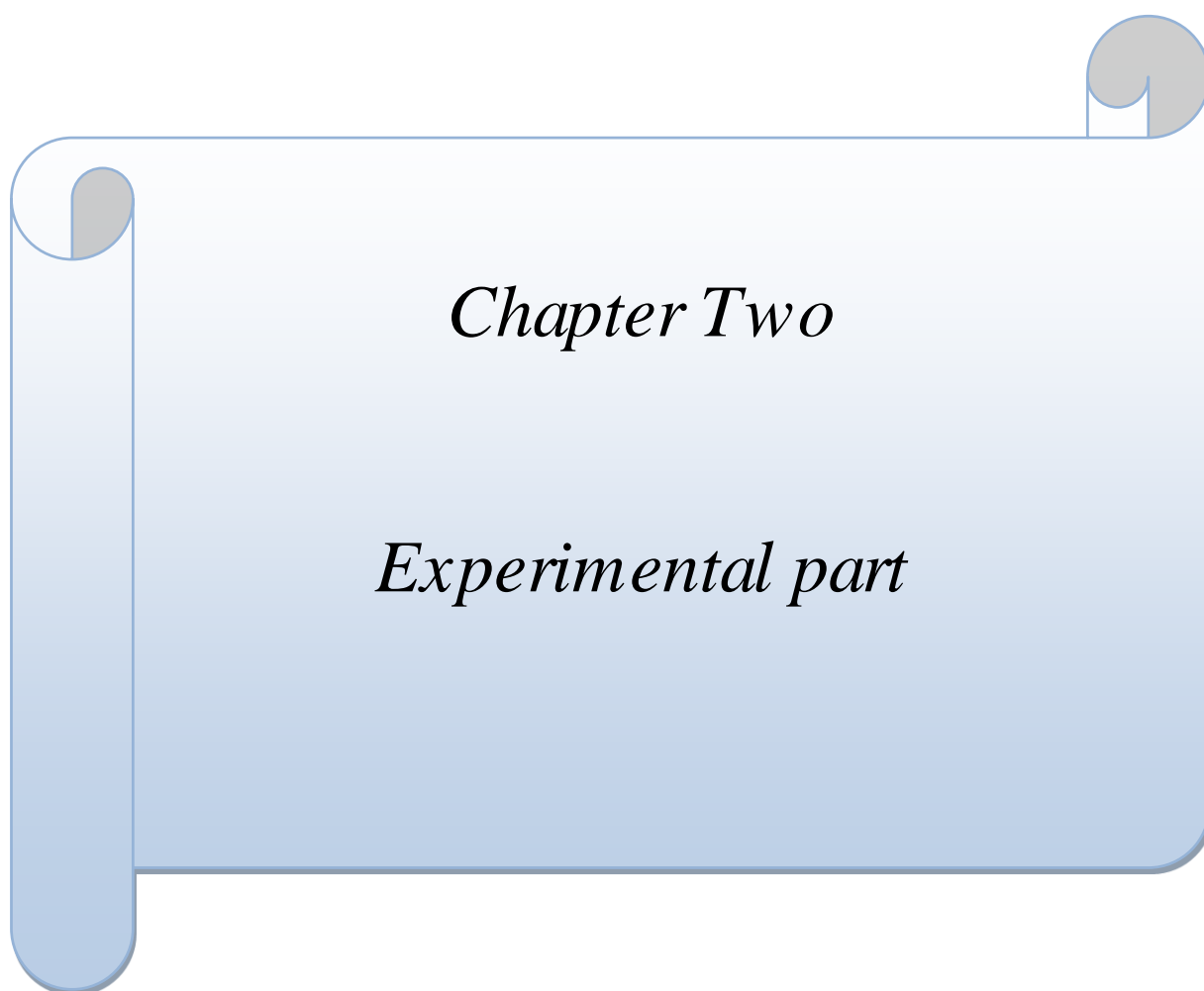
Chapter Two

Experimental part

2.1   Introduction

This chapter is dealing with techniques, and materials those were used to perform the plan of this project. It is also dealing with the specification of the equipment those were used in comparable with others were used globally. In the beginning, it is necessary to give more details about the sample preparation. The conventional method is the technique used which represented by solid state reaction (SSR).

2.2   The preparation condition of $K_{1-x}Na_xNbO_3$

In the beginning it was started the preparation condition at (x=0), by using Niobium pentoxide (Nb_2O_5) with Potassium carbonate (K_2CO_3) with a suitable ratio according to the following chemical equation.

$$\frac{1}{2}Nb_2O_5 + \frac{1}{2}K_2CO_3 \rightarrow KNbO_3 + \frac{1}{2}CO_2$$
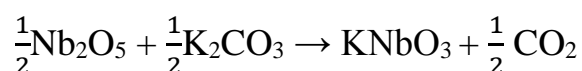
The sensitive balance with 4-digits is required to investigate these ratios. Then the powders were mixed together by using agate morter. The mixture should be homogenized by adding a sufficient quantity of high purity 2-propanol to form a past with a long period of grinding. The mixture was dried in the oven at temperature (100^oC) for (1 hr). This process is might by repeated many times to ensure the homogeneity. Later, the dried powder was calcined at temperature (700^0C) for (5 hr) to get ($KNbO_3$) powder, using a heating rate of ($350\ ^oC/hr$). Then cooling to room temperature is applied with a cooling rate of ($350\ ^oC/hr$) for the mixture. The phase formation was happened after the completely removing of CO_2 from the mixture.

The second sample was prepared with the substitution ration (x=0.5). The mixture ($K_{0.5}Na_{0.5}NbO_3$) was prepared by using Niobium pentoxide

(Nb_2O_5) with Potassium carbonate (K_2CO_3) and Sodium carbonate (Na_2CO_3) according to the following chemical equation.

$$\frac{1}{2}Nb_2O_5 + \frac{1}{4}K_2CO_3 + \frac{1}{4}Na_2CO_3 \rightarrow K_{0.5}Na_{0.5}NbO_3 + \frac{1}{2}CO_2$$
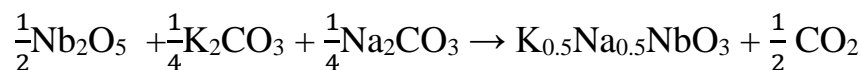
The powders were mixed together by using agate morter, the homogenized of the mixture is applied by regrinding with 2-propanol to form a past. The mixture was dried in the oven also and then calcined at temperature (700^0C) for (5 hr) with the same rate of heating and cooling to get ($K_{0.5}Na_{0.5}NbO_3$) powder. The amount of CO_2 is measured before to ensure the completely evolve of CO_2 from the mixture during the long heating.

The third concentration is at (x=1), it is prepared by using Niobium pentoxide (Nb_2O_5) with Sodium carbonate (Na_2CO_3) with a certain ratio according to the following chemical equation.

$$\frac{1}{2}Nb_2O_5 + \frac{1}{2}Na_2CO_3 \rightarrow KNbO_3 + \frac{1}{2}CO_2$$
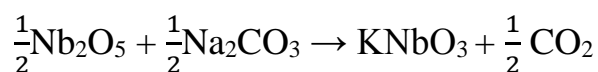
Then the powders were mixed together by using agate morter to ensure a homogenized powder as mention before. The dried powder mixture was calcined at temperature (700^0C) for (5 hr) to get ($NaNbO_3$) powder with the same value of heating and cooling rate.

Later, the pressing technique that has been applied to produce a pelletized shape before the sintering. The condition for this process is required a fine and homogenous powder for the pressing. It is a mechanical process used to press the powder into a pellet shape in order to reduce the vacancies and porosity between the particles under high temperature and long period of heating. There will be a shrinking in the size by packing the particles to each other. The pressing is considering very important step to

complete the sample preparation and produce the pellets shape samples for LCR measurements. This process is done by using a suitable electrical press and die. The powder after calcinations was putting in the die with diameter of (1.6cm) that was designed in solid state laboratory; as shown in figure (2-1). The powder is pressed using CARVAR electrical press at pressures, (150 MPa). The resulted pellet is subjected to sintering stage later.

Fig. 2.1:The die used for pressing the powders.

Finally, the sintering process is essential to investigate the dense sample. That is achieve by high temperature applied. The output of sintering stage is appeared clearly on the microstructure and physical properties on the product. During the sintering of a compacted powder, the densification and grain growth occur simultaneously through atomic diffusion mechanisms[47].

An atomic diffusion produces joining the particles and reduction the porosity [48].

The samples were sintered at different temperature, Table 2-1: shows the sintering temperature.

Table 2-1: Calcination and sintering temperature for the system $K_{x-1}Na_xNbO_3$.

Value of (x)	Calcination temperature (^{o}C)	Sintering temperature (^{o}C)
0	700	900
0	700	950
0	700	1000
0	700	1050
0.5	700	1000
1	700	1000

The rate of heating and cooling is very necessary in the sintering stages. It is clear that the heating rate was (100 ^{o}C/hr) until it reaches the desirable of sintering temperature. The long duration about (5 hr) of heating is preferable to make cohesion between the grains and reducing the prose size. The cooling to room temperature with cooling rate (100 ^{o}C/hr). It is suitable to rearrangement the atoms with the initial position in the unit cell so the slow cooling rate is favor for this stage.

2.3 Density estimation

Practically the density for all sintered samples is estimated according to geometrical shape , and calculated according to the following equation[48].

$$\rho = \frac{W}{Thickness \times Area} = \frac{W}{V} \qquad (2.1)$$

Where ρ = density (g/cm^3), W = mass of the sample (g), V= volume of the sample (cm^3).

2.4 Structural properties

After the successive preparation for the samples under study of the system ($K_{1-x}Na_xNbO_3$). The structural properties of the prepared samples

were done by using the X-ray diffraction analysis. That was carried out at room temperature. The lattice parameters was estimated according to the software that is constructed principally on Bragg and d-spacing laws as shown in the following equations [49]

$$n \lambda = 2d\sin \theta \qquad (2.2)$$

$$d = \frac{1}{\sqrt{\dfrac{h^2}{a^2} + \dfrac{k^2}{b^2} + \dfrac{l^2}{c^2}}} \qquad (2.3)$$

Where n = diffraction order, λ = wavelength of the XRD diffractometer, d= interplane distance, (a, b and c)= lattice constant and θ = diffracted angle.

The analysis was performed using XPowder v. 2004 software[50]. The second one was Refine95[51] for cell refinement. While crystallite sizes estimated from Scherrer equation[52]

$$L = \frac{K\lambda}{\beta.\cos\theta} \qquad (2.4)$$

Where λ = wavelength of the XRD diffractometer, K is a constant, β =Full width at half maximum of the peak.

2.5 The dielectric measurements

The study of dielectric properties for the samples was done experimentally by using the following set up mentioned by Fig. 2.2. The apparatus LCR is required for dielectric measurement using   TEGAM-

3550 LCR-meter at 5V. The pellet was placed in a suitable testing cell for dielectric measurement under high and low temperature with vacuum as shown in Fig.2.2. In this setup, there is a possibility to change the frequency applied but the temperature is fixed.

The changing of applied frequency from (42Hz - 5 MHz) with irregular steps at constant temperature. There is ability to calculate the capacitance(C) with loss tangent (D) experimentally and then define the dielectric properties. On the other hand, the temperature variation within the range (50-500 °C) at constant frequency (10 kHz, 100 kHz, and 1 MHz) is a suitable to define the phase change. The determination of dielectric constant during the estimation of the capacitance (C) with loss tangent (D) under the phase change condition.

Fig. 2.2: The setup of dielectric measurement

The refractive index also calculated from the LCR measurement with changing the frequency for the sample [(x=0 and TC =1000°C), (x=0.5) and , (x=1)]by using the flowing equation**[53]**

$$n = \sqrt{\varepsilon_r} \qquad\qquad (2.5)$$

2.6   Scanning electron microscope (SEM)

A scanning electron microscope (SEM) is a technique used to see the morphology of sample surface. The images of the sample were done by scanning the surface morphology. That is produced to give information about the grains and grains boundaries represented by the size of the grain. It is also used to predict the nanostructure appeared in the composite prepared during the obtainable results of grain and grain boundaries. The device that was used is the model Inspect S 50 SEM.

2.7   Energy gap measurement.

The calcinated powder of the system ($K_{1-x}Na_xNbO_3$) with (x=0, 0.5, and 1) was tested by using the spectrophotometer type SHIMADZU UV-1601PC UV-Visible. The thick films were prepared on the glass substrate with PVC-slab (PVC 70-24) taking into the account the ratio of PVC to the film prepared is (20:1). The PVC-slab on the glass is useful to make the adhesion of the film is simply. The spin coating technique was used to prepared the thick films for the solution of the mixture with 2-propanol. The optical band gap of the specimens was calculated by Kubelka–Munk method, using Tauc relation depending on the possible technique for the transition during the direct or indirect optical energy gap[54] .

$$(\alpha h\nu)^{1/n} = A\,(h\nu - E_g) \qquad\qquad (2.6)$$

in which α, ν , A, and E_g are absorption coefficient, light frequency, proportionality constant, and optical energy gap, respectively .In this relation n is chosen [(1/2) and (3/2)] for the specimens having direct transition and [(2) and (3)] for indirect transition. The plotting $(\alpha h\nu)^{1/n}$ versus (hν- E_g) can be estimated from the intersection of the tangent with the x-axis in order to determine the optical energy gap.

The refractive index for the system ($K_{1-x}Na_xNbO_3$) with (x=0, 0.5, and 1)was calculated using the flowing equation [55] :

$$n = \left(\frac{1+R}{1-R}\right) + \sqrt{\frac{4R}{(1-R)^2} - K^2} \qquad (2.7)$$

Where R is reflectance and K is the extinction coefficient.

Chapter Three

Results and Discussion

3.1 Introduction

During the performance of the project plan on such type of the ferroelectric material, which are apply in the solar harvesting energy system. Many successive samples were prepared like Potassium Niobate, Potassium Sodium Niobate and Sodium Niobate was prepared using solid state reaction method (SSR). The XRD analysis was used for determination of crystal structure (lattice parameters, crystallite size and space group) by using different software. The scanning electron microscope (SEM) is useful to determination the shape and size of grain and grain boundaries. LCR-measurement was done to determine the dielectric properties and Curie temperature for the phase transition with different frequency and temperature. The UV-Visible spectrophotometer was applied to find the band gap and the optical refractive index.

3.2 Density estimation

The density for the sintered samples is play an important role in the property of ceramic. The method was used for measuring the density is applied on the geometrical method. It is clear that there is a variation in a density of the samples between theoretical and experimental values as shown in Table 3-1. This variation is depending directly on different parameters, such as the particle size and sintering temperature. It is clear that the high value of (T_S =1000 ^{o}C) showed high density at a compacted press (P=150MPa).

Table 3.1: Indicate the density for different samples of the system $K_{1-x}Na_xNbO_3$.

Value of (x)	Sintering temperature (^{o} C)	Geometrical Density (g/cm^3)	Theoretical Density (g/cm^3)	Compactness (%)
0	900	2.24	4.62[56]	48.50
0	950	2.48	4.62[56]	53.67
0	1000	3.06	4.62[56]	66.23
0	1050	2.4	4.62[56]	51.94
0.5	1000	2.607	4.51[57]	57.80
1	1000	2.49	4.42[36]	56.33

It was clear that the density, of the sample with (x=0), was increased with increasing the sintering temperature of a compacted powder. The maximum value was recorded at (T_S=1000 ^{o}C). The densification and grain growth occur simultaneously through atomic diffusion mechanism. The density of the sample at (x=0) that was sintered at (1050 ^{o}C) showed a decreasing as a function of increasing the sintering temperature because this temperature might be approach to the melting point and start to liquid phase change. That is attributed to the big grains consuming the smaller grains, causing increasing in the porosity leads to lower density[58].

The density for the samples at (x=0, 0.5 and, 1) was decreased respectively at constant (T_S=1000 ^{o}C). This decreasing is agreement with the behavior of the theoretical values as a function of (x). The reason is related to insertion of of (Na^{+1}-ions) with respect to (K^{+1}-ions). There is a difference in the ionic radius is represented by (K^{+1}) radius = 1.33 Å and (Na^{+1}) radius= 0.95 Å [59].

3.3   XRD analysis (K $_{1-x}$Na$_x$NbO$_3$) system

The XRD is an important technique to determine the structural properties (crystal structure, lattice parameter, crystallite size and space group) of materials. The prepared samples were subjected to XRD diffractometer as mentioned in chapter two. XRD software were used to determine the structural properties of the prepared samples. The XRD pattern for (K $_{1-x}$Na$_x$NbO$_3$) with (x=0, 0.5, and 1) which has crystalline phase as shown in Fig. 3.1 ,3.2 and, 3.3.
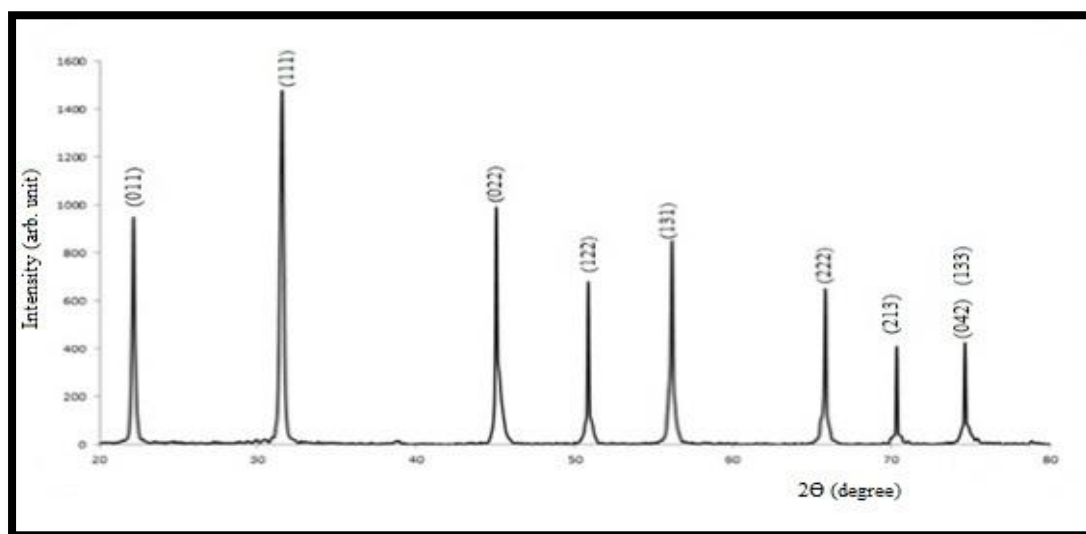

Fig. 3.1: X-ray diffraction patterns for KNbO$_3$

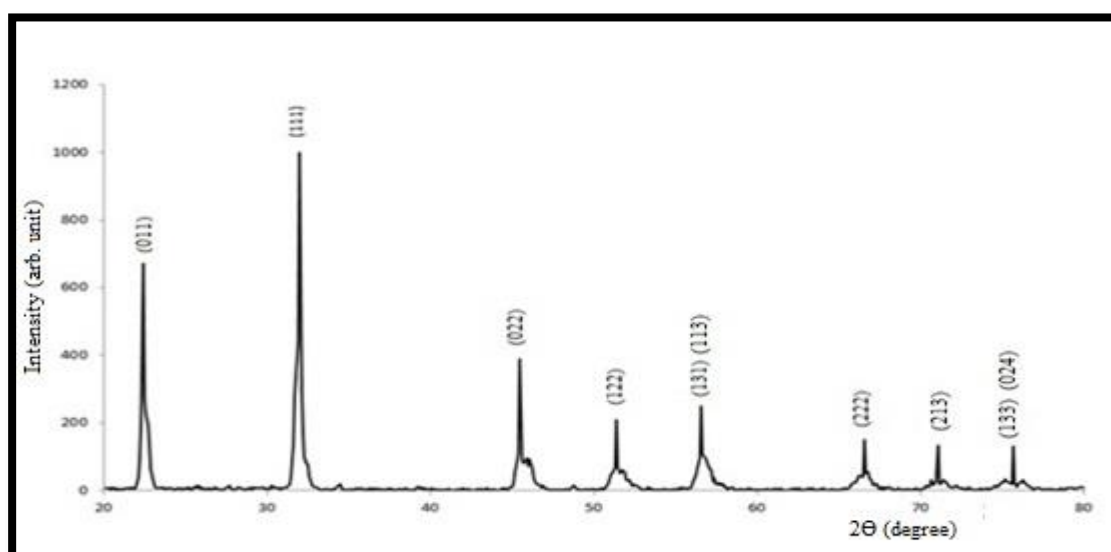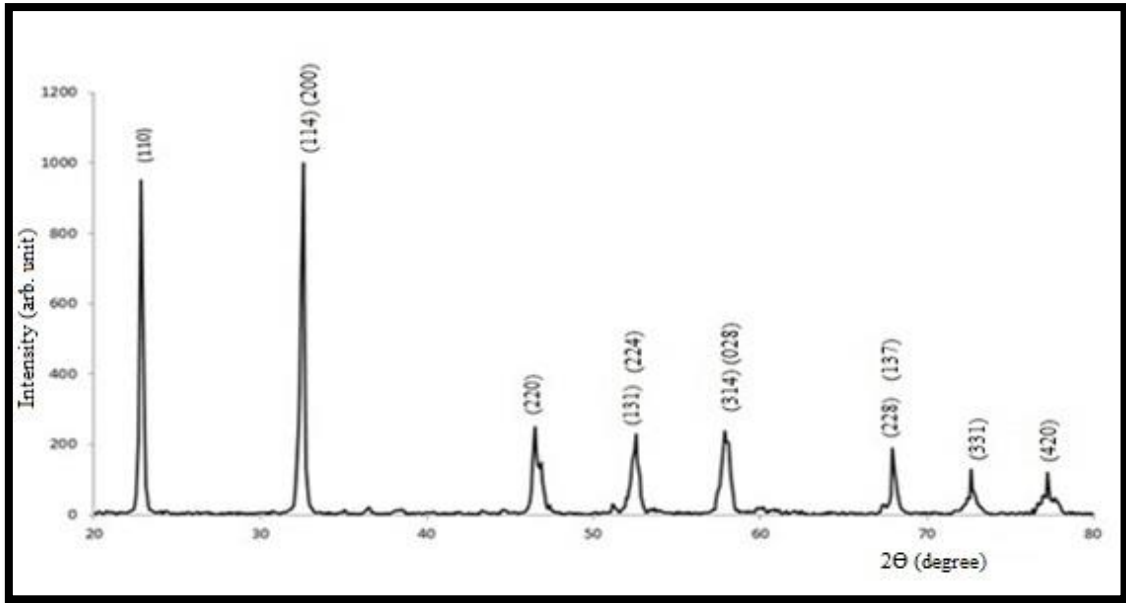Fig. 3.2: X-ray diffraction patterns for K$_{0.5}$Na$_{0.5}$NbO$_3$

Fig. 3.3: X-ray diffraction patterns for NaNbO$_3$

The XRD pattern for KNbO$_3$ as shown in Fig 3.1 the highest intensity peaks are mentioned by 2Θ (22.15, 31.5 and, 45) respectively. Normally, the high intensity of XRD-peaks means the presence of high concentration of these miller planes within the unit cell. The peak is mentioned at (2Θ = 74.65) has two miller indices. They are coinciding at the same angle. These data was comparable with XRD database(71-0946)from International Center for Diffraction Data (ICDD)[60]for KNbO$_3$. Regarding to the composition K$_{0.5}$Na$_{0.5}$NbO$_3$, the XRD-pattern is showed the appearance of all peaks mentioned in XRD-pattern for the composition KNbO$_3$, in comparable with XRD database(230-0499)crystallography open database from International Union for Crystallography (IUCr)[61],except the miller indices (042) that was disappear as shown in Fig(3.2).

The insertion of Na-ions in the unit cell tend to decrease the intensity of all peaks are decrees to about half value of pure one. That mean the density of these planes will decreased in the structure of K$_{0.5}$Na$_{0.5}$NbO$_3$ in spite of their presents. This decreasing is due to the replacement of (Na-ions) in the structure instead of (K-ions). In general, there is a limited increasing of

41

(2Θ) for the system at (x=0.5) in comparable with (x=0). This is the main reason for the partial variation of lattice constant calculated. The presence of all peaks are common is the meaning to remaining phase with the same bonds.

Just, there is appearance of (2Θ=56.55) $K_{0.5}Na_{0.5}NbO_3$ structure related to miller indices mentioned by (113) and (131) in comparable with pure component. This is possible because both are belonging to the set [313]. That is related to the insertion of Na-ions with respect to K-ions.

The results of XRD pattern for $KNbO_3$ was exhibited an Orthorhombic phase with space group (Amm2) and lattice constant (a =3.994 Å, b= 5.676 Å, c = 5.695 Å) , (α = β =γ = 90) and unit cell volume (128.92 $Å^3$).These results is comparable with the previous one published by Pribošič *et al*, they found that the $KNbO_3$ with Orthorhombic phase with lattice constant (a = 3.983 Å, b = 5.696 Å and c = 5.709 Å) [42]. Kittichai *et al*, found that the $KNbO_3$prepared by Solvo-thermal method has an Orthorhombic phase with lattice constant (a= 3.982-3.984Å, b=5.689-5.695 Å ,and c= 5.721-5.737Å) [34].

The results of XRD pattern for $K_{0.5}Na_{0.5}NbO_3$ was exhibited an Orthorhombic phase, with space group (Amm2) and lattice constant (a =3.961 Å, b =5.613 Å, c =5.621 Å) , (α = β = γ = 90) and unit cell volume (125.0$Å^3$).Zhuang[22] , Mahesh[31] and , Jenko [57] also found that the $K_{0.5}Na_{0.5}NbO_3$ has Orthorhombic phase.

The XRD pattern for $NaNbO_3$ as shown in Fig 3-3 in comparable these data was comparable with XRD database (73-0803)from International Center for Diffraction Data (ICDD)[60].The highest intensity peaks are mentioned by(2Θ) (22.85, 32.55 and, 46.45) respectively. The corresponding miller indices have high concentration of these peak in the structure regard to completely replacement of Na-ions. The other peaks that belong for $NaNbO_3$ structure are mentioned by (2Θ) (22.85, 32.55,

46.45, 57.85, 67.95, 72.65 and, 77.25) respectively. A thing was notice from the data concluded represented to the appearance the coincidence of many miller indices with the same value of (2Θ). That is possible for two reason, the first is regarding to the presence of two overlapping peaks with same value of (2Θ). Secondly, the completely insertion of Na-ions will make a new orthorhombic phase that was simulated.

The results of XRD pattern for $NaNbO_3$ was exhibited Orthorhombic phase with space group (Pbcm) and lattice constant (a = 5.523 Å, b = 5.564 Å, c = 15.59 Å), ($\alpha = \beta = \gamma = 90$) and the unit cell volume (480.57 Å^3). Bomlai has also Orthorhombic phase for$NaNbO_3$[40]. Mishra results showed that the $NaNbO_3$ with Orthorhombic phase and space group (Pbcm) [62].

The system with (x=1) is completely different from the other values of (x= 0 and 0.5) and different the space group but all of them are exhibited Orthorhombic phase but the difference is appearing in the rearrangement of atoms in the structure. So the difference in symmetry and redistribution for the atoms in the unite cell, is just the reason for the different (hkl) appear in the $NaNbO_3$.

The complete results those were concluded from XRD-analysis as shown in (Table 3-2). It was clear that the sharp increasing in the lattice parameters (a, c) with slightly decreasing of b-axis. That means the effect of Na-ions insertion is more clear. On the other hand, there is a sharp increasing in the volume of the unite cell as a function of (x). That is agreement with the result of density calculation, as mention before. The inversely proportional of the volume with density was a good tool to emphasize the result of XRD and their behavior as shown in Table 3-2. The crystallites size of the powders was about (14, 14.459 and 17.09 nm) for x= 0, 0.5 and 1 respectively.

Table (3-2): Variation of a, b, c (lattice parameter), and unite cell volume for the compounds $KNbO_3$, $K_{0.5}Na_{0.5}NbO_3$ and $NaNbO_3$.

Formula	a (Å)	b (Å)	c (Å)	Unit cell volume($Å^3$)	System
$KNbO_3$	3.994	5.676	5.695	128.92	Orthorhombic
$K_{0.5}Na_{0.5}NbO_3$	3.961	5.613	5.621	125	Orthorhombic
$NaNbO_3$	5.523	5.564	15.59	480.57	Orthorhombic

3.4 Scanning electron microscope (SEM)

It is considering a good tool to investigate the morphology of the surface and its homogeneity for the sample under study. The first group analyzed of photo is related to the effect of sintering temperature on the producing of the ($KNbO_3$) sample as mention in (Figs. 3.5 – 3.7). The effect of sintering is well defined by different value of (950 – 1000 – 1050 ^{o}C). It is clear that the appearance of grain size with a diameter range of about (2-5 μm). It seems that there is a homogeneous in the shape of grain. The cohesion between the grain is well define producing a big grain as shown in (Fig. 3.5). The effect of sintering temperature (1000°C) is well define in (Fig. 3.6). It is clear that there is state to produce a single crystal with small size and large size in the range (1-2μm) for small one. The large is well define of about (5-12μm). The large single crystal is return to the accumulation of small crystals. This result is return to success the sample preparation of ($KNbO_3$). Whereas the increasing of sintering temperature at (1050 ^{o}C) has a direct effect on the enhancement of producing of single crystal from the polycrystalline one as shown in (Fig.3.7). There is approaching and homogeneity in the size of single crystal producing rather than the sample prepared by (T_S=1000°C). It is clear the size of crystal

producing is about (1-3 μm). Another thing, the distribution of single crystal producing is more familiar and homogeneity rather than the sample prepared by (T_S=1000°C).
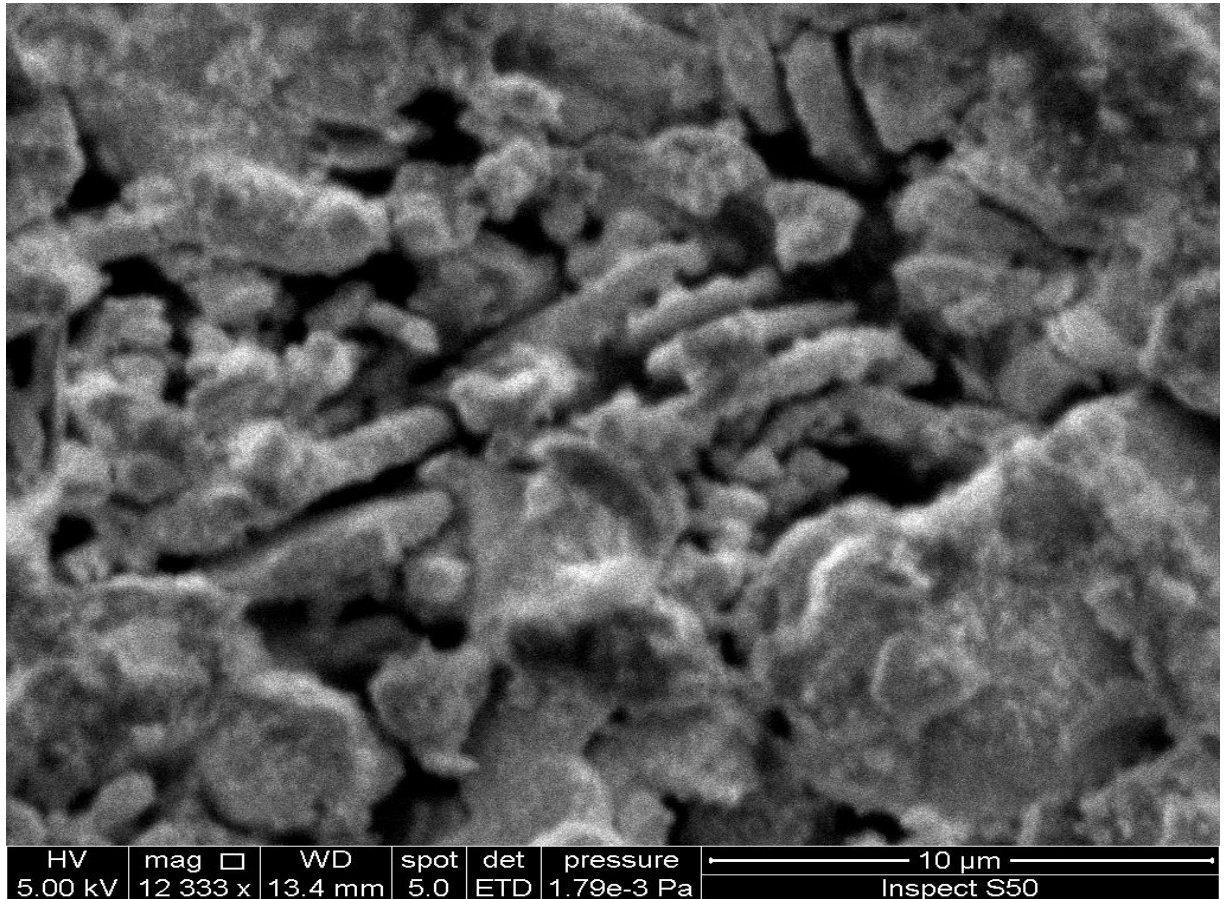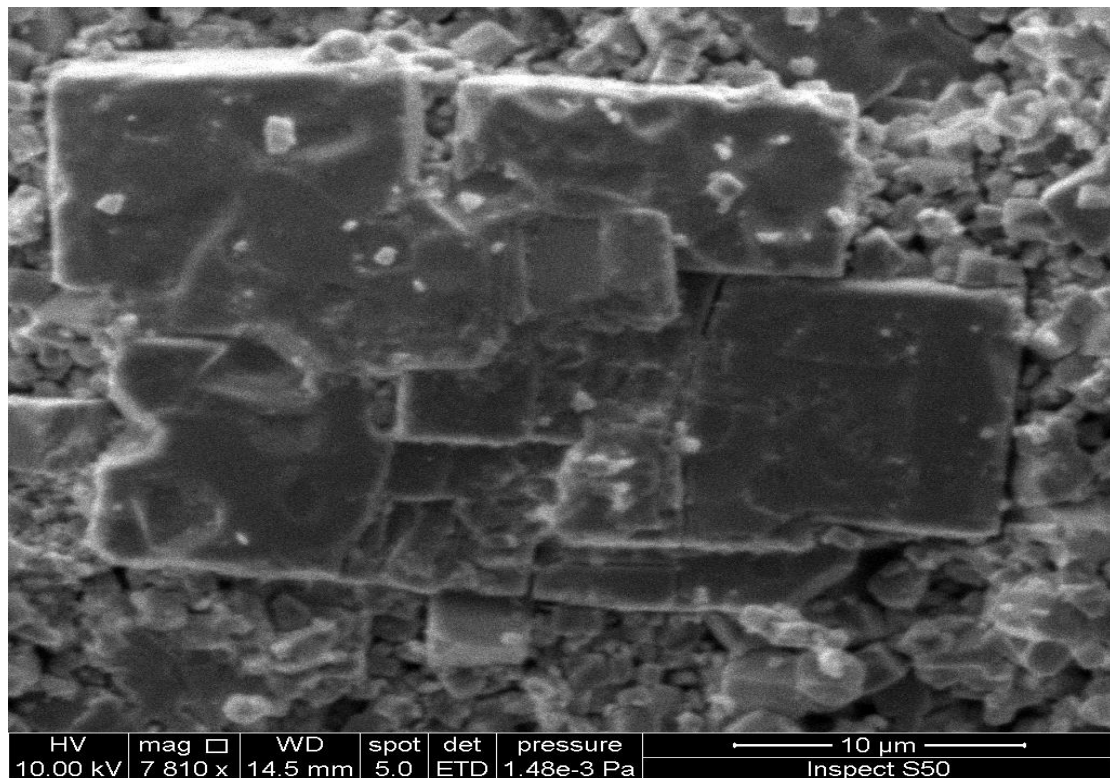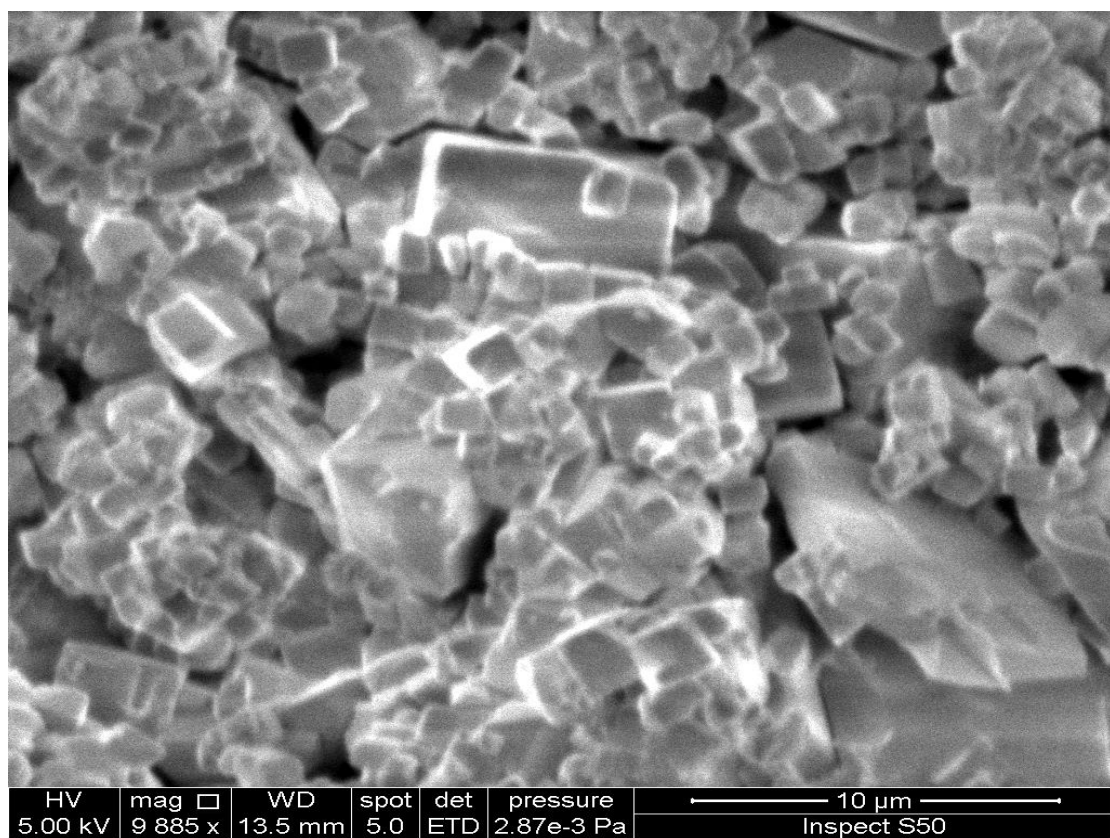

Fig. 3.4 SEM micrograph of $KNbO_3$ sample (T_S=950 °C)

Fig. 3.5 SEM micrograph of KNbO$_3$ sample (T$_S$=1000 ^{o}C)

Fig. 3.6 SEM micrograph of KNbO$_3$ sample (T$_S$=1050 ^{o}C)

Later, the SEM-photo is taken into account the effect of substitution of Na-ions with respect to k-ions at a constant sintering temperature (1000 ºC) as shown in (Fig. 4-6). There is start to producing of single crystal with different size of about (1-2 μm) for the sample ($KNbO_3$) as shown in (Fig. 3.7). The producing of single crystal from polycrystalline is still continues by the effect of substitution by Na-ions as shown in (Fig. 3.8). The size of single crystal is also in the range (1-2 μm) with small crystal created and homogeneity. The producing of small crystal size in ($NaNbO_3$) sample is appeared more and more in comparable with the previous one as shown in Fig. 3.9. The thing notice that the size of crystal producing is in the size small than (1μm) for homogeneous grain distribution. These results are in good agreement with that calculated from XRD where the fact of the synthesized powder consists of agglomerates of small crystallites[63].
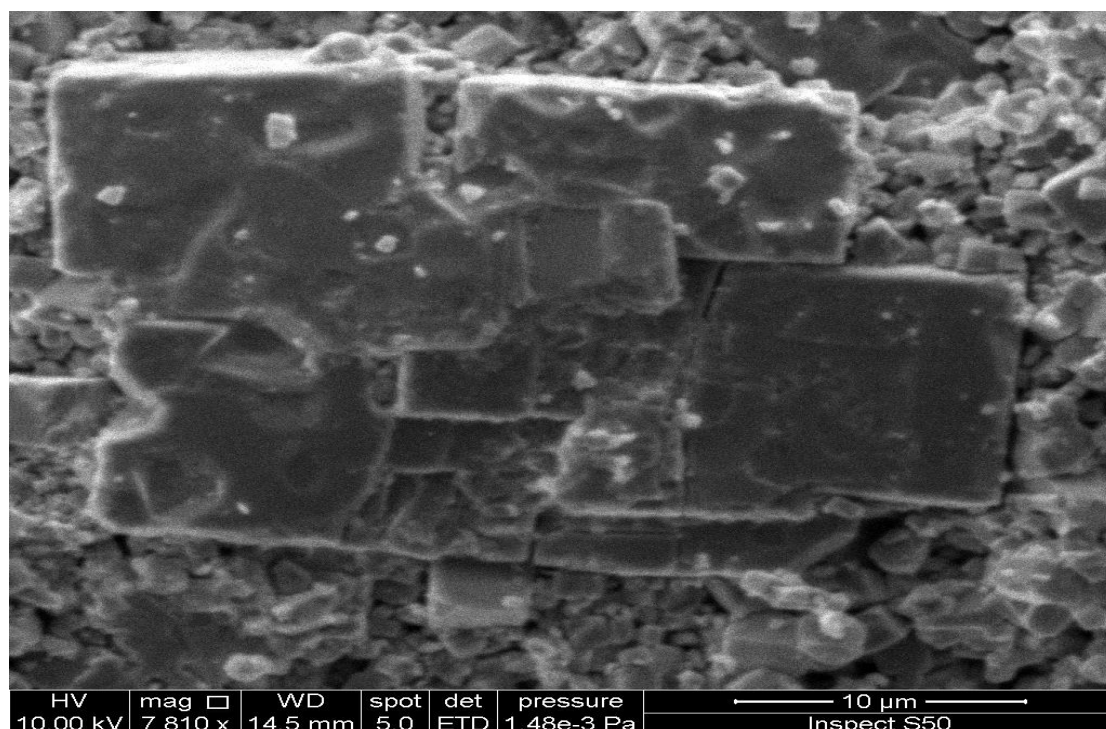

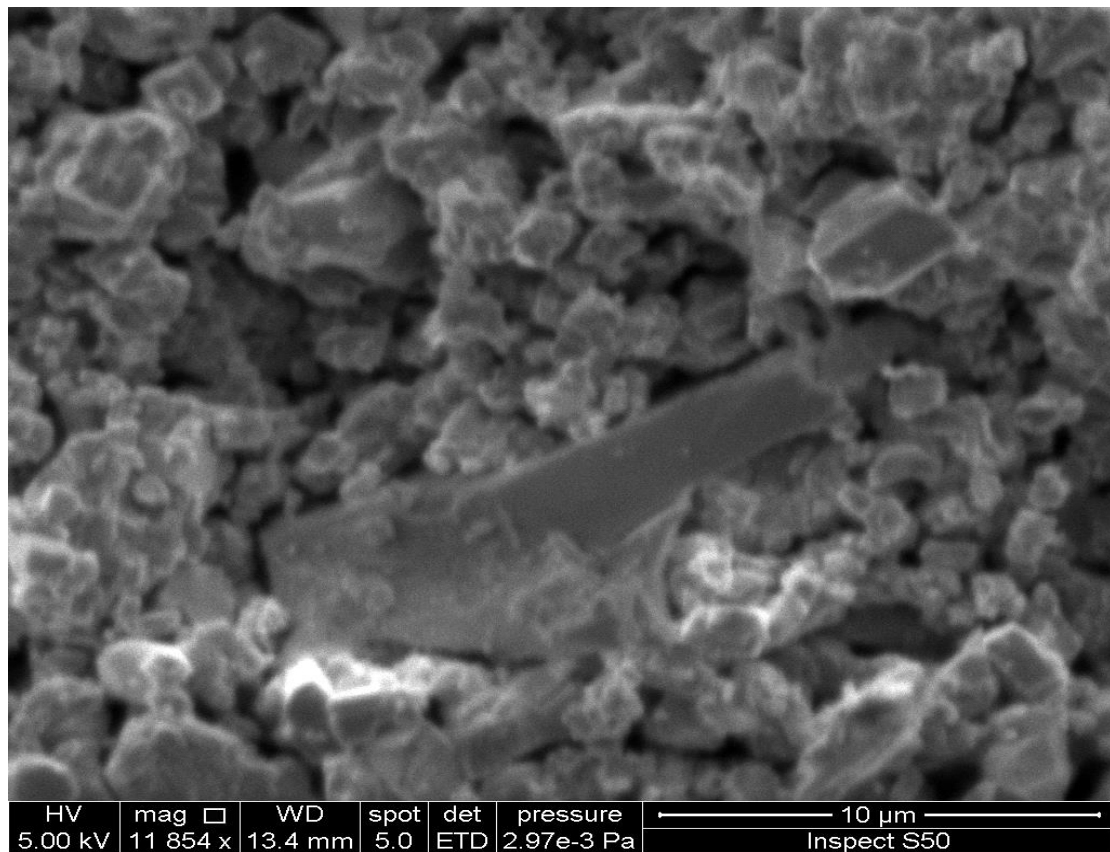| HV	mag □	WD	spot	det	pressure	10 μm
10.00 kV	7 810 x	14.5 mm	5.0	ETD	1.48e-3 Pa	Inspect S50

Fig. 3.7 SEM micrograph of $KNbO_3$ sample (T_S=1000ºC)

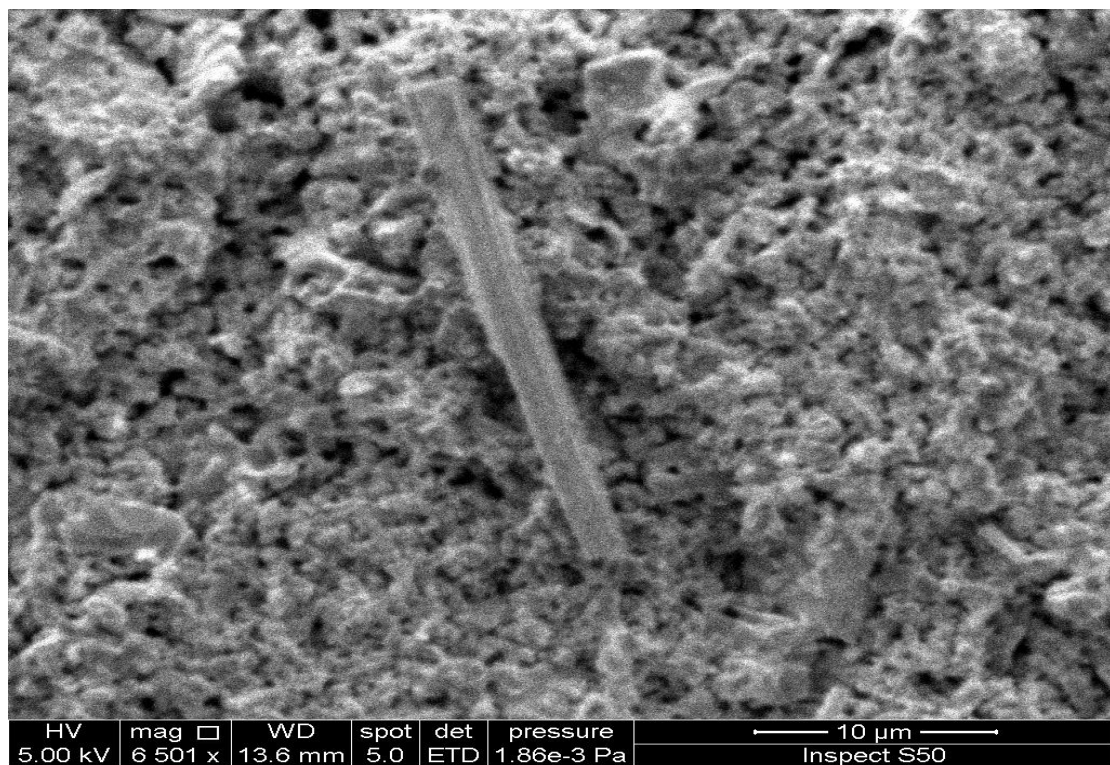Fig. 3.8 SEM micrograph of $K_{0.5}Na_{0.5}NbO_3$ sample (T_S=1000 ^{o}C)

Fig. 3.9 SEM micrograph of $NaNbO_3$ sample (T_S=1000 ^{o}C)

3.5 LCR measurements

   As we mentioned before, the LCR-measurement is benefit to find the dielectric properties, and the refractive index with different frequency. The temperature variation is necessary to find the phase transition point.

It is important to show the behavior of the samples with in frequency range (42 Hz – 5 MHz). The frequency dependence with dielectric constant for the system $K_{1-x}Na_xNbo_3$at (x =0) are shown in (Figs.3.10 –3.13) for different value of sintering temperature. Whereas the value of (x=0.5, 1) is mentioned in (Figs. 3.14 -3.15)
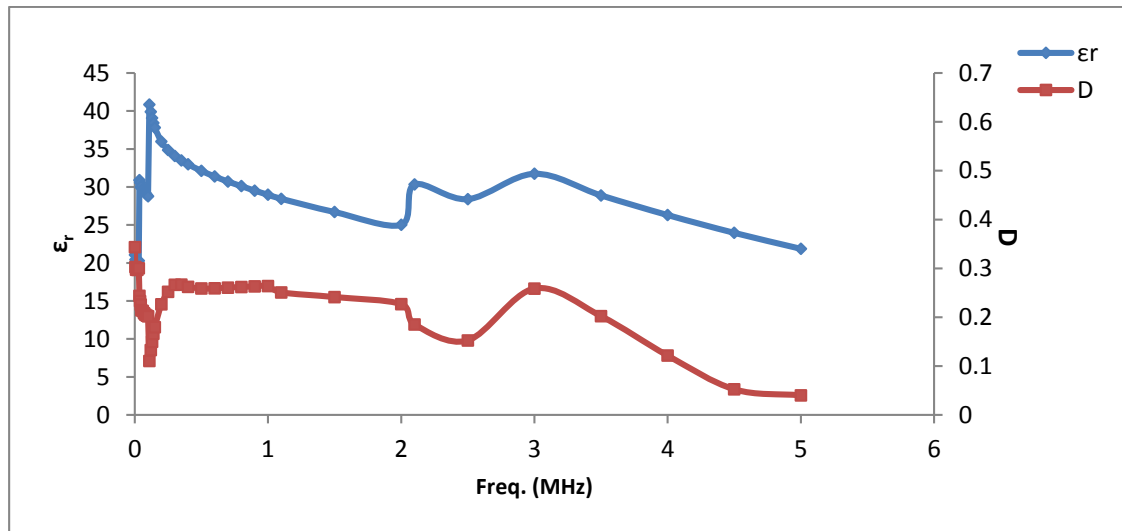

Fig 3.10: Dielectric constant and loss tangent *vs* frequency for (x=0) and $T_S = 900\ ^oC$
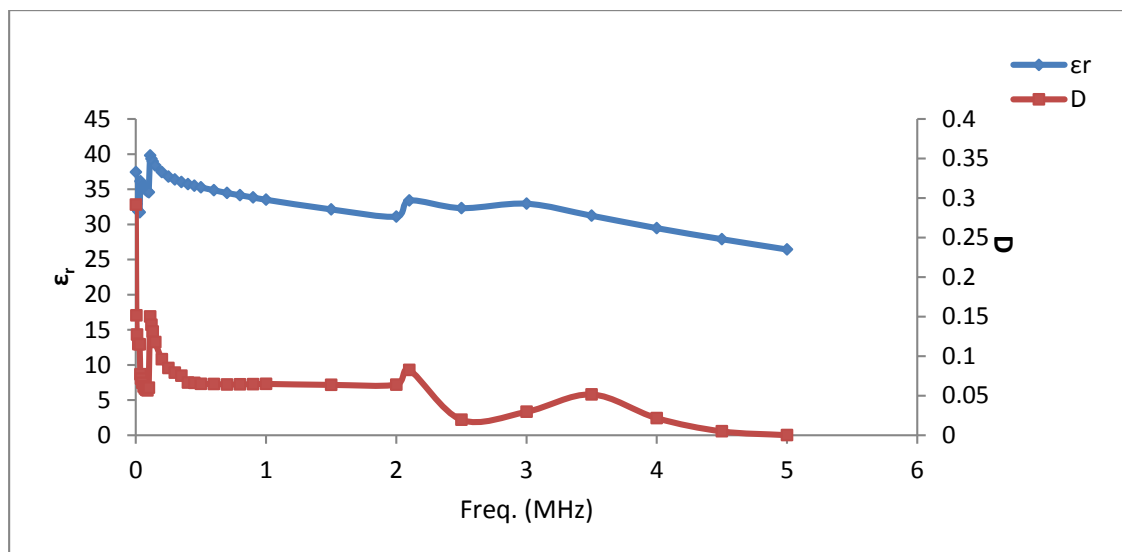
Fig. 3.11:Dielectric constant and loss tangent *vs* frequency for (x=0) and $T_S = 950\ ^oC$
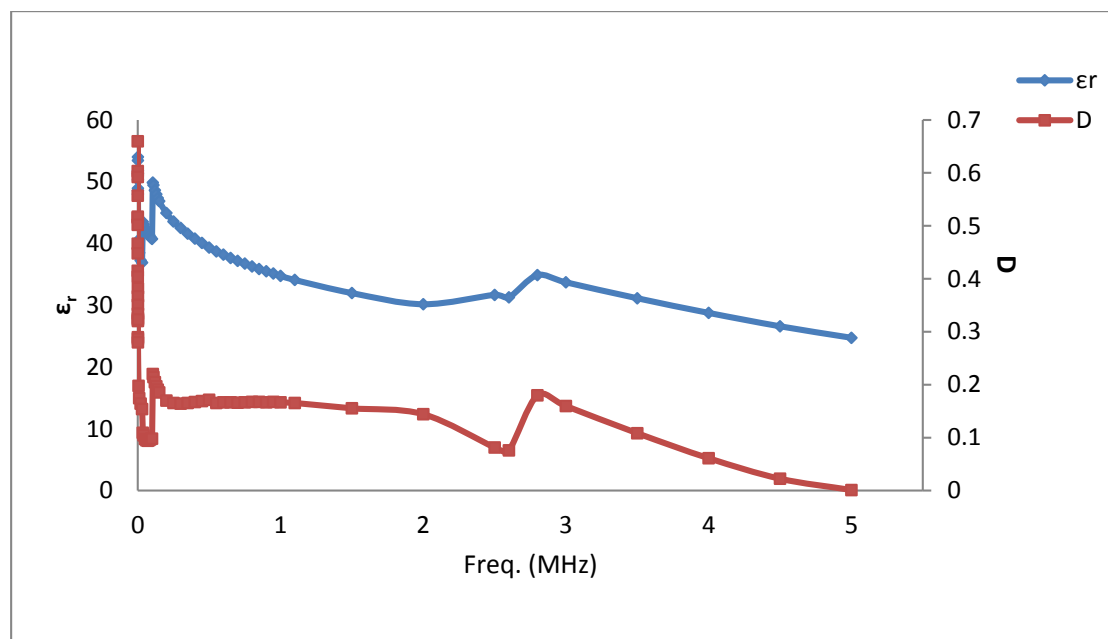
Fig.3.12: Dielectric constant and loss tangent *vs* frequency for (x=0) and $T_S = 1000$ °C.
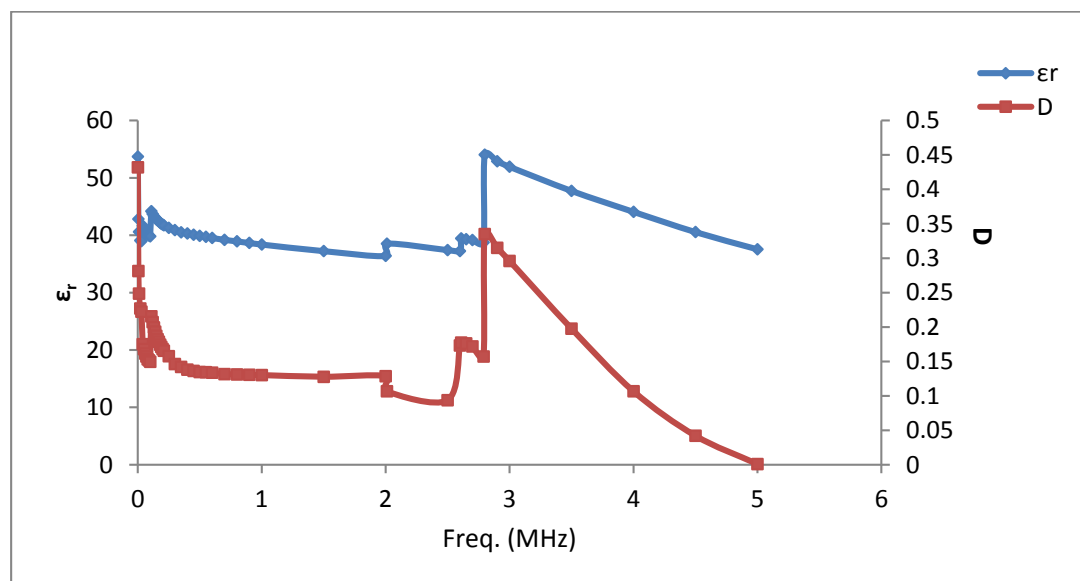
Fig. 3.13: Dielectric constant and loss tangent *vs* frequency for (x=0) and $T_S = 1050$ °C

The frequency dependence with the dielectric constant as a function of different sintering temperature at (x=0). It was clear that there are two peaks appeared (ε_{r1}, ε_{r2}), the first at low frequency within the range (1-

$1.3*10^5$Hz). The high dielectric constant is appeared at sintering temperature (T_S = 1000 ºC). This peak is related to dipolar polarization as discussed before in chapter one. The high dielectric constant that was appeared at (T_S = 1000 ºC). The second peak is appeared at the frequency range (2.1-2.8 $*10^6$ Hz), which is related to the ionic polarization as discussed before. The maximum value of dielectric constant was appeared at (T_S = 1000 ºC). Table (3-3) is showed the complete results for the compound KNbO$_3$ with different sintering temperature. The value of refractive index was measured for these frequencies by using the equation (2-5). Although the εr_2 at (T_S = 1050ºC) has high dielectric constant. That is might be attributed to the low bond length produced. The last is also related to the approaching of melting temperature as discussed before. Then the sintering temperature (T_S = 1000ºC) is dependent with LCR-measurement for the total system $K_{1-x}Na_xNbO_3$.

Table (3-3): The variation of dielectric constant and refractive index at the two peaks in the LCR-measurement for KNbO$_3$.

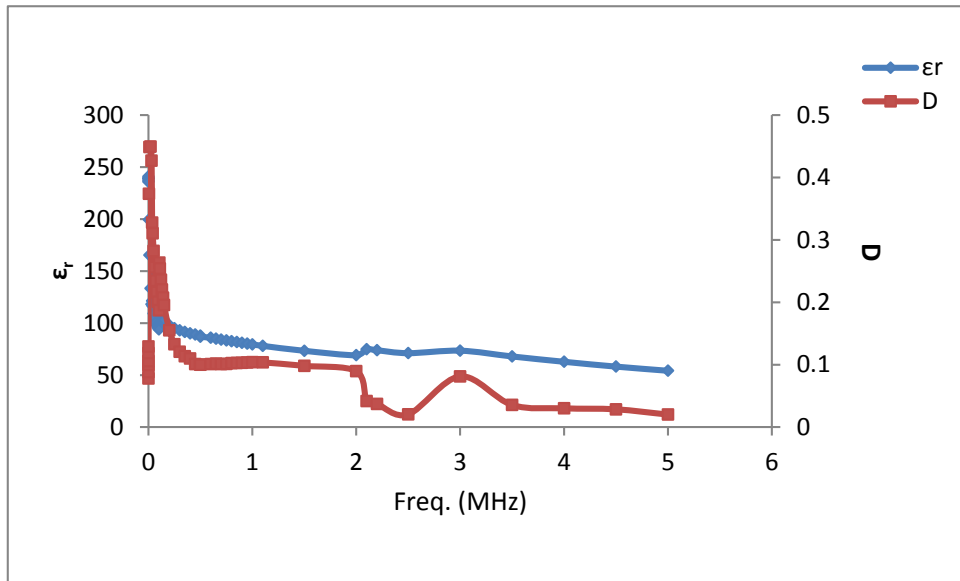| T_sºC	Peak1 $*10^5$(Hz)	ε_{r1}	n1	Peak1 (MHz)	ε_{r2}	n2
900	1.1	40.85	6.39	2.5	28.40	5.32
950	1.3	38.97	6.24	2.1	33.40	5.77
1000	1.05	49.86	7.06	2.8	34.88	5.9
1050	1.1	44.18	6.64	2.8	54.03	7.35

Fig.3.14: Dielectric constant and loss tangent *vs* frequency for (x=0.5) and $T_S = 1000$ ^{o}C.
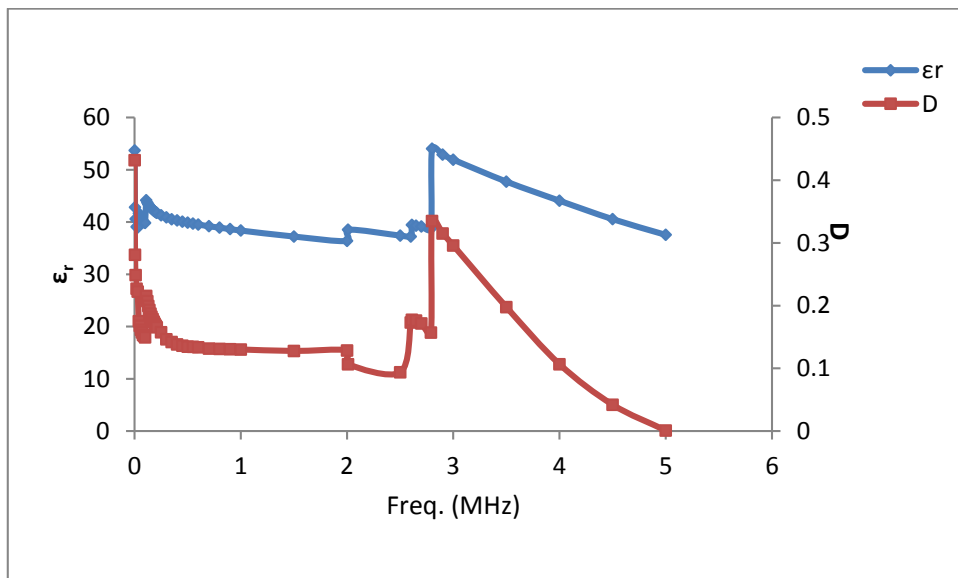
Fig.3.15: Dielectric constant and loss tangent *vs* frequency for (x=1) and $T_S = 1000$ ^{o}C

The effect of (x) on the results of LCR-measurements is clear in the Table (3-4) that was concluded from (Figs. 3.12, 3.14, and 3.15). The remaining of both peaks at low frequencies is appeared also. This is attributed to the presence of dipolar and ionic polarization although there is a replacement of Na-ions with respect to K-ions. The second thing, there is a maximum value appeared at (x=0.5) for both frequencies. That is

attributed to the difference in the ionic radius for both ions (Na, K). It has a direct effect on the producing of polarization. So we concluded that there is enhancement in the ionic polarization due to the substitution of Na-ions with respect to K-ions. This enhancement is tending to increase the (ε_r) for the peak.

Table (3-4): The variation of dielectric constant and refractive index at the two peaks in the LCR-measurement for the system $K_{1-x}Na_xNbO_3$.

X	Peak1($*10^5$Hz)	ε_{r1}	n1	Peak1(MHz)	ε_{r2}	n2
0	1.05	49.86	7.06	2.8	34.88	5.9
0.5	1.1	110.7	10.52	2.1	74.92	8.65
1	1.01	23.16	4.81	2.8	19.13	4.37

The temperature dependence at a constant frequency to find the dielectric constant and loss tangent for $KNbO_3$ at sintering temperature (900°C) is shown in Figs. (3-16,17,18). The dependence frequencies were (10 KHz, 100 KHz and 1 MHz) and temperature range was (50 – 500 °C). These are suitable to calculate the Curie temperature and determine phase transition from ferroelectric to paraelectric.
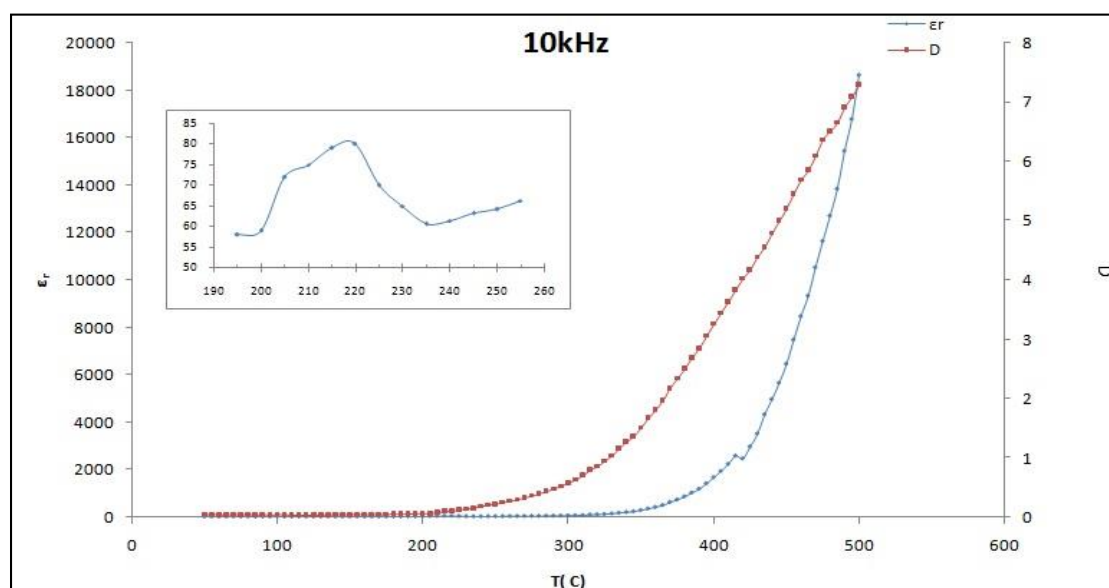

Fig. 3.16:The dielectric constant and loss tangent vs temperature at 10 kHz for $KNbO_3$ ceramic sintering at 900°C/5hr.

Fig. 3.17:The dielectric constant and loss tangent vs temperature at 100 kHz for KNbO$_3$ceramic sintering at 900°C/5hr.

Fig. 3.18:The dielectric constant and loss tangent vs temperature at 1 MHz for KNbO$_3$ceramic sintering at 900°C/5hr.

Normally, there are two phase transition appeared on this system, the first one from orthorhombic to tetragonal at lower temperature of about (225°C), and at high temperature of about (435°C) [16] showed phase transition tetragonal ferroelectric to cubic paraelectric. Actually, the first

54

peak is not necessary to appear because it is related to the crystal transition. Where the second peak is very important to appear because it is related to phase transition in the behavior. So that there is disappearance of the first peak at low temperature for the frequency (10- 100kHz) but on the other frequency (1MHz) the temperature for the first transition was about (220ºC). It is almost agreeing with the theoretical value. It was clear that the value of (T_C) at high temperature has high T_C of about (415ºC) at frequency (10 kHz and 1 MHz). The low T_C was appeared at (410ºC) for frequency (100 kHz). In general, both are approach to the theoretical value, but all these peaks have a small area. That means the strength of phase transition is low possibility.

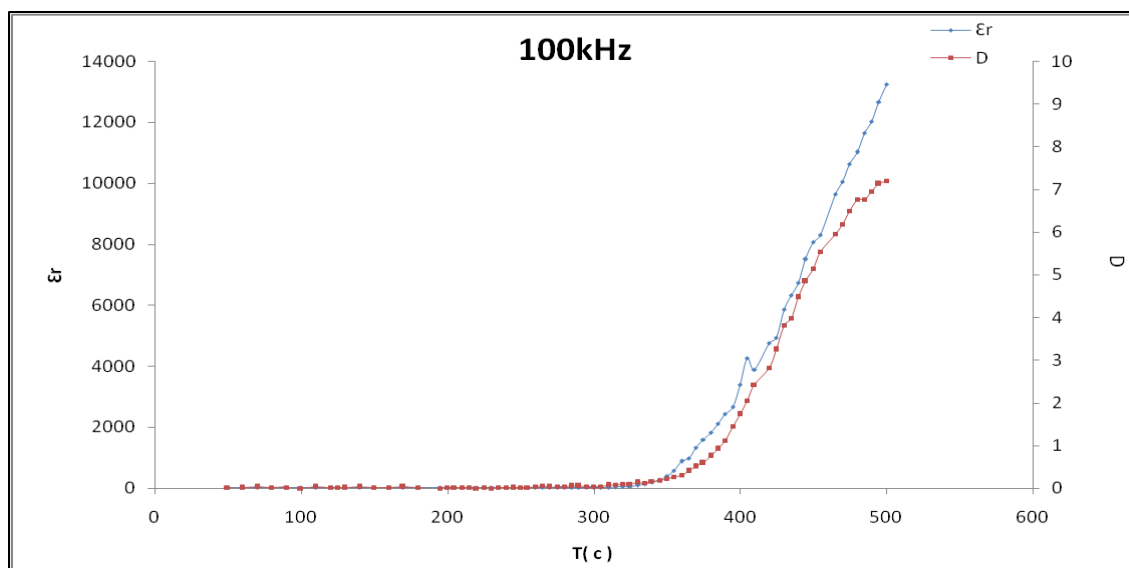Fig. 3.19:The dielectric constant and loss tangent vs temperature at 10 kHz for KNbO$_3$ceramic sintering at 950ºC/5hr.

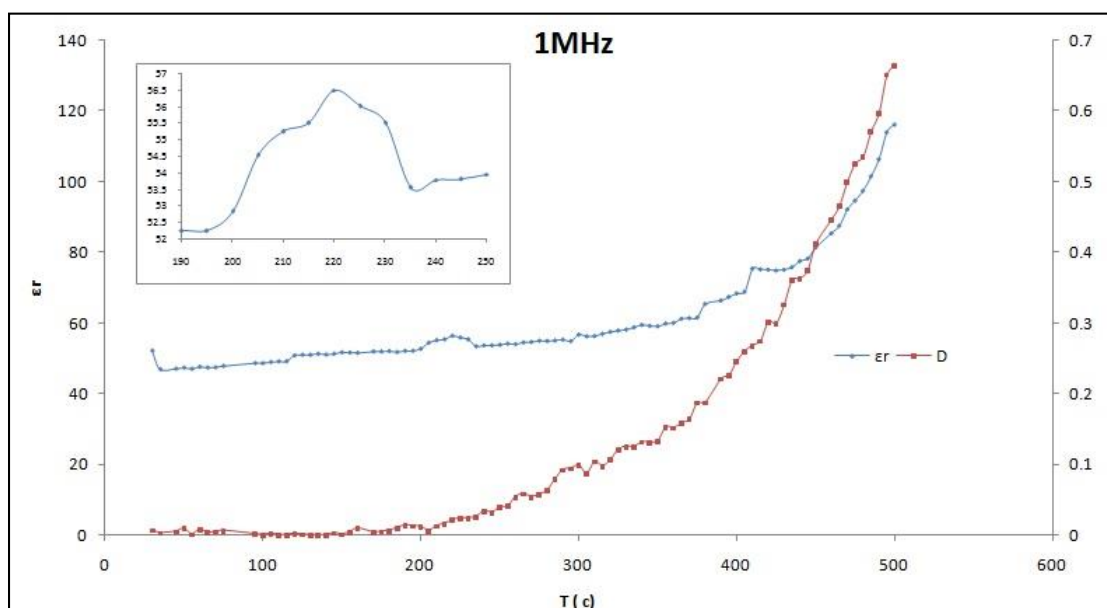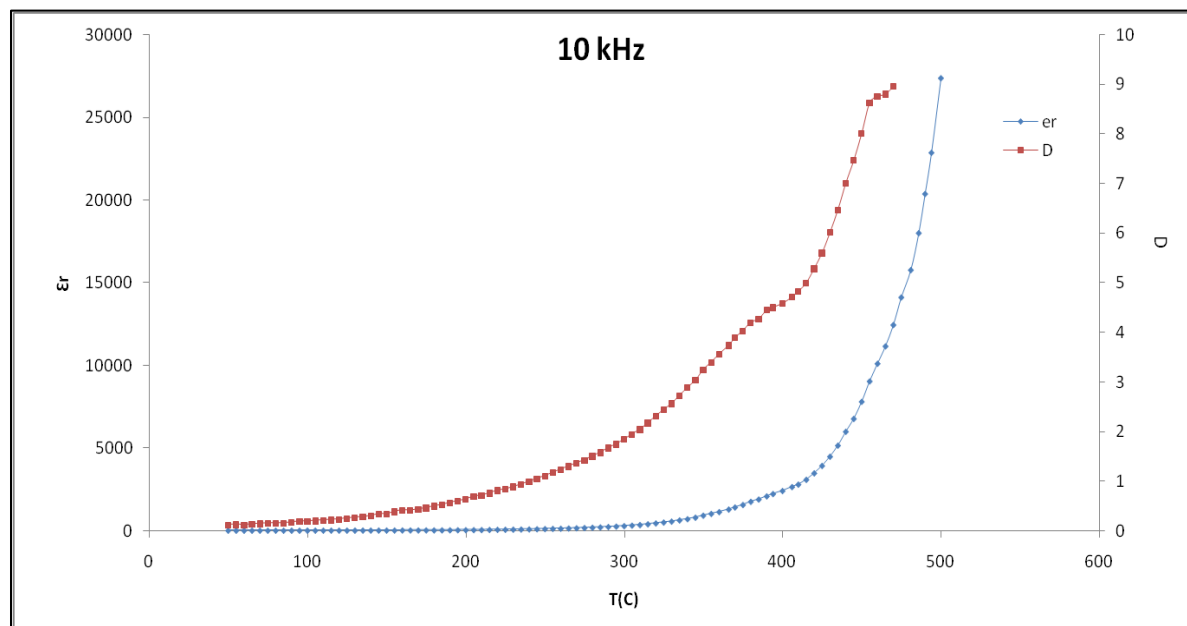Fig. 3.20:The dielectric constant and loss tangent vs temperature at 100 kHz for KNbO$_3$ceramic sintering at 950ºC/5hr.

Fig. 3.21:The dielectric constant and loss tangent vs temperature at 1 MHz for KNbO$_3$ ceramic sintering at 950ºC/5hr.

The temperature measurements of dielectric constant and loss tangent For the sample sintered at (950ºC) at different value of frequency are mention in (Figs. 3.19-21). The thing is notice represented by vanishing the (T$_C$) value at frequency (10 kHz). That is might be has the effect of relaxation ferroelectric behavior as mentioned in (Fig.3.19). It started the

56

appearance of the peak in the wide range and that may be happened greater than (500ºC). This thing is also applied on(Fig.3.14). It is well known that the ferroelectric to paraelectric transition needs a certain amount of energy for the transition. So it might be the amount of energy that is function of frequency is not compatible with this transition. Whereas the frequency (1MHz) is very important to appear this wide peak in a suitable value of temperature of about (417ºC). The thing that is emphasized this saying is the increasing of (T_C) for the sample prepared by different sintering temperature (900, and 950ºC).

The other transition temperature that which appear in the dielectric measurement is the temperature of transition from orthorhombic to tetragonal (T_{O-T}). The T_{O-T} was estimated for (100 kHz) is (220ºC) and for (1MHz) is (223ºC).

Fig. 3.22:The dielectric constant and loss tangent vs temperature at 10 kHz for KNbO$_3$ceramic sintering at 1000ºC/5hr.
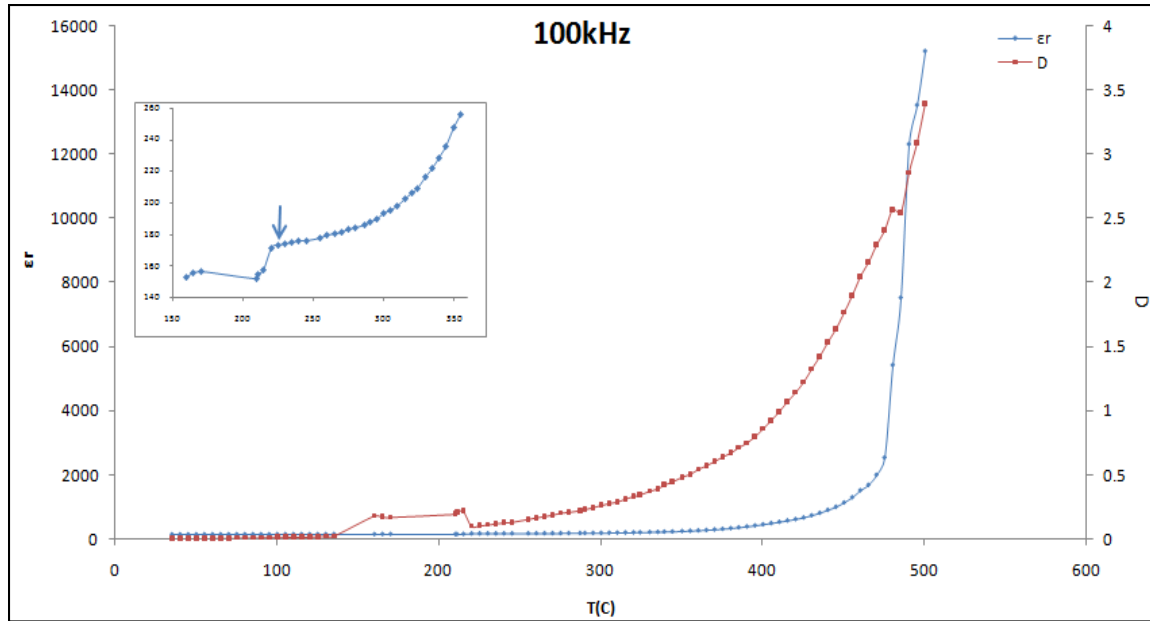
Fig. 3.23:The dielectric constant and loss tangent vs temperature at 100 kHz for KNbO$_3$ceramic sintering at 1000°C/5hr.
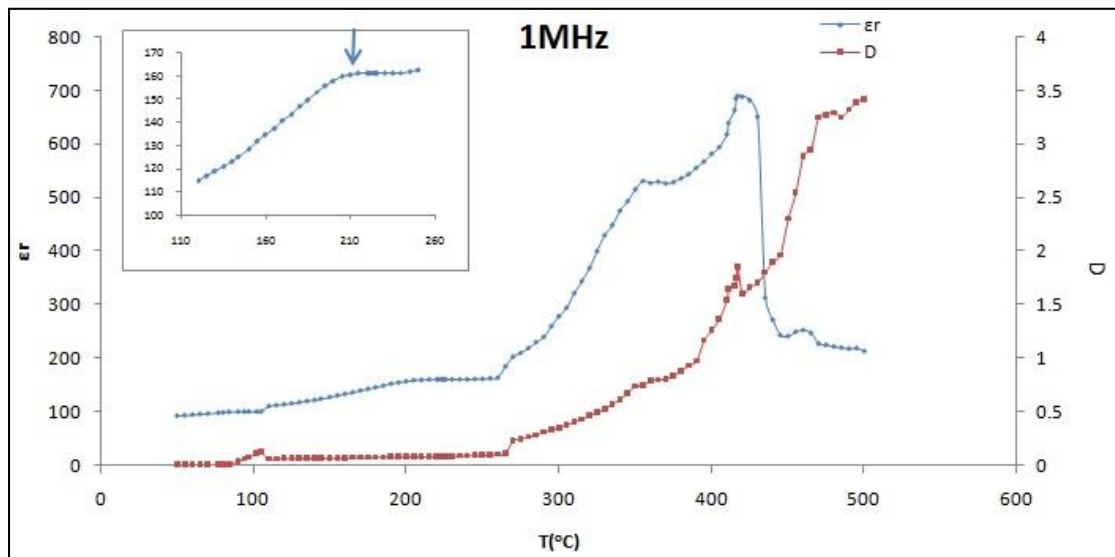

Fig. 3.24:The dielectric constant and loss tangent vs temperature at 1 MHz for KNbO$_3$ ceramic sintering at 1000°C/5hr.

On the other hand, the temperature dependence on dielectric behavior for the sample sintered at (1000°C) for different frequency is shown in (Figs. 3.22-24). This sintering temperature is more clear in the behavior of dielectric behavior during the appearance of phase transition temperature at temperature (400°C) at frequency (1MHz). Actually, it is lower than the sample sintered at (T$_S$= 900, and 950 °C). That is might be attributed to low

energy for transition in behavior. Also this energy represented by frequency is efficient to brake the ionic dipoles and producing the paraelectric behavior. Although, there is a weak appearance of the first peak for all value of frequency which is a function to investigate the crystalline phase transition. This is the true of considering the value of ($T_S=1000^{\circ}C$) as the better value in preparation.

The other transition temperature that which appear in the dielectric measurement is the temperature of transition from orthorhombic to tetragonal (T_{O-T}). The T_{O-T} was estimated for 10 kHz is $210^{\circ}C$, for 100 kHz is $220^{\circ}C$ and for 1MHz is $229^{\circ}C$.
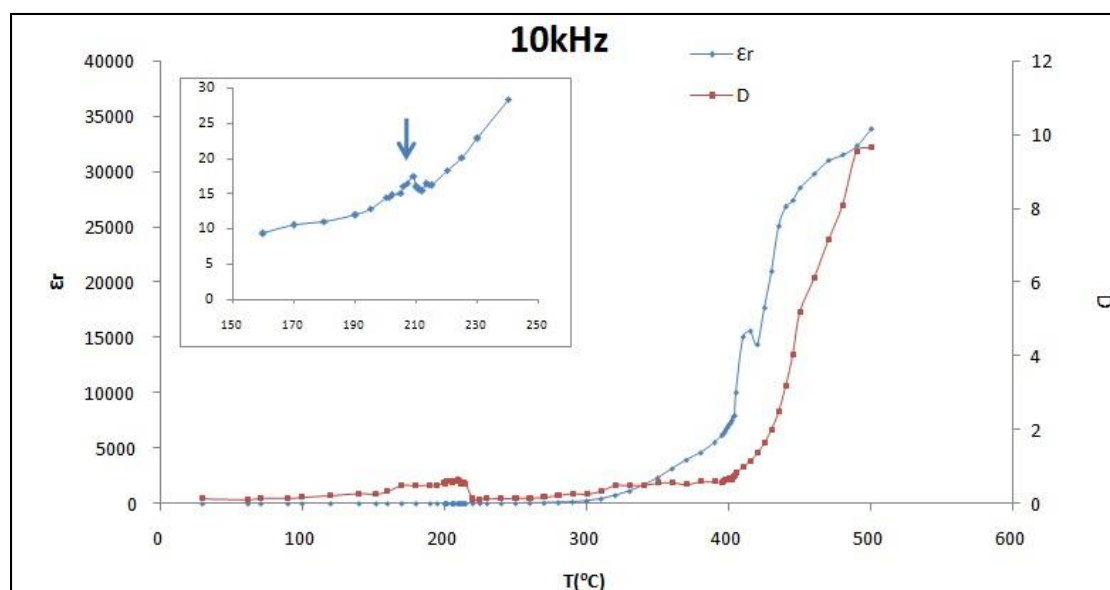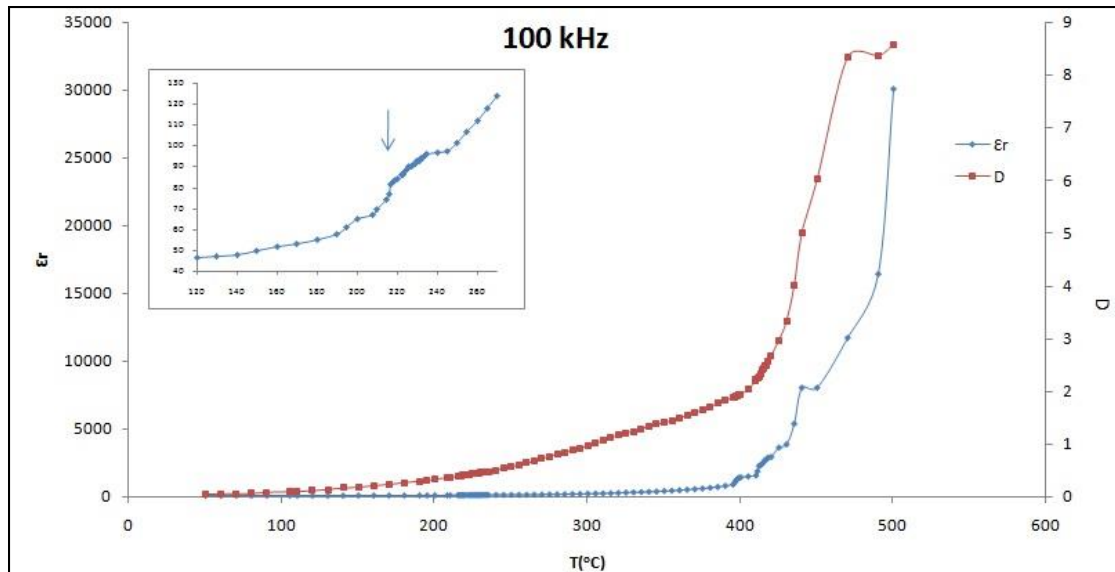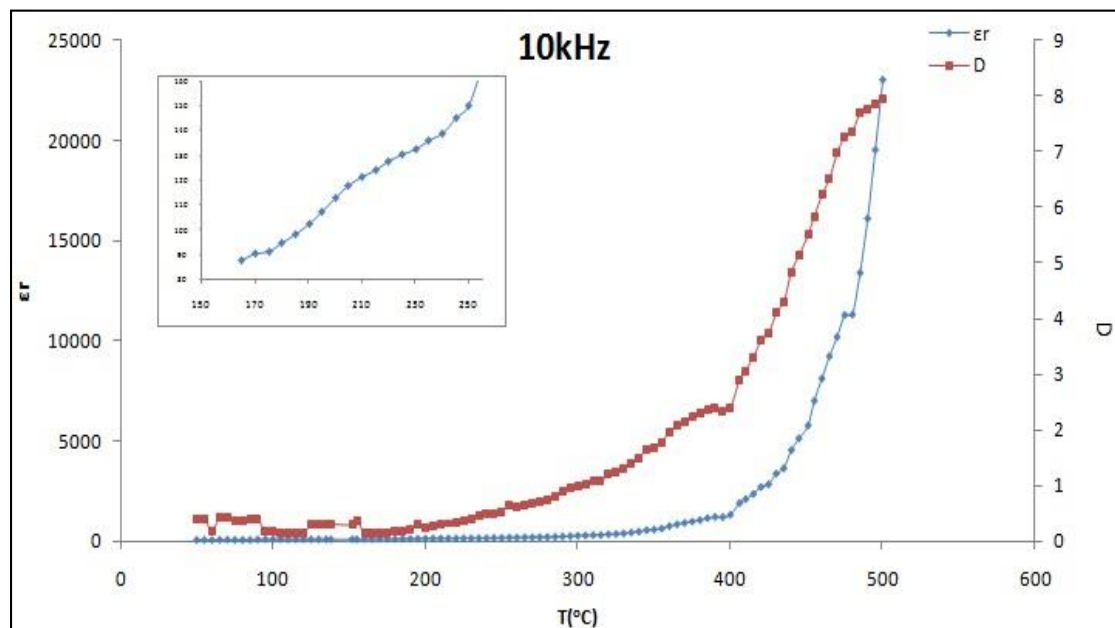

Fig. 3.25:The dielectric constant and loss tangent vs temperature at 10 kHz for KNbO$_3$ceramic sintering at $1050^{\circ}C/5hr$.

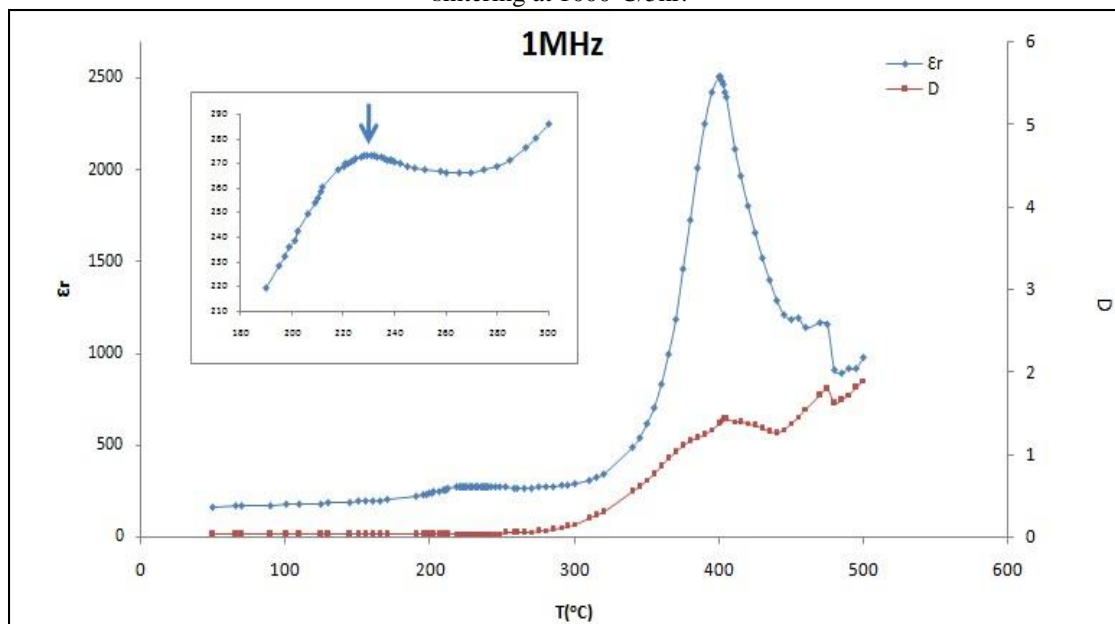Fig. 3.26:The dielectric constant and loss tangent vs temperature at 100 kHz for KNbO$_3$ceramic sintering at 1050ºC/5hr.

Fig. 3.27:The dielectric constant and loss tangent vs temperature at 1 MHz for KNbO$_3$ceramic sintering at 1050ºC/5hr.

Finally, the temperature dependence on the dielectric behavior for the sample sintered at (1050ºC) with different frequency is shown in (Figs.

3.25-27). There is no clear appearance for the peak of the phase transition in the behavior. That is might be attributed to stared for going to liquid phase and change the complete behavior. There is a narrow peak appeared at ($T_C=405^oC$) for the frequency (1MHz). The disappearance of this peak at other frequency is possible for the above reason.

The other transition temperature that which appear in the dielectric measurement is the temperature of transition from orthorhombic to tetragonal (T_{O-T}). The T_{O-T} was estimated for (10 kHz) is (210^oC), for (100 kHz) is (210^oC) and for (1MHz) is (212^oC).

Sundarakannan *et al*, found the two phase transition for $KNbO_3$ ceramic prepared by (SSR) method with caltination temperature (830^oC) and sintering temperature (1020^oC) for (2 hr) appeared about (213^oC) for the transition from orthorhombic to tetragonal, and the second transition from tetragonal to cubic about (420^oC) in the range of frequency (100 kHz-1MHz)[45]. The different in the result is might be due to the different in both calsination and sintering temperature and the period for both of them.
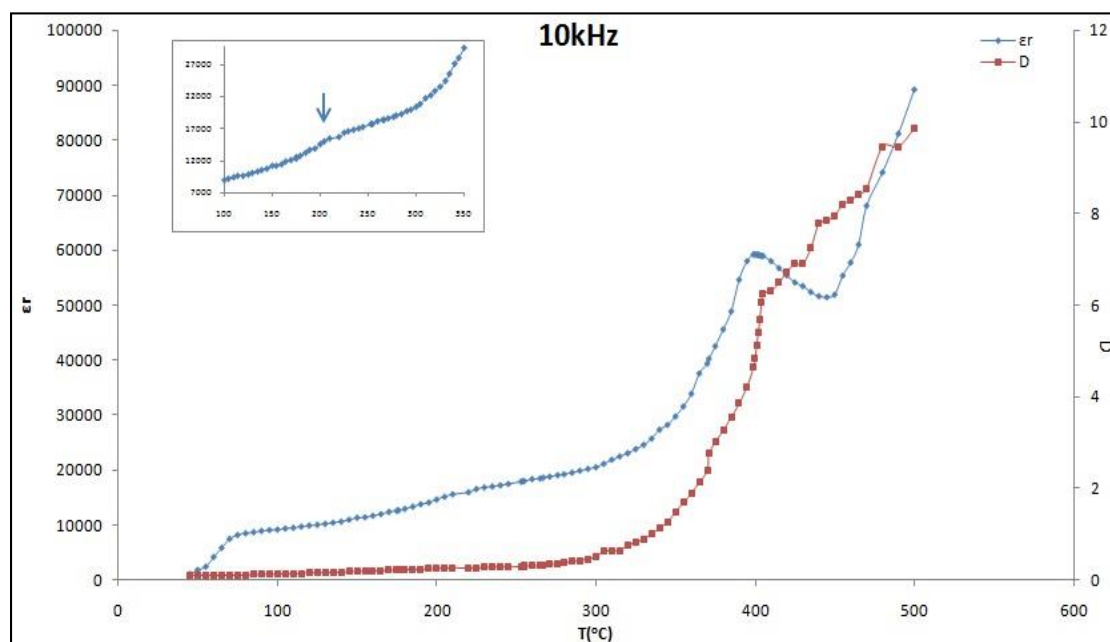
Fig. 3.28:The dielectric constant and loss tangent vs temperature at 10 kHz for $K_{0.5}Na_{0.5}NbO_3$ceramic sintering at $1000^oC/5hr$.
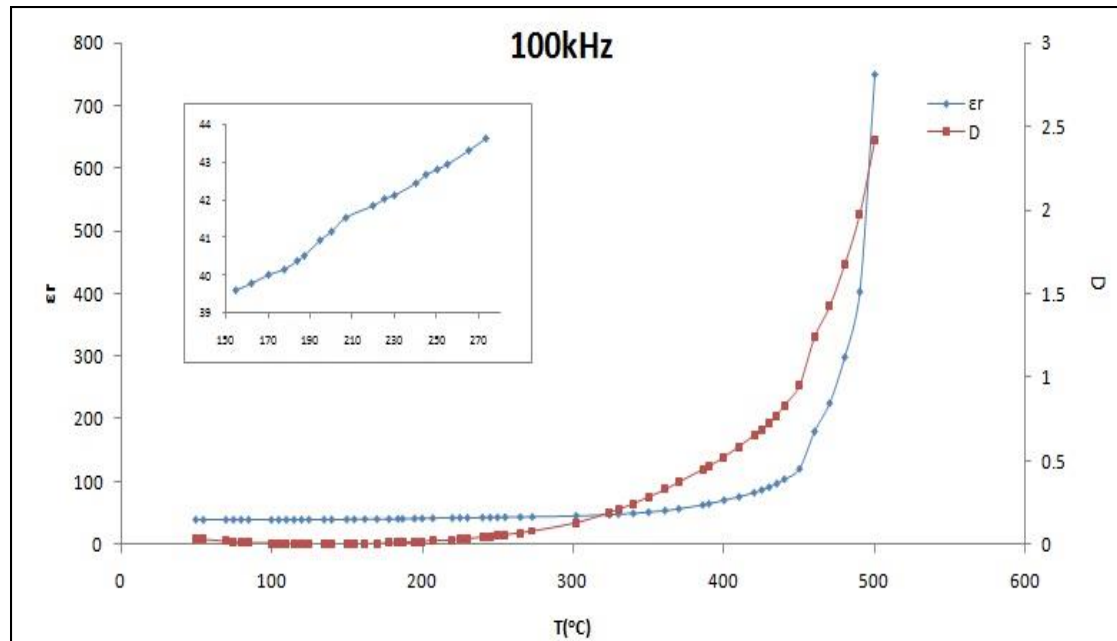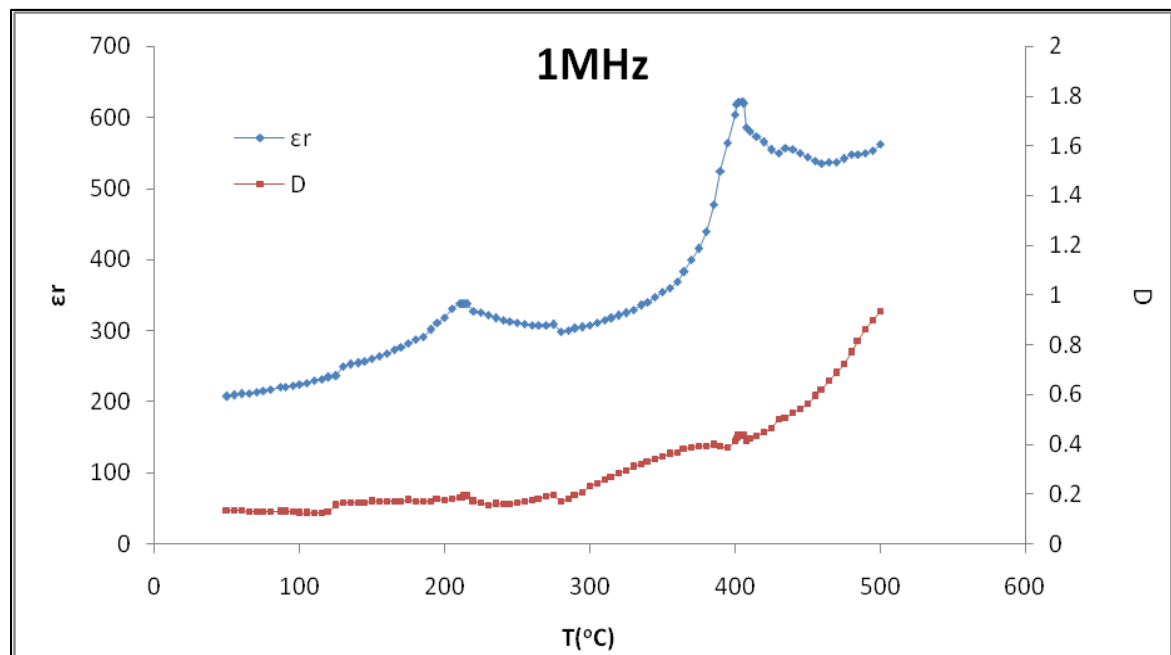
Fig. 3.29:The dielectric constant and loss tangent vs temperature at 100 kHz for $K_{0.5}Na_{0.5}NbO_3$ceramic sintering at $1000^oC/5hr$.

Fig. 3.30:The dielectric constant and loss tangent vs temperature at 1 MHz for $K_{0.5}Na_{0.5}NbO_3$ ceramic sintering at $1000^oC/5hr$.

The effect of Na-ions substitution with respect to K-ions was studied more and more. So the effect of ($T_S=1000^oC$) was dependent in calculation of dielectric constant as a function of temperature at different value of frequency represented by (Figs.3.28-30). It is well defining of (T_C) about

(399°C) is possible for the transition with the wide band of temperature range. This true is actually accepted in the behavior of phase transition from the ferroelectric to paraelectric. The frequency (1MHz) is the best value in this behavior. This mean the amount of energy required for this transition is compatible with this frequency. Although, there is a sharp T_C-value for the frequencies (10 and 100 kHz) represented by (400, and 395 °C) but the area of these peaks is so small. The comparison between $KNbO_3$ and $K_{0.5}Na_{0.5}NbO_3$ for the same frequency is well defining in (Figs. 3.24 and 3.30). It is clear that the peak has large area. This is regarded to amount of energy required to disperse the ionic dipoles forming paraelectric behavior. So it is clear the effect of Na-ions in the structure from the area of the peak at (T_C=399°C). The other transition temperature that which appear in the dielectric measurement is the temperature of transition from orthorhombic to tetragonal (T_{O-T}). The T_{O-T} was estimated for (10 kHz) is (215°C), for (100 kHz) is (218°C) and for (1MHz) is (200°C).

   Mahesh *et al*, observed the two transition at low and high temperature for $K_{0.5}Na_{0.5}NbO_3$ ceramic at (165°C) and (335°C) respectively [31].
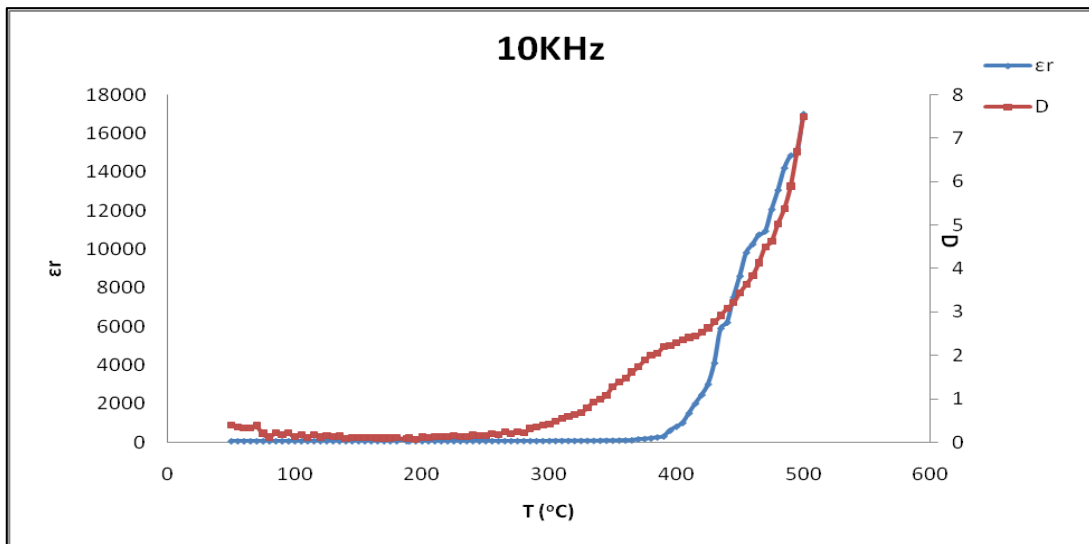
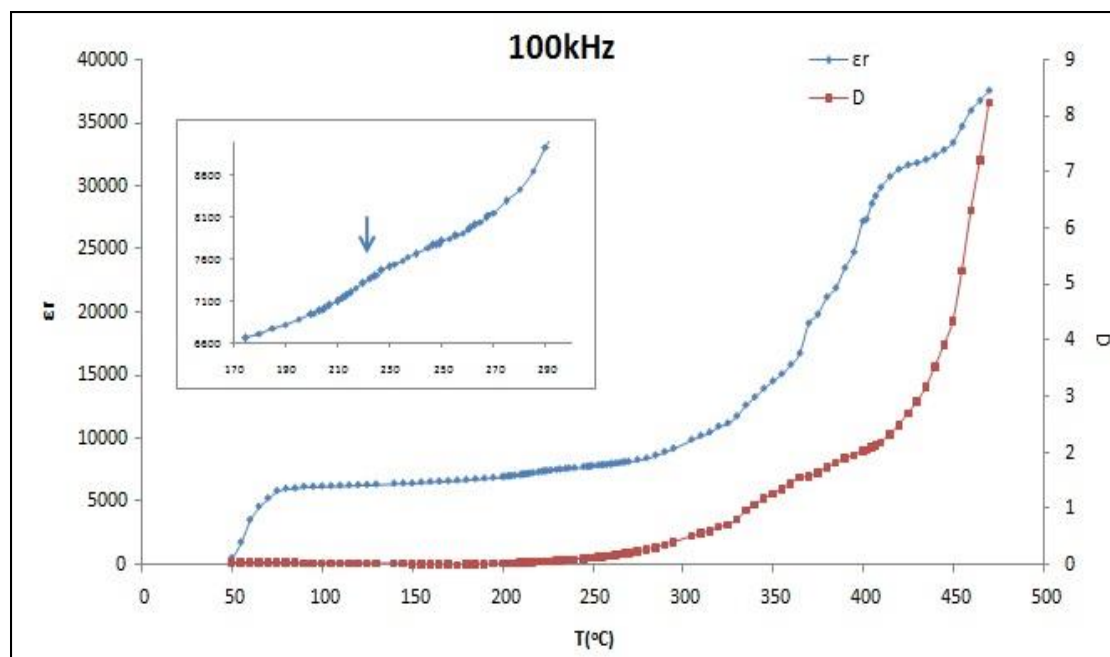

Fig. 3.31:The dielectric constant and loss tangent vs temperature at 10 kHz for $NaNbO_3$ceramic sintering at 1000°C/5hr.
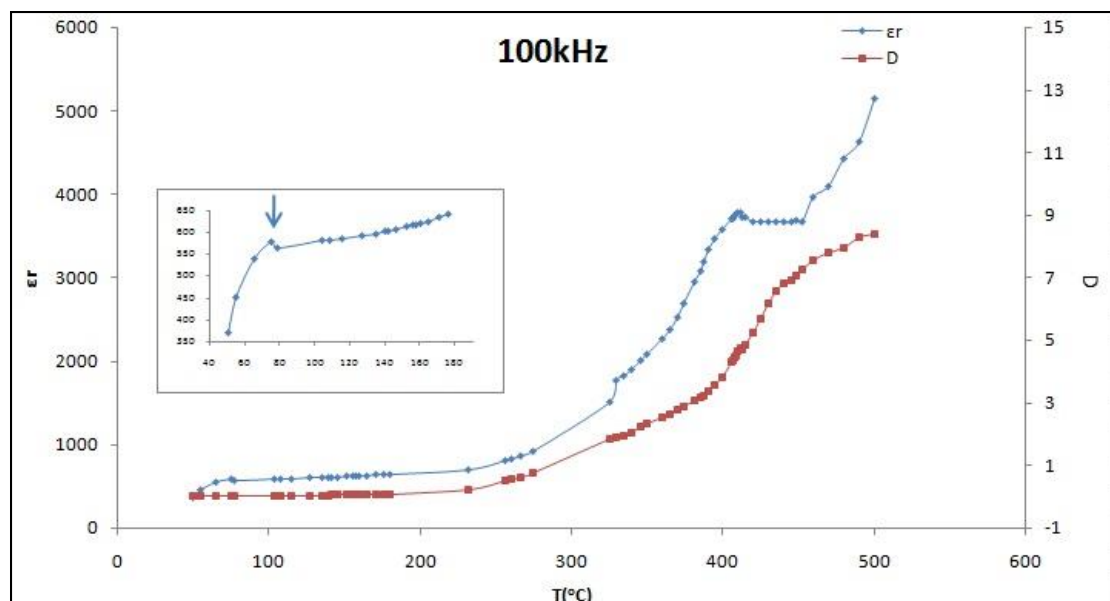
Fig. 3.32:The dielectric constant and loss tangent vs temperature at 100 kHz for NaNbO$_3$ceramic
sintering at 1000ºC/5hr.

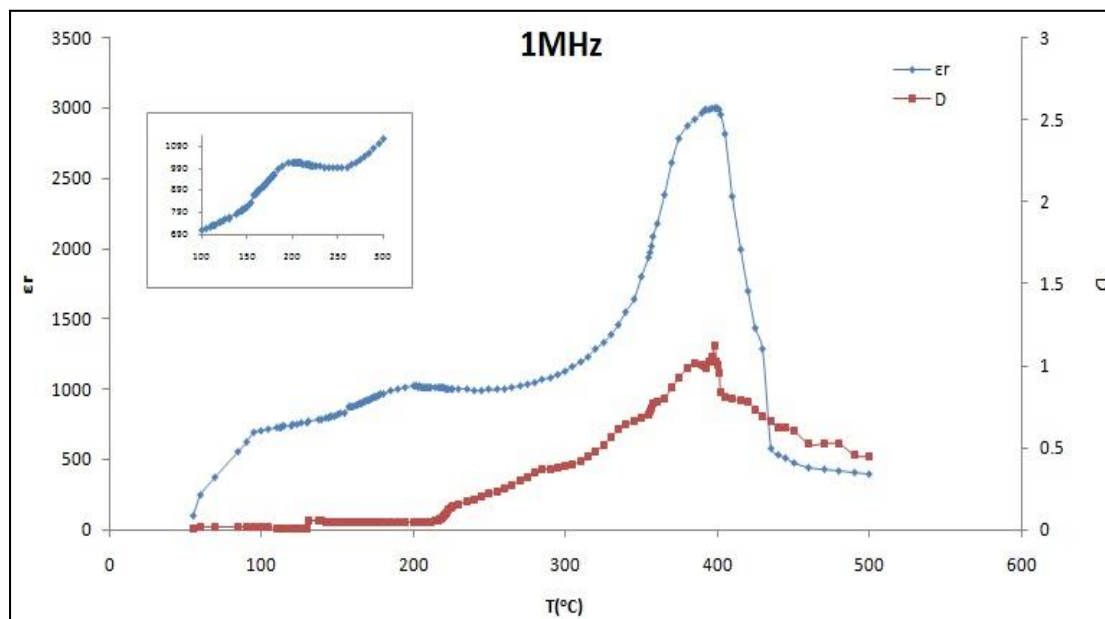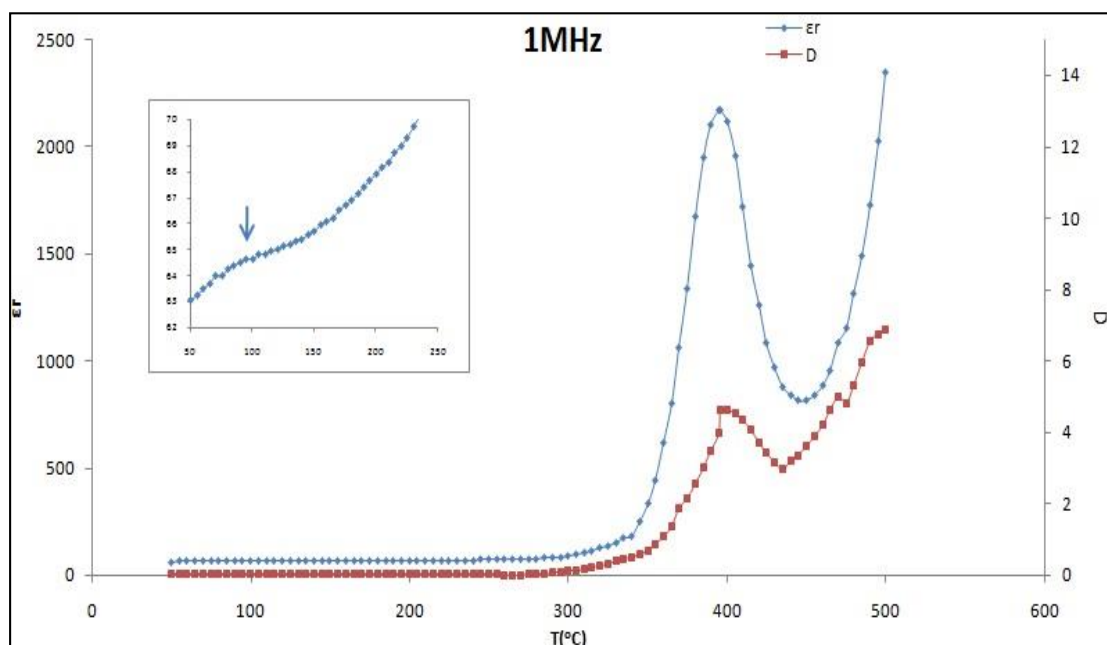Fig. 3.33:The dielectric constant and loss tangent vs temperature at 1 MHz for NaNbO$_3$ceramic
sintering at 1000ºC/5hr.

The completely substitution of Na-ions is more clear during the producing of NaNbO$_3$. The effect of temperature on the dielectric behavior is shown in (Figs.3.31-33) at different frequency. Normally, it is clear that the frequency (1MHz) is better in the definition the ferroelectric to paraelectric phase transition rather than the other frequencies such (10 and

64

100 kHz). The concluded (T_C) is appeared at ($T_C= 395°C$). The other transition temperature that which appear in the dielectric measurement was for (10kHz) is (140°C), for (100kHz) is (75°C) and for (1MHz) is (95°C).

The effect of Na-substitution on the mixture $K_{1-x}Na_xNbO_3$ is very clear during the decreasing of (T_C) to low value as a function of Na-ions concentration in the mixture.

That is agree with the true of the strength of the polarization. The last is normally depends on the ionic radii of K and Na ions, that has lower value of radius for Na ions with respect to K-ions. That means the strength of polarization in $NaNbO_3$ is lower than the $KNbO_3$, which are related to lower value of (T_C) as mention before. On the other hand, the area of the peak is very important to find the value of the thermal energy for transition.

System with (x=0.5) shows the maximum value of dielectric properties and this due to the best properties were achieved at morphotropic phase boundary (MPB) 50/50 Potassium sodium niobate composition [12].

Table (3-5): The T_C value of ferro-para transition in$K_{1-x}Na_xNbO_3$.

x-value	T_S (°C)	T_C(°C)		
		10 kHz	100 kHz	1 MHz
0	900	415	410	415
0	950			417
0	1000			400
0	1050			405
0.5	1000	400	395	399
1	1000	390	405	395

3.6   The optical energy gaps measurement

This type of material is classified as a dielectric material, so normally the energy gap is much large in the determination. The reason is return to a harvesting solar energy of this material type. It is necessary to measure the nature of coupling between the anion and cation during the band gap. That is similar the mechanism of the transition of electron from the top of the valance band to the bottom of the conduction band and producing electron hole pair (EHP) in semiconductor. Already there are two type of ions, anoin in the conduction band and cation in the valance band. There is electric field producing between them because of ferroelectric behavior so the coupling between them like exciton in semiconductor. The effect of electromagnetic radiation that was applied during the effect of electric field compound. It has direct effect to induce the strength of the electric field between the oppositely ions in the material. The measuring of this potential is the reason for producing the optical energy gap. The effective value of wavelength is about (280-300 nm) for the absorption spectrum as shown in Fig 3.34. That means the material is interact with the ultra-violet region. In reflectance spectrum, the effective region is about (298-550 nm) as shown in Fig 3.35. This is related to find the maximum value of the refractive index. The last is depending directly on the very high frequency to conclude the electronic polarization that should happened reasonably. The benefit of the both spectrum is very important in determination of the optical energy gap (E_g) and the refractive index (n) during the absorption and reflection spectrum respectively. There is a very sharp in the optical absorption within a limited wavelength. The reason is return to make all the mechanisms, direct and indirect are possible during the band gap. The reflection spectrum is a good tool to measure the refractive index for the same ray of wavelength.
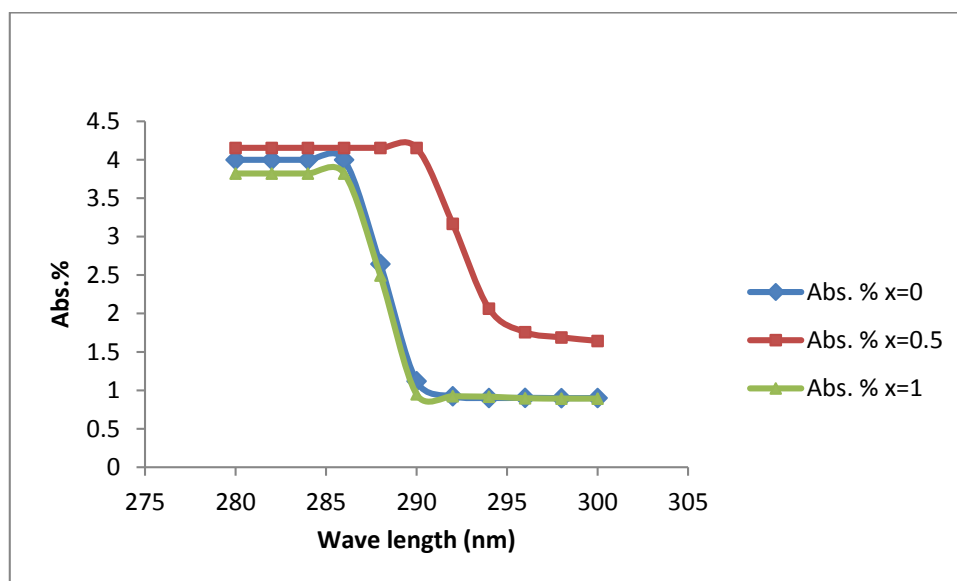
Fig. 3.34: Plots of absorption spectrum versus wavelength for [(K_xNa_{1-x}) NbO_3,] at (x=0,0.5 and, 1).
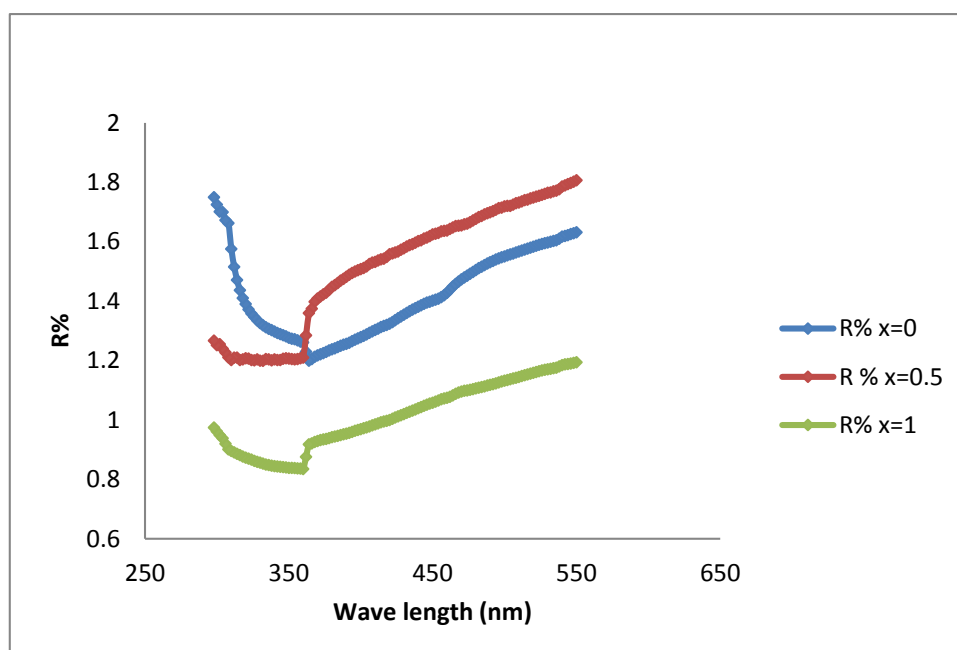
Fig. 3.35: Plots of reflectance spectrum versus wavelength for [(K_xNa_{1-x}) NbO_3,] at (x=0,0.5 and, 1)
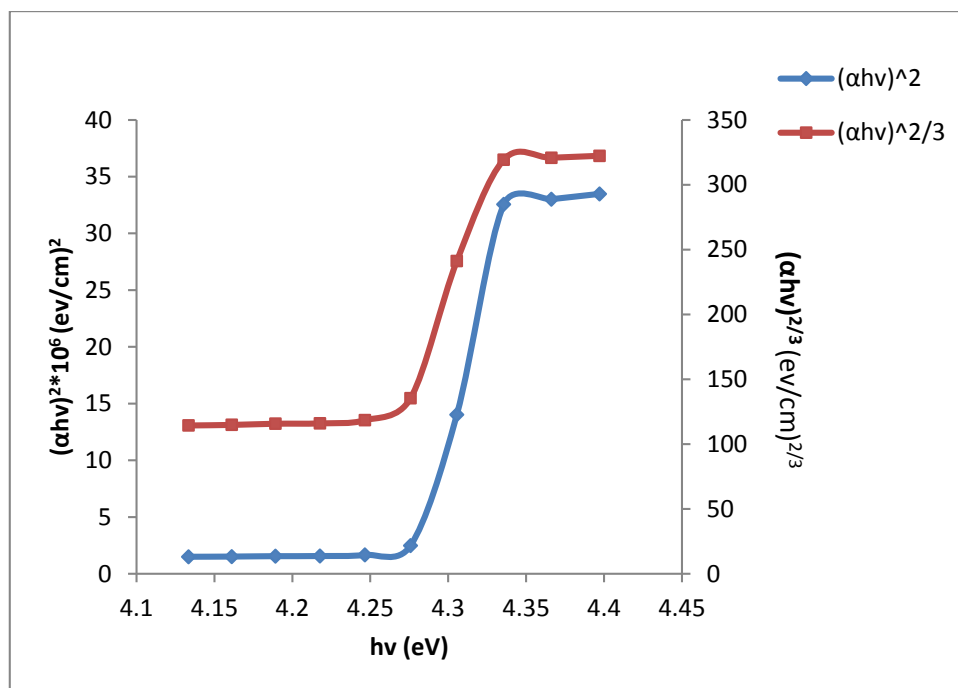
Fig. 3.36:Plots of $(\alpha h\nu)^2$ and $(\alpha h\nu)^{2/3}$ versus photon energy (hν) for (KNbO$_3$) for direct transition [$(\alpha h\nu)^2$ allowed and $(\alpha h\nu)^{2/3}$ forbidden].
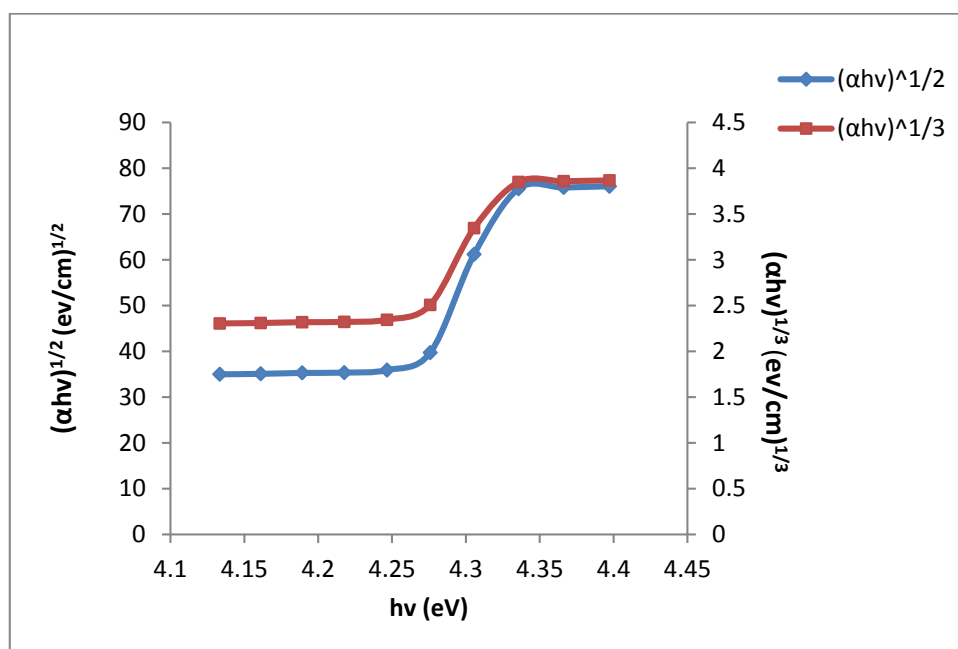
Fig. 3.37:Plots of $(\alpha h\nu)^{1/2}$ and $(\alpha h\nu)^{1/3}$ versus photon energy (hν) for (KNbO$_3$) indirect transition [$(\alpha h\nu)^{1/2}$ allowed and $(\alpha h\nu)^{1/3}$ forbidden].
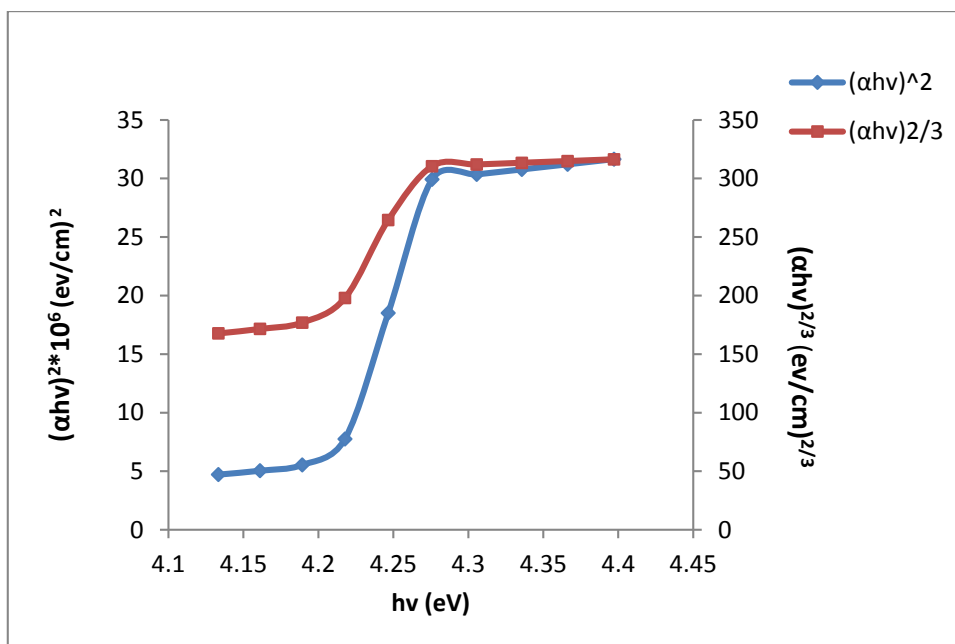
Fig. 3.38:Plots of $(\alpha h\nu)^2$ and $(\alpha h\nu)^{2/3}$ versus photon energy ($h\nu$) for $K_{0.5}Na_{0.5}NbO_3$ for direct transition [$(\alpha h\nu)^2$ allowed and $(\alpha h\nu)^{2/3}$ forbidden].

Fig. 3.39:Plots of $(\alpha h\nu)^{1/2}$ and $(\alpha h\nu)^{1/3}$ versus photon energy ($h\nu$) for $K_{0.5}Na_{0.5}NbO_3$ for indirect transition [$(\alpha h\nu)^{1/2}$ allowed and $(\alpha h\nu)^{1/3}$ forbidden].

Fig. 3.40:Plots of $(\alpha h\nu)^2$ and $(\alpha h\nu)^{2/3}$ versus photon energy (hν) for NaNbO$_3$,] at of direct transition [$(\alpha h\nu)^2$ allowed and $(\alpha h\nu)^{2/3}$ forbidden].

Fig. 3.41:Plots of $(\alpha h\nu)^{1/2}$ and $(\alpha h\nu)^{1/3}$ versus photon energy (hν) for NaNbO$_3$ of indirect transition [$(\alpha h\nu)^{1/2}$ allowed and $(\alpha h\nu)^{1/3}$ forbidden].

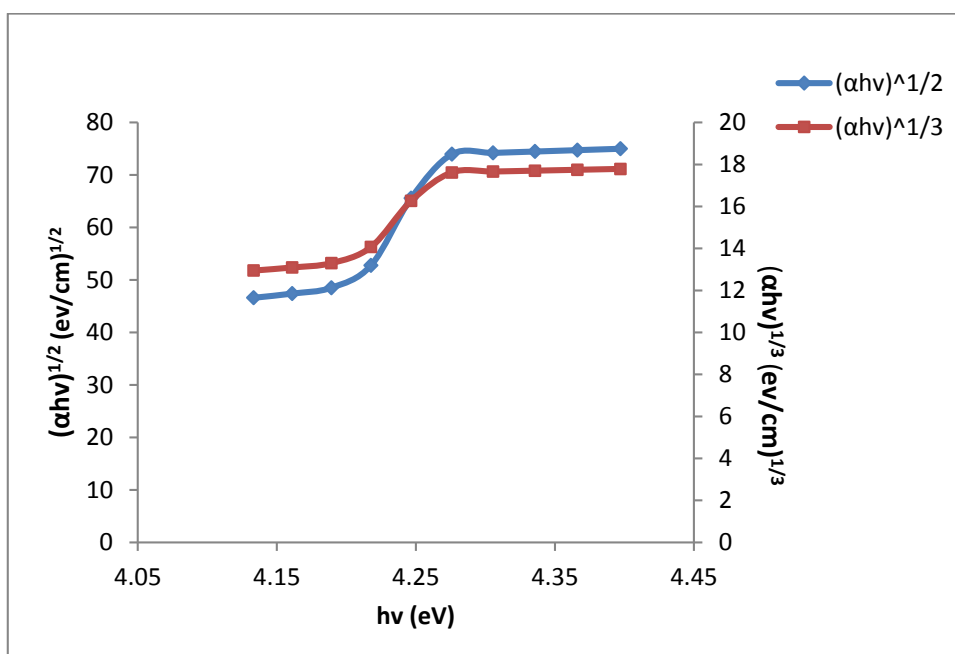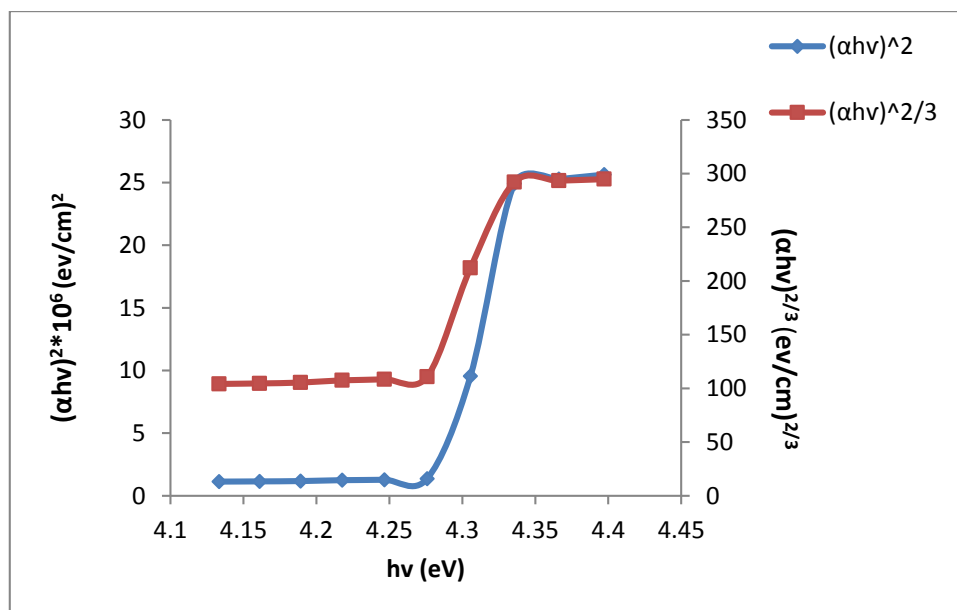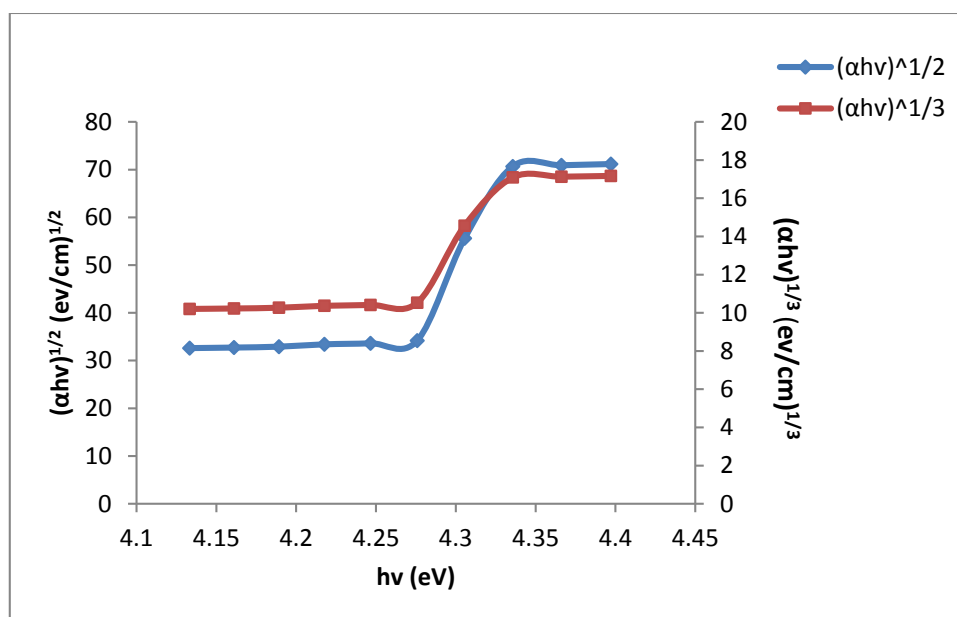The optical energy gaps for the system $K_x Na_{1-x} NbO_3$, composition is calculated for different value of (x) as shown in figures (Fig 3.36 – Fig. 3.41). It is clear that there are all possible of transition during the band gap,

direct and indirect transition. The most possible one is the direct transition because the absorption edge is smaller than that in indirect one. The values of the optical energy gap are nearly approach to each other for each value of (x). That is emphasized the statement said that the exaton is present between two opposite ions during the band gap. Generally, the range of energy gap was about (4.23 – 4.27 eV).

These calculated values are almost greater than the theoretical value of (KN =3.3eV[64] , KNN = 3.2 eV[65] and NN =3.4 eV[66]). Normally the peroviskite ferroelectric had a large energy gap in the range (3-5 eV) [3]. Kompany[65] calculated the energy gap and has result for $NaNbO_3$ was (3.8 eV) which is near our value.

Generally, the FE-PV devices, it is experimentally observed that the output photo voltage is proportional to the magnitude of electric polarization and electrode spacing. As a result, a unique and important characteristic of the FE-PV devices is the anomalous photovoltaic (APV) effect, i.e. the output V_{oc} can be a few orders of magnitude larger than the band gap of the FE materials [2]. That means the band gap is act as the depletion region in the normal semiconductor. This is the reason why this type of ferroelectric materials is favors in the solar energy applications.

Table (3-6): The optical energy gap in (eV)for $K_{1-x}Na_xNbO_3$for (x=0, 0.5 and 1) for direct and indirect transition

Sample	Direct		Indirect	
	Allowed	Forbidden	Allowed	Forbidden
KNbO3	4.27	4.23	4.21	4.18
$K_{0.5}Na_{0.5}NbO_3$	4.21	4.13	4.1	4.007
$NaNbO_3$	4.27	4.237	4.231	4.205

The reflectance spectrum is the way to measure the optical refractive index for the sample under study by using a suitable equation was mentioned in chapter two. The maximum values of the refractive index are appearing at the frequency (824, 847 and, 833 THz) was (1.2, 1.8 and, 1.243) for (x=0, 0.5 and 1) respectively as shown in the figures (Fig 3.42– Fig 3.44).
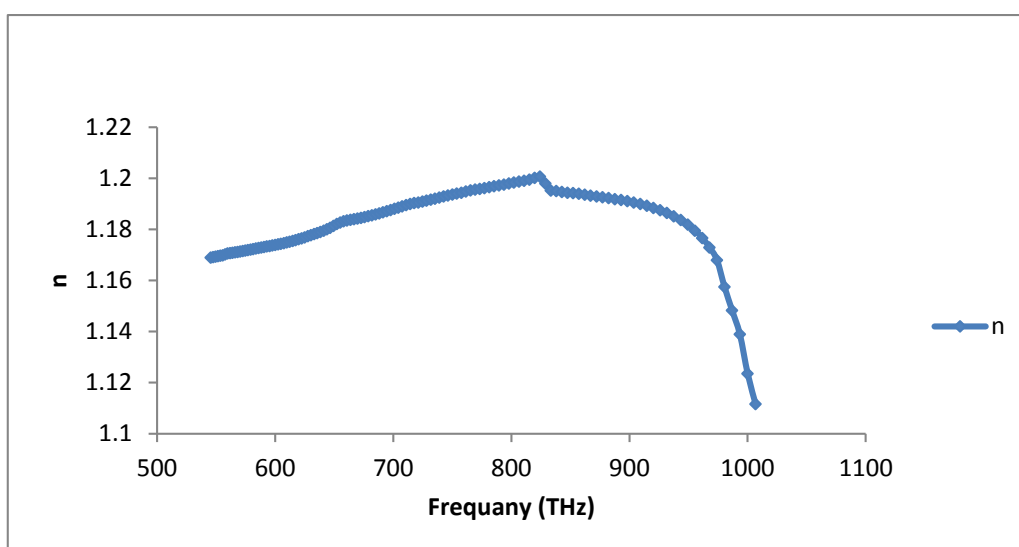
Fig. 3.42: The refractive index as a function of frequency for $KNbO_3$.
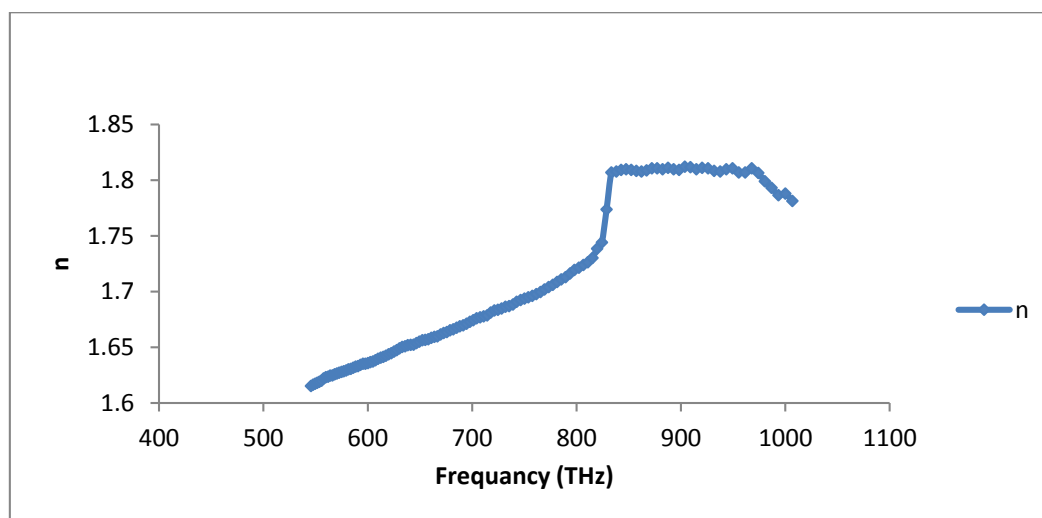
Fig. 3.43: The refractive index as a function of frequency for $K_{0.5}Na_{0.5}NbO_3$.
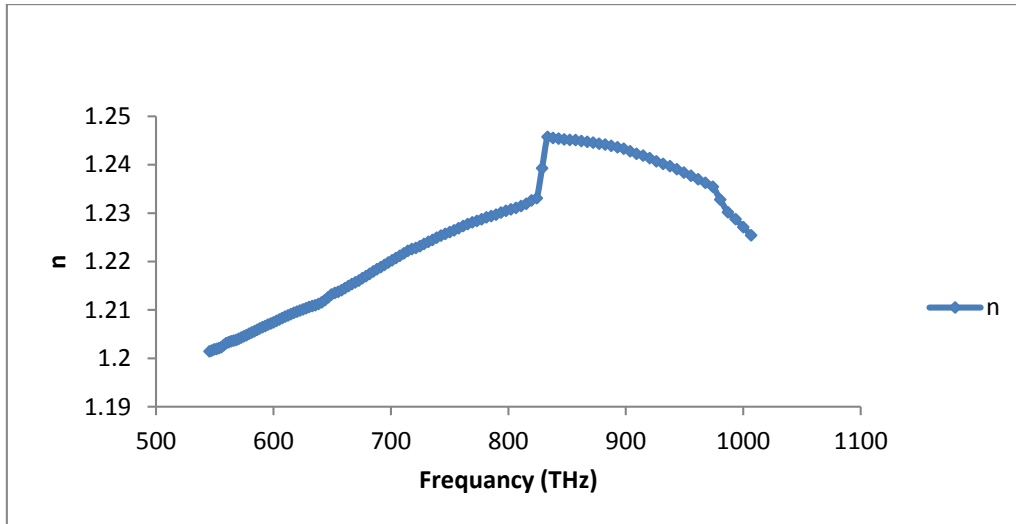
Fig. 3.44: The refractive index as a function of frequency for $NaNbO_3$.

It is clear that the value of the refractive index for $K_{0.5}Na_{0.5}NbO_3$is the highest value. This is normally due to high dielectric constant for this sample because the best dielectric properties were achieved at morphotropic phase boundary (MPB) 50/50 Potassium sodium niobate composition. and this agree with the LCR measurement. It notices that the maximum value of refractive index for the samples at different frequency and this might be due to the difference in the ionic radius between the K and Na ions.

The calculated refractive index that was concluded from the LCR-measurement as a function of frequency. It is about (4.97, 7.36 and, 3.71) at frequency (5 MHz) for all composition (x=0, 0.5 and, 1) respectively at room temperature. Under this region of frequency, the possible two type of polarization is happened represented by dipolar and ionic polarization. The last is more effective with high frequency.

It is clear that the value of the refractive index calculated from the reflection spectrum is much smaller than the refractive index calculated from the LCR measurements. The refractive index concluded from the reflection spectrum related to electronic polarization because it happened at high applied frequency by UV-source. Whereas, the values of (n)

calculated from the LCR measurement is related to the ionic polarization, which normally showed high refractive index.
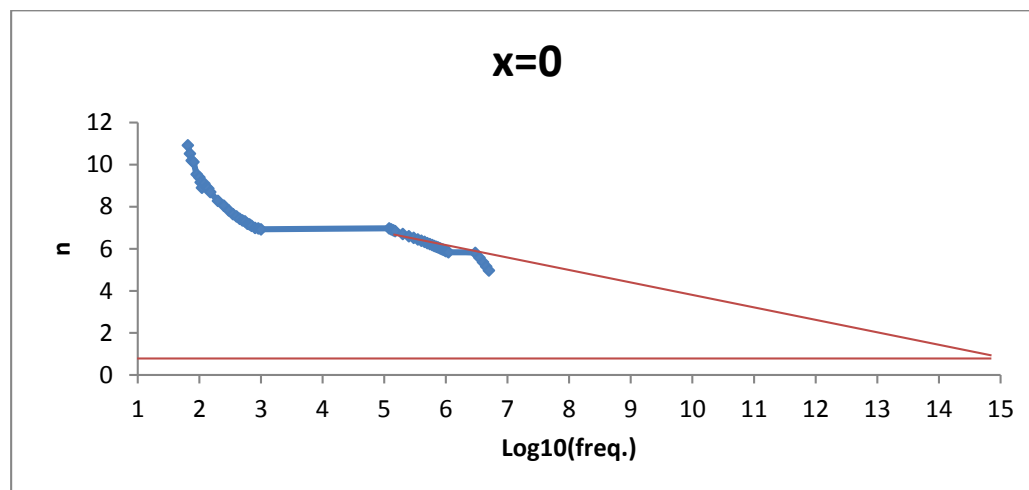
Fig. 3.45: The refractive index as a function to Log10(freq.) for the sample with (x=0) and

T_S=1000 ^oC
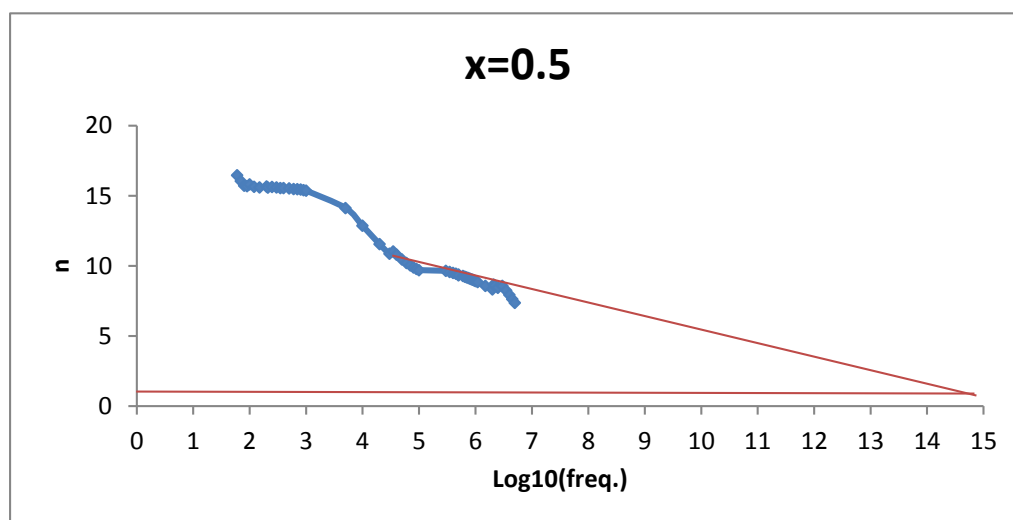
Fig. 3.46: The refractive index as a function to Log10(freq.) for the sample with (x=0.5) and
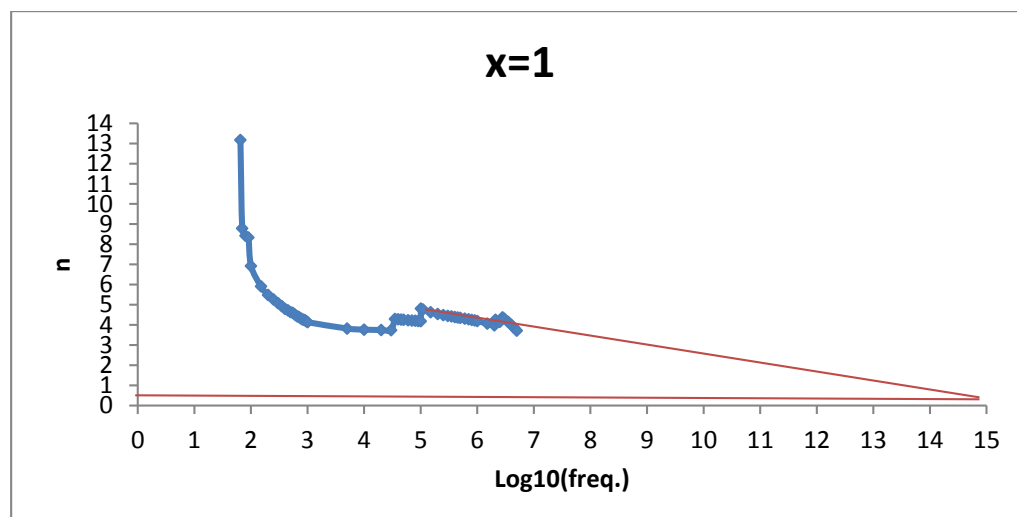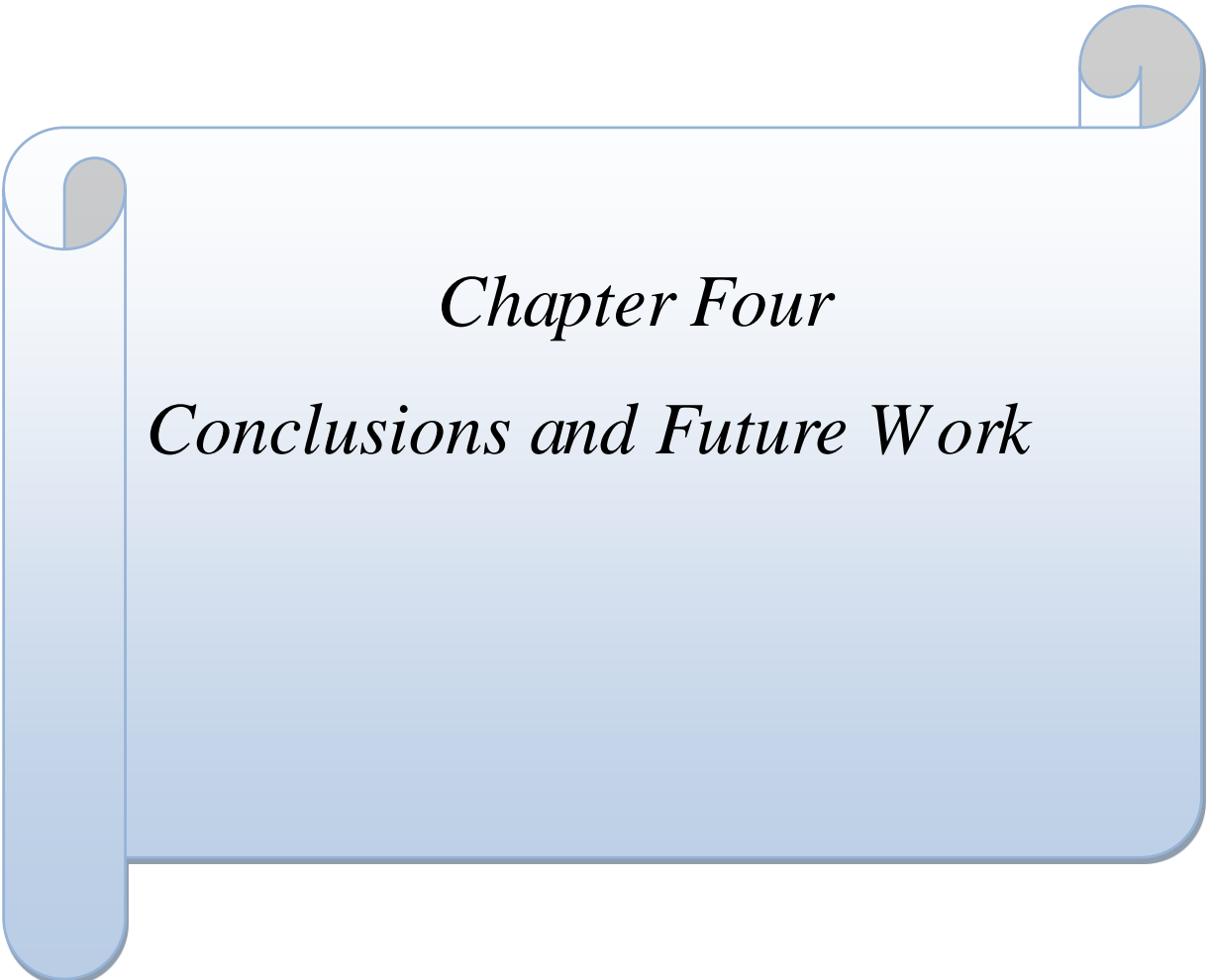
T_S=1000 ^oC.

Fig. 3.47: The refractive index as a function to Log10(freq.) for the sample with (x=0.5) and T_S=1000 °C.

The Log-linear relation between the refractive index and the frequency for the total results concluded by LCR-measurement is appeared in Figs. (3.45-47). Then the extension of the curve and intercepted with the frequency recording the maximum refractive index. It is founding that the value of refractive index is about (0.72, 0.96 and, 0.67) for (x=0, 0.5 and 1) respectively. These values are expected values and less than the calculated from the reflection spectrum.

Chapter Four

Conclusions and Future Work

4.1   Conclusions

From the result can be summarized the following conclusion:

1- For $KNbO_3$ samples, the best sintering temperature was found at (1000 ^{O}C) for it high density and dielectric properties.

2- The XRD showed that the full replacement of Na-ions in place of K-ions, a different miller indices and different space group from the other samples but with the same Orthorhombic phase due to the rearrange the atoms in the structure.

3- The samples sintered at (1000 ^{O}C), $K_{0.5}Na_{0.5}NbO_3$ showed the high dielectric properties, this due to its ratio between K and Na ions (50:50) which the best properties appeared in the ratio. This called (MPB).

4- The optical energy gap is showed that all possible transition during the band gap. But the most possible one is the direct transition because the absorption edge is smaller than that in indirect one. This mean that all the samples can operate in solar energy harvesting but the best one among them is $K_{0.5}Na_{0.5}NbO_3$ due to it low gap.

5- The highest refractive index appears in $K_{0.5}Na_{0.5}NbO_3$, the reason for it high dielectric constant measured in this sample.

6- The calculated refractive index from the reflectance spectrum and that was expected in LCR-measurement for the same frequency are almost the same value and showed the same behavior, which the maximum value of it appeared in $K_{0.5}Na_{0.5}NbO_3$.

4.2 Suggestions and Future Works

1- Studying the effect of the substitution factor(x) on the piezoelectric coefficient (d_{33}) and electrochemical coupling (κ) and pyroelectric coefficient (ρ_t).

2- Use a chemical method of preparation and compare its result with the result obtained in this research.

3- Studying the effect of frequency on d_{33}, κ and ρ t.

4- Trying to study the effect of sintering temperature on the properties of $K_{0.5}Na_{0.5}NbO_3$ and $NaNbO_3$.

5- Trying to fabricate the solar energy harvesting from the prepared system.

6- Studying the effect of another value of (x)

7- Studying the effect of substitution another component like Lithium instead of Sodium.

References

[1]   K. C. Kao, *Dielectric phenomena in solids*: Academic press, 2004.

[2]   Y. Yuan, Z. Xiao, B. Yang, and J. Huang, "Arising applications of ferroelectric materials in photovoltaic devices," *Journal of Materials chemistry A,* vol. 2, pp. 6027-6041, 2014.

[3]   I. Grinberg, D. V. West, M. Torres, G. Gou, D. M. Stein, L. Wu, *et al.*, "Perovskite oxides for visible-light-absorbing ferroelectric and photovoltaic materials," *Nature,* vol. 503, pp. 509-512, 2013.

[4]   E. Tsymbal, "Dielectric properties of insulators," *PHYSICS 927: Introduction to Solid-State Physics,* 2002.

[5]   S. Hoffmann-Eifert, D. Richter, and S. Trolier-Mc Kinstry, "Dielectric, Ferroelectric, and Optical Properties," 2012.

[6]   J. Fraden, *Handbook of modern sensors: physics, designs, and applications*: Springer Science & Business Media, 2004.

[7]   J. V. Mantese and S. P. Alpay, *Graded ferroelectrics, transpacitors, and transponents*: Springer, 2005.

[8]   R. Dittmer, "Lead-Free Piezoceramics–Ergodic and Nonergodic Relaxor Ferroelectrics Based on Bismuth Sodium Titanate," 2013.

[9]   P. W. Barnes, "Exploring structural changes and distortions in quaternary perovskites and defect pyrochlores using powder diffraction techniques," The Ohio State University, 2003.

[10]   M. Johnsson and P. Lemmens, "Crystallography and chemistry of perovskites," *Handbook of magnetism and advanced magnetic materials,* 2007.

[11]   F. Rubio-Marcos, J. Romero, M. S. Martín-Gonzalez, and J. Fernández, "Effect of stoichiometry and milling processes in the synthesis and the piezoelectric properties of modified KNN nanoparticles by solid state reaction," *Journal of the European Ceramic Society,* vol. 30, pp. 2763-2771, 2010.

[12]   K. T. P. Seifert, "Lead-Free Piezoelectric Ceramics," TU Darmstadt, 2010.

[13]   C.-H. Lu, S.-Y. Lo, and Y.-L. Wang, "Glycothermal preparation of potassium niobate ceramic particles under supercritical conditions," *Materials Letters,* vol. 55, pp. 121-125, 2002.

[14]   T. Zhang, W. Lei, P. Liu, J. A. Rodriguez, J. Yu, Y. Qi, *et al.*, "Insights into the structure–photoreactivity relationships in well-defined perovskite ferroelectric $KNbO_3$ nanowires," *Chemical Science,* 2015.

[15]   B. Li, Y. Hakuta, and H. Hayashi, "Hydrothermal Synthesis of $KNbO_3$ powders in Supercritical water," 2008.

References

[16] L. Liang, Y. Li, L.-Q. Chen, S. Y. Hu, and G.-H. Lu, "Thermodynamics and ferroelectric properties of $KNbO_3$," *Journal of Applied Physics,* vol. 106, p. 104118, 2009.

[17] S. Mishra, N. Choudhury, S. Chaplot, P. Krishna, and R. Mittal, "Competing antiferroelectric and ferroelectric interactions in $NaNbO_3$: Neutron diffraction and theoretical studies," *Physical Review B,* vol. 76, p. 024110, 2007.

[18] K. E. Johnston, J. M. Griffin, R. I. Walton, D. M. Dawson, P. Lightfoot, and S. E. Ashbrook, "93Nb NMR and DFT investigation of the polymorphs of $NaNbO_3$," *Physical Chemistry Chemical Physics,* vol. 13, pp. 7565-7576, 2011.

[19] R. Machado, M. Sepliarsky, and M. Stachiotti, "Relative phase stability and lattice dynamics of $NaNbO_3$ from first-principles calculations," *Physical Review B,* vol. 84, p. 134107, 2011.

[20] Y. Yang, J. H. Jung, B. K. Yun, F. Zhang, K. C. Pradel, W. Guo, *et al.*, "Flexible Pyroelectric Nanogenerators using a Composite Structure of Lead-Free $KNbO_3$ Nanowires," *Advanced Materials,* vol. 24, pp. 5357-5362, 2012.

[21] F. Wang, I. Grinberg, and A. M. Rappe, "Semiconducting ferroelectric photovoltaics through Zn^{2+} doping into $KNbO_3$ and polarization rotation," *Physical Review B,* vol. 89, p. 235105, 2014.

[22] Y. Zhuang, Z. Xu, F. Li, Z. Liao, and W. Liu, "Fabrication of flexible energy harvesting device based on $K_{0.5}Na_{0.5}NbO_3$ nanopowders," *Journal of Alloys and Compounds,* vol. 629, pp. 113-117, 2015.

[23] J. Macutkevic, A. Molak, and J. Banys, "Dielectric Properties of $NaNbO_3$ Ceramics," *Ferroelectrics,* vol. 479, pp. 48-55, 2015.

[24] X. Vendrell, J. García, X. Bril, D. Ochoa, L. Mestres, and G. Dezanneau, "Improving the functional properties of $(K_{0.5}Na_{0.5})NbO_3$ piezoceramics by acceptor doping," *Journal of the European Ceramic Society,* vol. 35, pp. 125-130, 2015.

[25] R. Gaur, K. C. Singh, and R. Laishram, "Piezoelectric properties of $(K_{0.5}Na_{0.5})_{1-x}Li_x(Nb_{0.96}Sb_{0.04})O_3$ ceramics prepared from nanocrystalline powders," *Ceramics International,* vol. 41, pp. 1413-1420, 2015.

[26] D.-H. Kim, M.-R. Joung, I.-T. Seo, J. Hur, J.-H. Kim, B.-Y. Kim, *et al.*, "Influence of sintering conditions on piezoelectric properties of $KNbO_3$ ceramics," *Journal of the European Ceramic Society,* vol. 34, pp. 4193-4200, 2014.

[27] X. Cheng, J. Wu, T. Zheng, X. Wang, B. Zhang, D. Xiao, *et al.*, "Rhombohedral–tetragonal phase coexistence and piezoelectric properties based on potassium–sodium niobate ternary system," *Journal of Alloys and Compounds,* vol. 610, pp. 86-91, 2014.

References

[28] F. Li, D. Xiao, J. Wu, Z. Wang, C. Liu, and J. Zhu, "Phase structure and electrical properties of ($K_{0.5}Na_{0.5}$) NbO_3–($Bi_{0.5}Na_{0.5}$) ZrO_3 lead-free ceramics with a sintering aid of ZnO," *Ceramics International,* vol. 40, pp. 14601-14605, 2014.

[29] J. Acker, H. Kungl, R. Schierholz, S. Wagner, R.-A. Eichel, and M. J. Hoffmann, "Microstructure of sodium-potassium niobate ceramics sintered under high alkaline vapor pressure atmosphere," *Journal of the European Ceramic Society,* vol. 34, pp. 4213-4221, 2014.

[30] F. K. Rezaie, D. Panjwani, J. Nath, C. J. Fredricksen, I. O. Oladeji, and R. E. Peale, "Junctionless thin-film ferroelectric oxides for photovoltaic energy production," in *SPIE Sensing Technology+ Applications*, 2014, pp. 91150Q-91150Q-7.

[31] P. Mahesh, A. Kumar, A. James, and D. Pamu, "Dielectric and ferroelectric studies on lead free piezoelectric KNN ceramics," in *SOLID STATE PHYSICS: PROCEEDINGS OF THE 57TH DAE SOLID STATE PHYSICS SYMPOSIUM 2012*, 2013, pp. 62-63.

[32] W. M. Roberts, "The synthesis and characterisation of lead-free piezoelectric ceramics," University of Birmingham, 2012.

[33] Q. Chen, J. X. Li, L. H. Zhang, Y. Bai, Y. J. Su, L. J. Qiao, *et al.*, "Preparation and Characterization of Lead-free Piezoelectric Ceramics," in *Key Engineering Materials*, 2012, pp. 189-193.

[34] K. Jinachai, A. Ngamjarurojana, and A. Rujiwatra, "Solvothermal synthesis, sintering behavior and dielectric properties of potassium niobate fine powders," 2011.

[35] H. Song and W. Ma, "Hydrothermal synthesis of submicron $NaNbO_3$ powders," *Ceramics International,* vol. 37, pp. 877-882, 2011.

[36] K. Kanie, Y. Numamoto, S. Tsukamoto, H. Takahashi, H. Mizutani, A. Terabe, *et al.*, "Hydrothermal Synthesis of Sodium and Potassium Niobates Fine Particles and Their Application to Lead-Free Piezoelectric Material," *Materials Transactions,* vol. 52, pp. 2119-2125, 2011.

[37] H. Bruncková, L. Medvecky, and J. Durisin, "Sol-gel prepared ferroelectric lead-free $KNBO_{(3)}$ and $NaNBO_{(3)}$ thin films and thire microstructure," *Powder Metallurgy Progress,* vol. 10, pp. 169-176, 2010.

[38] G. Wang, S. M. Selbach, Y. Yu, X. Zhang, T. Grande, and M.-A. Einarsrud, "Hydrothermal synthesis and characterization of $KNbO_3$ nanorods," *CrystEngComm,* vol. 11, pp. 1958-1963, 2009.

[39] A. J. Paula, R. Parra, M. A. Zaghete, and J. A. Varela, "Synthesis of $KNbO_3$ nanostructures by a microwave assisted hydrothermal method," *Materials letters,* vol. 62, pp. 2581-2584, 2008.

References

[40] P. Bomlai, W. Saengchote, S. Muensit, and S. J. Milne, "Phase and morphology evolution of $(Na_{1-x}K_x)NbO_3$ powders related to calcinations and K_2CO_3 content."

[41] Y.-J. Hsiao, Y.-H. Chang, Y.-S. Chang, T.-H. Fang, Y.-L. Chai, G.-J. Chen*, et al.*, "Growth and characterization of $NaNbO_3$ synthesized using reaction-sintering method," *Materials Science and Engineering: B,* vol. 136, pp. 129-133, 2007.

[42] I. Pribošič, D. Makovec, and M. Drofenik, "Chemical synthesis of $KNbO_3$ and $KNbO_3$–$BaTiO_3$ ceramics," *Journal of the European Ceramic Society,* vol. 25, pp. 2713-2717, 2005.

[43] T. Rojac, M. Kosec, B. Malič, and J. Holc, "Mechanochemical synthesis of $NaNbO_3$, $KNbO_3$ and $K_{0.5}Na_{0.5}NbO_3$," *Science of Sintering,* vol. 37, pp. 61-67, 2005.

[44] G. K. Goh, F. F. Lange, S. M. Haile, and C. G. Levi, "Hydrothermal synthesis of $KNbO_3$ and $NaNbO_3$ powders," *Journal of materials research,* vol. 18, pp. 338-345, 2003.

[45] B. Sundarakannan, K. Kakimoto, and H. Ohsato, "Frequency and temperature dependent dielectric and conductivity behavior of $KNbO_3$ ceramics," *Journal of applied physics,* vol. 94, pp. 5182-5187, 2003.

[46] J.-Y. Yun, J.-H. Jeon, and S.-J. L. Kang, "Synthesis of sodium niobate powders by mechanochemical processing," *Materials transactions,* vol. 49, pp. 2166-2168, 2008.

[47] A. Lakshmanan, "Sintering of ceramics: new emerging techniques," *InTech, Rijeka,* p. 324, 2012.

[48] M. N. RAHAMAN, "4.1 Sintering of Ceramics," *Handbook of Advanced Ceramics: Materials, Applications, Processing and Properties,* vol. 2, p. 187, 2003.

[49] R. Guinebretière, *X-ray diffraction by polycrystalline materials*: John Wiley & Sons, 2013.

[50] *Xpowder Ver. 2004.04.70 PRO*. Available: http://www.xpowder.com .

[51] *Refine95 software*. Available: downs@geo.arizona.edu

[52] A. Monshi, M. R. Foroughi, and M. R. Monshi, "Modified Scherrer equation to estimate more accurately nano-crystallite size using XRD," *World Journal of Nano Science and Engineering,* vol. 2, p. 154, 2012.

[53] S. J. Orfanidis, *Electromagnetic waves and antennas*: Rutgers University New Brunswick, NJ, 2002.

[54] R. Al-Gaashani, S. Radiman, Y. Al-Douri, N. Tabet, and A. Daud, "Investigation of the optical properties of $Mg(OH)_2$ and MgO nanostructures obtained by microwave-assisted methods," *Journal of Alloys and Compounds,* vol. 521, pp. 71-76, 2012.

References

[55] S. S. Chiad, N. F. Habubi, S. F. Oboudi, and M. H. Abdul-Allah, "Effect of Thickness on The Optical Parameters of PVA: Ag," *Diyala Journal for Pure Sciences,* vol. 7, pp. 153-161, 2011.

[56] T.-W. Huang, Y.-S. Chang, G.-J. Chen, and Y.-H. Chang, "Preparation and structures of the $La_{1-x}K_xCo_{1-x}Nb_xO_3$ (x= 0–l) system," *Journal of alloys and compounds,* vol. 430, pp. 205-211, 2007.

[57] D. Jenko, A. Bencan, B. Malic, J. Holc, and M. Kosec, "Electron microscopy studies of potassium sodium niobate ceramics," *Microscopy and microanalysis,* vol. 11, pp. 572-580, 2005.

[58] B. Jaffe, *Piezoelectric ceramics* vol. 3: Elsevier, 2012.

[59] C. Kittel, *Introduction to solid state physics*: Wiley, 2005.

[60] "PDF2 database (powder diffraction file) from International Center for Diffraction Data, http://www.icdd.com/," ed.

[61] "Crystallography Open Database (COD) , from International Union for Crystallography (IUCr) , http://www.crystallography.net/ .".

[62] S. Mishra, R. Mittal, V. Y. Pomjakushin, and S. Chaplot, "Phase stability and structural temperature dependence in sodium niobate: A high-resolution powder neutron diffraction study," *Physical Review B,* vol. 83, p. 134105, 2011.

[63] B. Akbari, M. P. Tavandashti, and M. Zandrahimi, "Particle Size Characterization of Nanoparticles–A Practicalapproach," *Iranian Journal of Materials Science and Engineering,* vol. 8, pp. 48-56, 2011.

[64] S. Cabuk, "Electronic structure and optical properties of $KNbO_3$: First principles study," *OPTOELECTRONICS AND ADVANCED MATERIALS-RAPID COMMUNICATIONS,* vol. 1, pp. 100-107, 2007.

[65] A. Kompany, "Structural and optical properties of $(K, Na)NbO_3$ nanoparticles synthesized by a modified sol–gel method using starch media," *Advanced powder technology,* vol. 26, 2015.

[66] P. Li, S. Ouyang, G. Xi, T. Kako, and J. Ye, "The effects of crystal structure and electronic structure on photocatalytic H_2 evolution and CO_2 reduction over two phases of perovskite-structured $NaNbO_3$," *The Journal of Physical Chemistry C,* vol. 116, pp. 7621-7628, 2012.

الخلاصة

في هذه الدراسة تم تحضير مادة $K_{1-x}Na_xNbO_3$ حيث يمثل (x) عامل التعويض و هو x = 0, 0.5 , 1 بطريقة تفاعل الحالة الصلبة. النماذج التي تمتلك قيمة x=0 تم تحضيرها بدرجات حرارة تلبيد مختلفة (٩٠٠ و ٩٥٠ و ١٠٠٠ و ١٠٥٠ درجة مئوية). بينما كانت درجة حرارة التلبد للنماذج مع قيمة x=0.5 , 1 (١٠٠٠ درجة مئوية).

إن المسحوق الناتج هو متعدد التبلور و لكن هناك بداية للتحول إلى أحادي التبلور في درجة حرارة التلبد ١٠٠٠ درجة مئوية للنماذج مع قيم x=0 . و هذه الحالة أيضا تظهر في النماذج مع قيمة x=0.5, 1 . تم تحديد كل من التركيب البلوري و المجموعة الفراغية Space group و الإبعاد البلورية و الحجم الحبيبي باستخدام عدة تطبيقات تحليلية مثل حيود الأشعة السينية و المجهر الالكتروني الماسح . و تم تحليلي النتائج باستخدام عدة برامج خاصة بالفحوص التركيبية كبرامج تحليل حيود الأشعة السينية و التي سهلت أيضا من إجراء المقارنات ببعض قواعد البيانات العالمية مثل قاعدة بيانات حيدو الأشعة السينية PDF 2 و قاعدة بيانات علوم البلورات و المواد ICDD، COD.

تم دراسة بعض الخواص الفيزيائية مثل قياس الكثافة و خواص العزل الكهربائية و فجوة الطاقة و معامل الانكسار. درست خواص العزل الكهربائي هي بطريقتين الأولى هي بتغيير التردد و ثبوت درجة الحرارة (درجة حرارة الغرفة) ، و الثانية هي بتغيير درجة الحرارة و ثبوت التردد لقياس ثابت العزل و الخسارة الكهربائية .و كذلك تم تحديد درجات حرارة كيوري (درجه جرارة الانقلاب) و ثابت العزل الكهربائي.

من خلال حسابات العزل الكهربائي لمركب $KNbO_3$ وجد إن أعلى قيم لثابت العزل الكهربائي في النموذج مع درجة حرارة التلبيد ١٠٠٠ درجة مئوية . و بالنسبة للنماذج التي درجة حرارة تلبدها ١٠٠٠ درجة مئوية كانت أعلى قيم لثابت العزل في النموذج مع x=0.5. لوحظ إن درجة حرارة كيوري أنها انحرفت نحو درجات حرارة اقل مع زيادة نسبة الصوديوم في المركب.

تم حساب فجوة الطاقة للنظام و كانت قيمها تتراوح بين (٤,٢٣- ٤,٢٧ إلكترون-فولت). و أيضا تم احتساب معامل الانكسار للنظام من خلال نمط الانعكاس و من خلال الحسابات الكهربائية . ان اعلى قيمة لمعامل الانكسار للمركب لقيم اكس (٠ – ٠,٥ و ١) والذي احتسبت من نمط الانعكاس كانت(١,٢ – ١,٨ و ١,٢٤) على التوالي. أما قيم معامل الانكسار التي حسبت من خلال الحسابات الكهربائية كانت قيمتها ت (٠,٧٢ – ٠,٩٦ و ٠,٦٧) لقيم اكس تساوي (٠ – ٠,٥ و ١) على التوالي.

لقد اظهرت النتائج الكلية النهائية امكانية استخدام المركب المستخدم في هذه الدراسة في محال حاصدات الطاقة الشمسية .

تحضير متراكب فيروالكترك $K_{1-x}Na_xNbO_3$ لتطبيقات جمع الخلايا الشمسية

رسالة

مقدمة إلى كلية العلوم \ جامعه النهرين

كجزء من متطلبات نيل درجة ماجستير في علوم الفيزياء

من قبل

عامر عبد الله سلمان

بكالوريوس جامعة النهرين ٢٠١٠

بأشراف

أ.د. عماد خضير الشكرجي

2016   *1437*